

# A scalable and robust variance components method reveals insights into the architecture of gene-environment interactions underlying complex traits

## Authors

Ali Pazokitoroudi, Zhengtong Liu, Andrew Dahl,  
Noah Zaitlen, Saharon Rosset,  
Sriram Sankararaman

## Correspondence

[alipazoki@cs.ucla.edu](mailto:alipazoki@cs.ucla.edu) (A.P.),  
[sriram@cs.ucla.edu](mailto:sriram@cs.ucla.edu) (S.S.)

**Pazokitoroudi et al. introduced a scalable method to estimate trait variance explained by gene-environment interactions across the genome and within specific genomic annotations. Application of the method in the UK Biobank uncovered significant genome-wide GxE heritability and enrichment of GxE heritability within population and functional genomic annotations.**



# A scalable and robust variance components method reveals insights into the architecture of gene-environment interactions underlying complex traits

Ali Pazokitoroudi,<sup>1,7,8,\*</sup> Zhengtong Liu,<sup>1</sup> Andrew Dahl,<sup>5</sup> Noah Zaitlen,<sup>2,3,4</sup> Saharon Rosset,<sup>6</sup> and Sriram Sankararaman<sup>1,2,3,\*</sup>

## Summary

Understanding the contribution of gene-environment interactions (GxE) to complex trait variation can provide insights into disease mechanisms, explain sources of heritability, and improve genetic risk prediction. While large biobanks with genetic and deep phenotypic data hold promise for obtaining novel insights into GxE, our understanding of GxE architecture in complex traits remains limited. We introduce a method to estimate the proportion of trait variance explained by GxE (GxE heritability) and additive genetic effects (additive heritability) across the genome and within specific genomic annotations. We show that our method is accurate in simulations and computationally efficient for biobank-scale datasets.

We applied our method to common array SNPs (MAF  $\geq 1\%$ ), fifty quantitative traits, and four environmental variables (smoking, sex, age, and statin usage) in unrelated white British individuals in the UK Biobank. We found 68 trait-E pairs with significant genome-wide GxE heritability ( $p < 0.05/200$ ) with a ratio of GxE to additive heritability of  $\approx 6.8\%$  on average. Analyzing  $\approx 8$  million imputed SNPs (MAF  $\geq 0.1\%$ ), we documented an approximate 28% increase in genome-wide GxE heritability compared to array SNPs. We partitioned GxE heritability across minor allele frequency (MAF) and local linkage disequilibrium (LD) values, revealing that, like additive allelic effects, GxE allelic effects tend to increase with decreasing MAF and LD. Analyzing GxE heritability near genes highly expressed in specific tissues, we find significant brain-specific enrichment for body mass index (BMI) and basal metabolic rate in the context of smoking and adipose-specific enrichment for waist-hip ratio (WHR) in the context of sex.

## Introduction

Variation in a complex trait is modulated by an interplay between genetic and environmental factors. Characterizing the effects of gene-environment interactions (GxE) on complex trait variation has the potential to shed light on biological mechanisms underlying the trait,<sup>1–3</sup> inform public health measures,<sup>4</sup> identify sources of missing heritability,<sup>5</sup> and improve the accuracy and portability of trait prediction.<sup>6,7</sup> The growth of biobanks that collect genetic and deep phenotypic data (that span disease outcomes, clinical labs, lifestyle factors, and environmental exposures) across large numbers of individuals offers the possibility to gain novel insights into GxE.<sup>3,8</sup> Nevertheless, characterizing GxE has proved challenging due, in part, to the small effect sizes of individual genetic variants.<sup>9,10</sup>

A potentially powerful methodological approach aims to quantify GxE effects aggregated across a set of variants without needing to pinpoint individual variants. In this approach, the proportion of trait variation explained by GxE (GxE heritability or  $h_{gxe}^2$ ) is estimated by fitting a class of variance components models where the model param-

eters, i.e., the variance components, are informative of  $h_{gxe}^2$ . Methods for estimating  $h_{gxe}^2$  using this approach include GCTA-GxE,<sup>11</sup> multitrait GREML (MV-GREML),<sup>5</sup> random regression GREML (RR-GREML),<sup>5,12</sup> and whole-genome reaction norm model (RNM) and its multitrait version (MRNM).<sup>13</sup> All of these methods (except RNM) are able to account for differences in the noise or residual variance across environments (noise heterogeneity), which is important to mitigate biases in GxE heritability estimates.<sup>13,14</sup> However, these methods work with discrete-valued environmental variables, with RNM and MRNM further restricted to fit bivariate and univariate environments, respectively. A more recent general framework, GxEMM,<sup>14</sup> can be applied to both discrete and continuous environmental variables while modeling noise heterogeneity. However, none of these methods are practical for biobank-scale datasets with sample sizes in the hundreds of thousands and genetic variants in the millions. Two recent methods, GPLEMMA<sup>15</sup> and MEMMA,<sup>16</sup> attempt to scale GxE heritability estimation to large-scale datasets but do not model noise heterogeneity. A more recent method, MonsterLM,<sup>17</sup> has been shown to be feasible for biobank-scale datasets and to produce

<sup>1</sup>Department of Computer Science, UCLA, Los Angeles, CA, USA; <sup>2</sup>Department of Human Genetics, David Geffen School of Medicine, UCLA, Los Angeles, CA, USA; <sup>3</sup>Department of Computational Medicine, David Geffen School of Medicine, UCLA, Los Angeles, CA, USA; <sup>4</sup>Department of Neurology, UCLA, Los Angeles, CA, USA; <sup>5</sup>Section of Genetic Medicine, Department of Medicine, University of Chicago, Chicago, IL, USA; <sup>6</sup>Department of Statistics, Tel-Aviv University, Tel-Aviv, Israel; <sup>7</sup>Department of Epidemiology, Harvard School of Public Health, Boston, MA, USA; <sup>8</sup>Program in Medical and Population Genetics, Broad Institute of MIT and Harvard, Cambridge, MA, USA

\*Correspondence: [alipazoki@cs.ucla.edu](mailto:alipazoki@cs.ucla.edu) (A.P.), [sriram@cs.ucla.edu](mailto:sriram@cs.ucla.edu) (S.S.)

<https://doi.org/10.1016/j.ajhg.2024.05.015>.

© 2024 The Authors. This is an open access article under the CC BY-NC-ND license (<http://creativecommons.org/licenses/by-nc-nd/4.0/>).



unbiased estimates in many scenarios. However, MonsterLM requires SNPs to be filtered to common variants with low levels of linkage disequilibrium (LD), which may limit its application to discover GxE. As a result, current methods for estimating GxE heritability either do not scale to the biobank setting or are susceptible to biased estimates. Additional insights into the architecture of GxE can be gleaned if we can move beyond genome-wide estimates of GxE heritability and estimate GxE heritability across specific genomic annotations such as minor allele frequency (MAF), LD, and functional genomic annotations.

We propose a scalable and robust method, GENIE (gene-environment interaction estimator) that can estimate the proportion of trait variance explained by GxE and additive genetic effects (additive heritability). Using extensive simulations and real data analysis, we show that GENIE accurately estimates  $h_{gxe}^2$  and provides calibrated tests of  $h_{gxe}^2$  due to its ability to account for noise that is heterogeneous across environments. Importantly, GENIE is scalable: able to estimate GxE on datasets with hundreds of thousands of individuals, millions of SNPs, and tens of environmental variables in several hours. The ability of GENIE to be applied to large-scale datasets is important for power: we show that GENIE has adequate power to detect  $h_{gxe}^2$  as low as 2% across a sample of  $\approx 300,000$  unrelated individuals. Finally, GENIE is versatile: able to handle multiple environmental variables (discrete or continuous) and to estimate not only genome-wide  $h_{gxe}^2$  but also partition  $h_{gxe}^2$  across genomic annotations (both overlapping and non-overlapping).

To demonstrate its utility, we first applied GENIE to estimate the genome-wide  $h_{gxe}^2$  on common SNPs ( $M = 454,207$  SNPs with  $MAF > 1\%$ ) and four environmental variables (smoking, sex, age, and statin usage) for fifty quantitative phenotypes measured across 291,273 unrelated white British individuals in the UK Biobank (UKB). Second, we leveraged the scalability of GENIE to partition  $h_{gxe}^2$  across common and low-frequency imputed SNPs ( $M = 7,774,235$  with  $MAF > 0.1\%$ ) in UKB. We partitioned  $h_{gxe}^2$  into genomic annotations based on the MAF and local LD score of each SNP to investigate the variation in GxE effects with population genetic features and to estimate genome-wide  $h_{gxe}^2$  that includes the contribution of both common and low-frequency SNPs. Finally, we applied GENIE to assess whether  $h_{gxe}^2$  shows tissue-specific enrichment by analyzing each of 53 tissue-specific gene sets identified from the GTEx dataset.<sup>18</sup>

## Material and methods

### Generalized GxE linear mixed model

Let  $\mathbf{X}$  denote a  $N \times M$  genotype matrix,  $\mathbf{E}$  denote a  $N \times L$  matrix of environmental variables,  $\mathbf{C}$  denote a  $N \times P$  matrix of fixed-effect covariates, and  $\mathbf{y}$  denote an  $N$ -vector of phenotypes. We assume the following linear mixed model:

$$\begin{aligned} \mathbf{y} &= \mathbf{X}\boldsymbol{\beta} + \sum_{l=1}^L (\mathbf{X} \odot \mathbf{E}_{\cdot l}) \boldsymbol{\alpha}_l + \sum_{l=1}^L (\mathbf{I}_N \odot \mathbf{E}_{\cdot l}) \boldsymbol{\delta}_l + \mathbf{C}\boldsymbol{\gamma} + \boldsymbol{\epsilon} \\ \boldsymbol{\beta} &\sim D\left(\mathbf{0}, \frac{\sigma_g^2}{M} \mathbf{I}_M\right) \\ \boldsymbol{\alpha}_l &\sim D\left(\mathbf{0}, \frac{\sigma_{gxe,l}^2}{M} \mathbf{I}_M\right) \\ \boldsymbol{\delta}_l &\sim D\left(\mathbf{0}, \sigma_{nxe,l}^2 \mathbf{I}_N\right) \\ \boldsymbol{\epsilon} &\sim D\left(\mathbf{0}, \sigma_e^2 \mathbf{I}_N\right) \end{aligned} \quad (\text{Equation 1})$$

Here,  $D(\boldsymbol{\mu}, \boldsymbol{\Sigma})$  denotes an arbitrary distribution with mean  $\boldsymbol{\mu}$  and covariance  $\boldsymbol{\Sigma}$ ,  $\mathbf{E}_{\cdot l}$  denotes  $l$ -th column of  $\mathbf{E}$ , and  $\odot$  denotes row-wise Kronecker product.  $\boldsymbol{\beta}$  denotes the  $M$ -vector of SNP effect sizes,  $\boldsymbol{\gamma}$  denotes the  $P$ -vector of fixed effects,  $\boldsymbol{\alpha}_l$  denotes the  $M$ -vector of genetic effect sizes in the context of environment  $l$  (GxE effects) while  $\boldsymbol{\delta}_l$  denotes the  $N$ -vector of noise-by-environment effect sizes for environment  $l$ , and  $\boldsymbol{\epsilon}$  denotes the  $N$ -vector of noise.  $\sigma_e^2$ ,  $\sigma_g^2$ ,  $\sigma_{gxe,l}^2$ , and  $\sigma_{nxe,l}^2$  denote the residual variance, additive genetic, gene-by-environment, and noise-by-environment variance components, respectively. These variance components can then be transformed into the additive heritability or the proportion of variance explained by additive effects ( $h_g^2$  associated with  $\sigma_g^2$ ) and the GxE heritability or the proportion of variance explained by interactions of genetics with a given environment ( $h_{gxe,l}^2$  associated with  $\sigma_{gxe,l}^2$ ). The noise-by-environment matrix for environment  $l$  is obtained as the row-wise Kronecker product between the  $N \times N$  identity matrix  $\mathbf{I}_N$  and the environment vector  $\mathbf{E}_{\cdot l}$  so that the vector of environment-specific noise for each individual  $i$  (due to environment  $l$ ) will be given by  $E_{il} \boldsymbol{\delta}_l$ . In the simplest case of a binary environment that is coded as  $\{0, 1\}$ , the phenotype of an individual whose environmental variable is set to value 1 will have an additional contribution of noise ( $\boldsymbol{\delta}_l$ ) relative to an individual whose environmental variable is set to 0. Further, all individuals whose environmental variable takes the value 1 will have an additional term that contributes to their phenotypic variance, quantified by  $\sigma_{nxe,l}^2$  relative to individuals with environmental variable 0. This formulation generalizes to settings where the environment is coded as categorical (but with values different from  $\{0, 1\}$ ) and to continuous-valued environments. We now refer to the noise-by-environment (or heterogeneous noise) component as the NxE component and the variance  $\sigma_{nxe}^2$  as the NxE variance in the following sections.

### Estimation in the GxE linear mixed model

We assume without loss of generality that  $\mathbf{y}$  is centered, and the columns of  $\mathbf{X}$  and  $\mathbf{E}$  are standardized. To estimate the variance components of our linear mixed model (LMM), we use a method-of-moments (MoM) estimator that searches for parameter values so that the population moments are close to the sample moments. Since  $E[\mathbf{y}] = 0$ , we derived the MoM estimates by equating the population covariance to the empirical covariance. For simplicity, we exclude the matrix of covariates  $\mathbf{C}$  from the model in the following derivation as the covariates can be efficiently projected out of the phenotype, genotypes, and interaction terms with minimal additional cost (Note S1).

For compactness, we denote  $\mathbf{Z}_0 = \mathbf{X}$ ,  $\mathbf{Z}_l = \mathbf{X} \odot \mathbf{E}_{\cdot l}$  for  $l = 1, \dots, L$ ,  $\mathbf{Z}_l = \mathbf{I}_N \odot \mathbf{E}_{\cdot l}$  for  $l = L + 1, \dots, 2L$ , and  $\mathbf{Z}_{2L+1} = \mathbf{I}_N$ . The population covariance is given by

$$\text{cov}(\mathbf{y}) = E[\mathbf{y}\mathbf{y}^T] - E[\mathbf{y}]E[\mathbf{y}^T] = \sum_{l=0}^{2L+1} \sigma_l^2 \mathbf{K}_l \quad (\text{Equation 2})$$

where

$$\mathbf{K}_l = \begin{cases} \frac{\mathbf{Z}_l \mathbf{Z}_l^T}{M}, & l = 0, \dots, L \\ \mathbf{Z}_l \mathbf{Z}_l^T, & l = L + 1, \dots, 2L + 1 \end{cases}$$

and

$$\sigma_l^2 = \begin{cases} \sigma_s^2, & l = 0 \\ \sigma_{gxe,l}^2, & l = 1, \dots, L \\ \sigma_{nxe,l}^2, & l = L + 1, \dots, 2L \\ \sigma_e^2, & l = 2L + 1 \end{cases}$$

Using  $\mathbf{y}\mathbf{y}^T$  as our estimate of the empirical covariance, we need to solve the following least squares problem to find the variance components.

$$\hat{\sigma}^2 = \underset{\sigma^2}{\operatorname{argmin}} \|\mathbf{y}\mathbf{y}^T - \sum_{l=0}^{2L+1} \sigma_l^2 \mathbf{K}_l\|_F^2 \quad (\text{Equation 3})$$

The MoM estimator satisfies the following normal equations:

$$\mathbf{T}\boldsymbol{\sigma}^2 = \mathbf{q} \quad (\text{Equation 4})$$

where  $\mathbf{T}$  is matrix with entries  $T_{ij} = \operatorname{tr}(\mathbf{K}_i \mathbf{K}_j)$ ,  $i, j \in \{0, \dots, 2L + 1\}$ , and  $\mathbf{q}$  and  $\boldsymbol{\sigma}^2$  are vectors with entries  $c_l = \mathbf{y}^T \mathbf{K}_l \mathbf{y}$  and  $\sigma_l^2$ , respectively, for  $l \in \{0, \dots, 2L + 1\}$ .

The heritability associated with component  $i$  for a component that represents additive genetic or GxE effects (equivalently, the proportion of variance explained by component  $i$ ) is defined as follows:

$$h_i^2 = \frac{\sigma_i^2 \operatorname{tr}(\mathbf{K}_i)}{\sum_k \sigma_k^2 \operatorname{tr}(\mathbf{K}_k)} \quad (\text{Equation 5})$$

The aforementioned definition of heritability holds when the columns of each of the  $\mathbf{Z}$  matrices have zero means and  $N$  is large. To explicitly ensure that the columns of GxE matrices also have zero means, a column consisting of all ones is included in the covariate matrix. Consequently, when the covariates are projected out of the GxE matrices (Note S1), it guarantees that all columns have zero means.

### Computational challenges

Computing the coefficients of the system of linear Equation 4 presents computational challenges. The main computational bottleneck is the evaluation of the quantities  $T_{ij}$  for  $i, j \in \{0, \dots, 2L + 1\}$ , which requires  $\mathcal{O}(N^2 ML)$ . Therefore, the total time complexity for exact MoM is  $\mathcal{O}(N^2 ML + L^3)$ , imposing challenging memory or computation requirements for Biobank-scale data ( $N$  in the hundreds of thousands,  $M$  in the millions, and  $L$  in the hundreds or thousands).

### Scalable estimation

Instead of computing the exact value of  $T_{ij}$ , GENIE uses a randomized estimator of the trace.<sup>19</sup> This estimator uses the fact that for a given  $N \times N$  matrix  $\mathbf{C}$ ,  $\mathbf{w}^T \mathbf{C} \mathbf{w}$  is an unbiased estimator of  $\operatorname{tr}(\mathbf{C})$  ( $E[\mathbf{w}^T \mathbf{C} \mathbf{w}] = \operatorname{tr}[\mathbf{C}]$  where  $\mathbf{w}$  is a random vector with mean zero and covariance  $\mathbf{I}_N$ ). Hence, we can estimate the values  $T_{ij}$ ,  $i, j \in \{0, \dots, 2L + 1\}$  as follows:

$$T_{ij} = \operatorname{tr}(\mathbf{Z}_i \mathbf{Z}_i^T \mathbf{Z}_j \mathbf{Z}_j^T) \approx \widehat{T}_{ij} = \frac{1}{B} \sum_b \mathbf{w}_b^T \mathbf{Z}_i \mathbf{Z}_i^T \mathbf{Z}_j \mathbf{Z}_j^T \mathbf{w}_b \quad (\text{Equation 6})$$

Here,  $\mathbf{w}_1, \dots, \mathbf{w}_B$  are  $B$  independent random vectors with zero mean and covariance  $\mathbf{I}_N$ . In GENIE, we draw these random vectors independently from a standard normal distribution. Note that computing  $T_{ij}$  by using the above estimator involves matrix-vector multiplications, which are repeated  $B$  times. Therefore, the total running time is  $\mathcal{O}(LNMB)$ .

Moreover, we can leverage the structure of the genotype matrix, which only contains entries in  $\{0, 1, 2\}$ . For a fixed genotype matrix  $\mathbf{X}_k$ , we can improve the per iteration time complexity of matrix-vector multiplication from  $\mathcal{O}(NM)$  to  $\mathcal{O}\left(\frac{NM}{\max(\log_3(N), \log_3(M))}\right)$  by using the Mailman algorithm.<sup>20</sup> Solving the normal equations takes  $\mathcal{O}(L^3)$  time so that for a small number of components ( $L$ ), the overall time complexity of our algorithm is  $\mathcal{O}\left(\frac{LNMB}{\max(\log_3(N), \log_3(M))} + L^2(NB + L)\right)$ .

### Standard errors of the estimates

We used a computationally efficient block jackknife<sup>21</sup> to compute standard errors of the estimates, which does not require any assumptions on the distribution of the effect sizes. Each jackknife subsample was created by removing a block of the genotype matrix, and we approximated the true SE by the jackknife estimate. Specifically, if we partition the genotype  $\mathbf{X}$  into  $J$  non-overlapping blocks  $[\mathbf{X}^{(1)}, \dots, \mathbf{X}^{(J)}]$ ,  $\widehat{SE} = \sqrt{\frac{J-1}{J} \sum_j (\widehat{h}_{(j)}^2 - \widehat{h}_{jack}^2)^2}$ , where  $\widehat{h}_{(j)}^2$  is the heritability estimate based on  $\mathbf{X}^{(-j)}$  (removing  $\mathbf{X}^{(j)}$  from  $\mathbf{X}$ ), and  $\widehat{h}_{jack}^2$  is the mean of estimates across  $J$  jackknife subsamples. The jackknife estimator was implemented efficiently in GENIE to compute the estimate in time  $\mathcal{O}\left(\frac{LNMB}{\max(\log_3(N), \log_3(M))} + JL^2(NB + L)\right)$ . In our analysis, we used  $J = 100$  blocks defined over SNPs to compute the standard errors of the estimates.

### Partitioning GxE heritability across the genome

Although the model defined in Equation 1 is beneficial in quantifying genome-wide GxE effects for a given E, it is interesting to identify and interpret the interaction of E with specific regions of the genome, such as SNPs with a particular range of minor allele frequencies or SNPs that lie within genes expressed specifically in a tissue. Following our previous work,<sup>21</sup> the genotype component  $\mathbf{X}$  can be assigned to  $T$  (potentially overlapping) components with respect to a set of annotations (such as MAF/LD or functional annotations). Thus, we extend our model as follows:

$$\begin{aligned} \mathbf{y} &= \sum_{t=1}^T \mathbf{X}_t \boldsymbol{\beta}_t + \sum_{t=1}^T \sum_{l=1}^L (\mathbf{X}_t \odot \mathbf{E}_{:l}) \boldsymbol{\alpha}_{tl} + \sum_{l=1}^L (\mathbf{I}_N \odot \mathbf{E}_{:l}) \boldsymbol{\delta}_l + \mathbf{C}\boldsymbol{\gamma} + \boldsymbol{\epsilon} \\ \boldsymbol{\beta}_t &\sim \mathcal{D}\left(\mathbf{0}, \frac{\sigma_{s,t}^2}{M_t} \mathbf{I}_{M_t}\right) \\ \boldsymbol{\alpha}_{tl} &\sim \mathcal{D}\left(\mathbf{0}, \frac{\sigma_{gxe,tl}^2}{M_t} \mathbf{I}_{M_t}\right) \\ \boldsymbol{\delta}_l &\sim \mathcal{D}\left(\mathbf{0}, \sigma_{nxe,l}^2 \mathbf{I}_N\right) \\ \boldsymbol{\epsilon} &\sim \mathcal{D}(\mathbf{0}, \sigma_e^2 \mathbf{I}_N) \end{aligned} \quad (\text{Equation 7})$$

Here,  $\mathbf{X}_t$  is the genotype of annotation  $t$  with  $M_t$  SNPs, and  $\boldsymbol{\alpha}_{tl}$  refers to the effect sizes of SNPs in annotation  $t$  in the context of environment  $l$ . Analogously,  $\sigma_{gxe,tl}^2$  refers to the variance component for SNPs in annotation  $t$  in the context of environment  $l$ .

while  $h_{gxe,t}^2$  refers to the GxE heritability associated with annotation  $t$  in the context of environment  $l$ .

Given estimated GxE heritabilities under the above model, we define the enrichment of genetic effects in annotation  $t$  in the context of environment  $l$  (also termed GxE enrichment) as follows:

$$Enrichment(gxe, t, l) = \frac{h_{gxe,t}^2 / \sum_{t=1}^T h_{gxe,t}^2}{M_t/M}, t \in \{1, \dots, T\}, l \in \{1, \dots, L\} \quad (\text{Equation 8})$$

### Estimating GxE in the UK Biobank

We applied GENIE to the UKB<sup>8</sup> where we considered environmental variables such as smoking status, sex, age, and statin medication. The analyses utilized the UKB Resource under application 331277, with participants' informed consents verified by the UKB.<sup>22</sup> For every environmental variable, we applied GENIE to estimate additive heritability ( $h_g^2$ ) and GxE heritability ( $h_{gxe}^2$ ) across 50 quantitative phenotypes (in a model that included the environmental variable as a main effect and accounted for noise heterogeneity) (Table S2). In this study, we restricted our analysis to SNPs that were present in the UKB Axiom array used to genotype the UK Biobank. SNPs with greater than 1% missingness and MAF smaller than 1% were removed. Moreover, SNPs that failed the Hardy-Weinberg test at significance threshold  $10^{-7}$  were removed. We restricted our study to self-reported British white ancestry individuals who are  $> 3^{rd}$  degree relatives that are defined as pairs of individuals with kinship coefficient  $< 1/2^{(9/2)}$ .<sup>8</sup> Furthermore, we removed individuals who are outliers for genotype heterozygosity and/or missingness. Finally, we obtained a set of  $N = 291,273$  individuals and  $M = 454,207$  SNPs for real data analyses. No LD pruning or filtering was required by GENIE subsequently.

We included age, sex, age<sup>2</sup>, age  $\times$  sex, age<sup>2</sup>  $\times$  sex, and the top 20 genetic principal components (PCs) as covariates in our analysis for all traits. We always include the environmental variable as a covariate in these analyses. We used PCs precomputed by the UKB from a superset of 488,295 individuals. Additional covariates were used for waist-to-hip ratio (adjusted for body mass index [BMI]) and diastolic/systolic blood pressure (adjusted for cholesterol-lowering medication, blood pressure medication, insulin, hormone replacement therapy, and oral contraceptives). We standardized environmental variables in our primary analyses. The standardized coding for binary environmental variables has an invariant property in the sense that the covariance matrix would be the same regardless of flipping the 0/1 coding. We also considered the binary coding of environmental variables to be relevant. Statin usage is defined as a binary environmental variable based on C10AA (the American Therapeutic Chemical [ATC] code of statin), which corresponds to taking any subtype of statin medications. Smoking status is defined as a categorical variable with three possible values (never, previous, and current).

We considered an additional analysis of genotypes at high-quality imputed SNPs (with a hard call threshold of 0.2 and an INFO score  $\geq 0.8$ ) with MAF  $\geq 0.1\%$  in the  $N = 291,273$  unrelated white British individuals. We further restricted our analyses to SNPs that are under Hardy-Weinberg equilibrium ( $p < 10^{-7}$ ) and are confidently imputed in more than 99% of the individuals. Additionally, we excluded SNPs in the MHC region, resulting in a total of  $M = 7,774,235$  SNPs.

In our analysis of heritability partitioned based on MAF-LD annotations (primarily for the imputed SNPs), we divided SNPs into

eight annotations based on quartiles of the LD scores (computed in-sample using GCTA) and two MAF bins (MAF  $< 5\%$  and MAF  $\geq 5\%$ ). In our analyses of heritability partitioned based on tissue-specific gene expression annotations, we used the annotations for the 53 tissue-specific genes generated by Finucane et al.<sup>18</sup> using a matrix of normalized gene expression values from the Genotype-Tissue Expression (GTEx) database, which included samples from various tissues, including the focal tissue. The authors calculated a  $t$  statistic for each gene to determine its specific expression in the focal tissue and ranked all genes based on their  $t$ -statistics. They defined the top 10% of genes with the highest  $t$  statistic as the set of specifically expressed genes for the focal tissue. To improve the accuracy of the gene set construction, 100-kb windows are added on either side of the transcribed region of each gene in the set of specifically expressed genes to generate a genome annotation that corresponds to the focal tissue.

## Results

### Calibration and power

We assessed the false positive rate of tests of GxE heritability based on GENIE in simulations under different genetic architectures with no GxE heritability. For each architecture, we simulated 100 phenotype replicates across  $N = 291,273$  unrelated white British individuals in the UKB and  $M = 454,207$  SNPs with MAF  $> 1\%$  genotyped on the UKB genotyping array. We chose statin usage in the UKB as the environmental variable. We varied the percentage of causal SNPs while fixing the additive heritability at  $h_g^2 = 0.25$ . We ran GENIE with  $B = 10$  random vectors (see the following section on the choice of the number of random vectors).

Across all simulations, the false positive rate of rejecting the null hypothesis of no GxE heritability is controlled at levels 0.05 and 0.05/200 (we consider this threshold, which controls for the number of trait-environmental variable [trait-E] pairs that we test in UKB): the average  $P(\text{rejection at } p < t)$  is 7.5% and 0% for  $t = 0.05$  and  $t = 0.05/200$ , respectively (Figure 1A).

To measure the power of GENIE to detect GxE heritability, we simulated phenotypes with a non-zero GxE heritability. Across genetic architectures, we varied the GxE heritability with no noise heterogeneity while fixing the additive heritability at 0.25 and the percentage of causal SNPs at 10% (these are default values of additive heritability and causal ratio across our simulations unless otherwise specified). We also tested GENIE by varying the sample size from 30,000 to 300,000. We simulated 100 replicates for every genetic architecture. Let  $h_{gxe}^2(i)$  be the estimate of  $h_{gxe}^2$  and  $SE_i$  be the jackknife estimate of the standard error on the  $i$ -th replicate for  $i \in \{1, \dots, 100\}$ . We computed the  $p$  value of a test of the null hypothesis of no  $h_{gxe}^2$  on the  $i$ -th replicate from the  $Z$  score defined as  $h_{gxe}^2(i)/SE_i$  for  $i \in \{1, \dots, 100\}$ . We reported the percentage of replicates with  $p$  value  $< t$  as the power of GENIE on a given genetic architecture for a  $p$  value threshold of  $t$ .



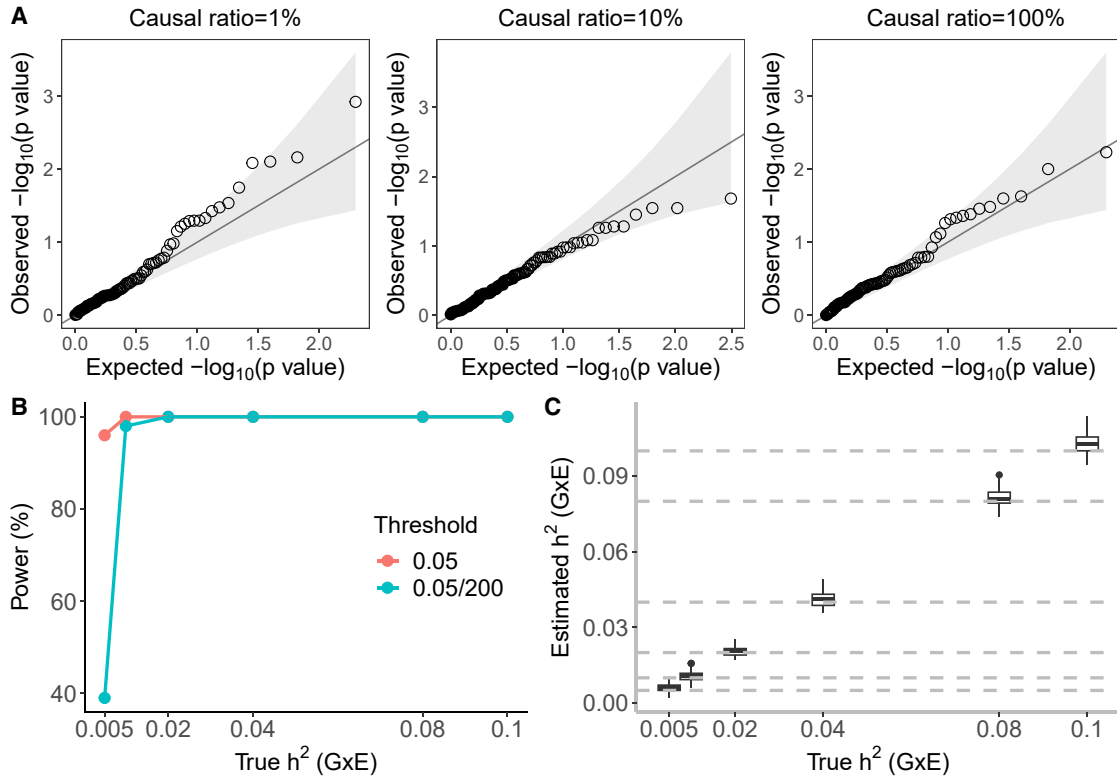


**Figure 1. Calibration and power of GENIE in simulations ( $N = 291,273$  unrelated individuals,  $M = 454,207$  SNPs)**

(A) Q-Q plot of  $p$  values (of a test of the null hypothesis of zero GxE heritability) when GENIE is applied to phenotypes simulated in the absence of GxE effects. Each panel contains 100 replicates of phenotypes simulated with additive heritability  $h_g^2 = 0.25$  and varying proportions of causal variants. The causal ratios are the same for the G and GxE components (10%), and the causal SNPs for the GxE component are independently sampled to those for the additive genetic component. Across all architectures, the mean of  $P(\text{rejection at } p < t)$  is 7.5% and 0% for  $t = 0.05$  and  $t = \frac{0.05}{200}$ , respectively (7.5% is not significantly different from the nominal rate of 5%).

(B) The power of GENIE across genetic architectures as a function of GxE heritability. We report power for  $p$  value thresholds of  $t \in \{0.05, \frac{0.05}{200}\}$ .

(C) The accuracy of  $h_{gxe}^2$  estimates obtained by GENIE. Across all simulations, statin usage in UKB was used as the environmental variable.

GENIE has adequate power to detect GxE effects with  $h_{gxe}^2 \geq 0.005$  in a sample of 300,000 unrelated individuals at  $p < 0.05$  (Figure 1B). The power increases from around 20% to 100% as the sample size grows from 30,000 to 300,000 when  $h_{gxe}^2 = 0.01$  at  $p < 0.05$  and remains almost 100% for  $h_{gxe}^2 \geq 0.05$  as the sample size reaches 50,000 (Figure S2A). Additionally, GENIE yields unbiased estimates of GxE heritability (Figure 1C), and the SEs estimated by GENIE were concordant with the true SEs (Figure S3).

Next, we assessed the accuracy of GENIE in a setting with multiple environmental variables. We simulated phenotypes from a sub-sampled set of UKB genotypes, choosing a subset of  $N = 10,000$  individuals and 20,000 SNPs on chromosome 1 of the UKB Axiom array. We considered a setting with  $L = 10$  environmental variables with  $\sigma_g^2 = 0.2$ , five environmental variables with  $\sigma_{gxe}^2 = 0$ , three environmental variables with  $\sigma_{gxe}^2 = 0.1$ , and two with  $\sigma_{gxe}^2 = 0.01$ . We generated 100 replicates of simulated phenotypes for each set of parameters. We find that GENIE ob-

tains estimates of  $h_{gxe}^2$  that are accurate across the environmental variables (Figure S1; Table S1).

#### Impact of randomization on GxE estimates

We investigated the impact of randomization on the estimates obtained by GENIE by comparing it to the exact MoM. Since exact MoM is computationally infeasible for large sample sizes, we choose to experiment on a small-scale dataset consisting of  $N = 10,000$  unrelated white British individuals and  $M = 60,000$  SNPs selected from the UK Biobank array SNPs on chromosome 1. We generated 100 replicates of phenotypes with no noise heterogeneity,  $h_g^2 = 0.1$ , and varying  $h_{gxe}^2$  with standardized smoking status as the environment variable. We ran GENIE using the G + GxE + Nx E model with  $B = 10$  random vectors and compared the estimated G and GxE heritability with the results from GCTA-HE regression<sup>11</sup> (exact MoM) on G and GxE GRM matrices. We see that exact MoM has a slightly higher statistical power than GENIE (with an increase in power of 2% to 8% across the values tested; Figure S4A). Further, the relative contribution of randomization to the

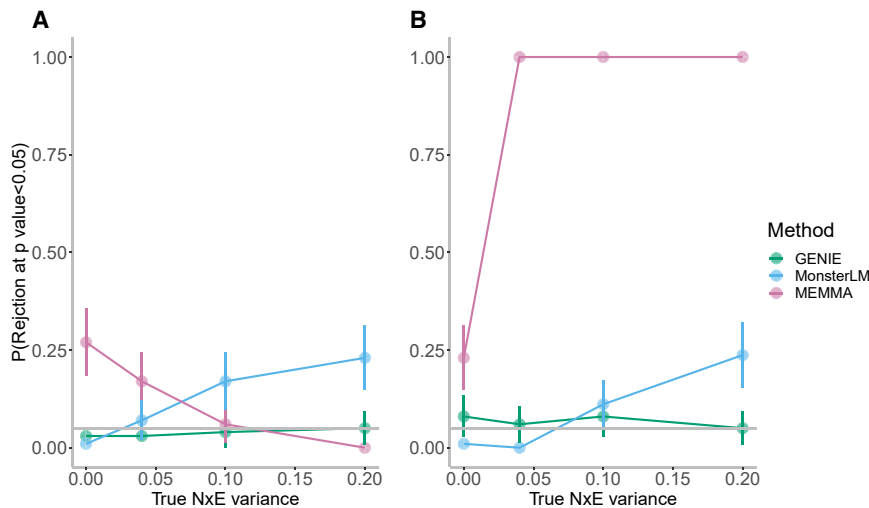


**Figure 2. Comparisons of false positive rates with existing methods with the presence of noise heterogeneity**

False positive rates for GxE heritability across GENIE, MEMMA, and MonsterLM using (A) continuous and (B) discrete environment exposures. We performed simulations with no GxE heritability but with varying magnitudes of the variance of the Nx/E effect. We computed the false positive rate as the fraction of rejections ( $p$  value of a test of the null hypothesis of zero GxE heritability  $< 0.05$ ) over 100 replicates of phenotypes. The phenotypes were simulated from  $N = 40,000$  individuals and  $M = 223,591$  SNPs filtered from  $M = 454,207$  SNPs with the genotype QC steps in MonsterLM: SNPs that failed the Hardy-Weinberg test at the significance threshold  $10^{-10}$  were excluded, and highly correlated SNPs with LD  $r^2 > 0.9$  and SNPs with MAF  $< 0.05$  were removed. Error bars correspond to the estimated 95% CI of the rejection rate.

SE of GENIE remains around 30% despite the variation of power difference across simulations (Figure S4B).

Confirming that randomization makes a modest difference on the power of GENIE, we quantified the effect of the number of random vectors. We explored the choice of the number of random vectors in two ways. First, we quantified the contribution of randomization to the SE of the GxE estimator in GENIE. We simulated 100 phenotypes where  $h_{gxe}^2 = 0$ . We compared the SE of GxE estimates with  $B = 10$  random vectors run 100 times over one of the replicates (the contribution of the randomization to the SE) to the SE of GxE estimates across 100 replicates to determine that, with  $B = 10$ , randomization contributes to about 30% of the total SE across various sample sizes (Figure S5). Second, we verified that our GxE estimates are highly correlated for the choice of random vectors  $B = 10$  vs.  $B = 100$  (Pearson's correlation  $r = 0.99$ ; Figure S6). These results lead us to conclude that  $B = 10$  random vectors provide stable estimates, and we use this setting in our remaining analyses.

### Noise heterogeneity

Previous studies have shown that accounting for noise heterogeneity (Nx/E component) is essential to avoid false positives and inflation in estimates of GxE effects.<sup>13,14,23</sup> To demonstrate the importance of modeling Nx/E, we simulated phenotypes in the presence of Nx/E effect such that  $h_{gxe}^2 = \sigma_{nxe}^2 \in \{0, 0.04, 0.08, 0.10\}$  (we set  $\sigma_{nxe}^2$  to 0.04 when  $h_{gxe}^2 = 0$ ). We ran GENIE, in turn, with and without the Nx/E component. Across all simulations, the model that does not account for the Nx/E component ( $G + GxE$ ) yields statistically significant upward bias in its GxE estimates (relative bias ranges from 2.5% to 69% across genetic architectures) while the model that fits a noise heterogeneity component ( $G + GxE + Nx/E$ ) achieves unbiased estimates of GxE (Figure S7).

### Comparison with existing methods in simulations

We compared the calibration of tests of GxE from GENIE with MEMMA<sup>16</sup> and MonsterLM.<sup>17</sup> GPLEMMA<sup>15</sup> was excluded due to its focus on multiple environmental variables. We conducted the benchmark experiments on  $M = 454,207$  SNPs from a subset of  $N = 40,000$  unrelated white British individuals. To ensure a fair comparison with MonsterLM, which requires genotype QC steps, we filtered SNPs by removing those with high LD ( $r^2 > 0.9$ ) and low MAF (MAF  $< 0.05$ ), resulting in 223,591 SNPs (we report results for GENIE and MEMMA on unfiltered SNPs in Figure S8). We then simulated phenotypes with both continuous (cystatin-C) and discrete (statin usage) environmental variables on the filtered SNPs. In simulations with no GxE or Nx/E effects, MEMMA had inflated false positive rates while GENIE and MonsterLM were calibrated (Figure 2). The inflated false positive rate for MEMMA in the absence of the Nx/E effect can be explained by a bias in their estimates of the SE of the variance components (Figure S9). Under scenarios with noise heterogeneity, GENIE remained calibrated while MonsterLM displayed inflation in its false positive rate with increasing Nx/E variance for both continuous and discrete environment variables. MEMMA showed elevated false positive rates with discrete environment variables, and lower but still inflated false positives with continuous environmental variables (Figure 2).

### Robustness of GENIE in simulations

We tested the robustness of GENIE by varying the correlation between the phenotype ( $Y$ ) and the environment ( $E$ ), simulating heritable  $E$ , imposing that the causal SNPs are the same for the  $G$  and GxE components, simulating  $Y$  that has the same causal SNPs with the heritable  $E$ , and simulating a collider bias scenario. In addition, we also considered a scenario where the environment noise is

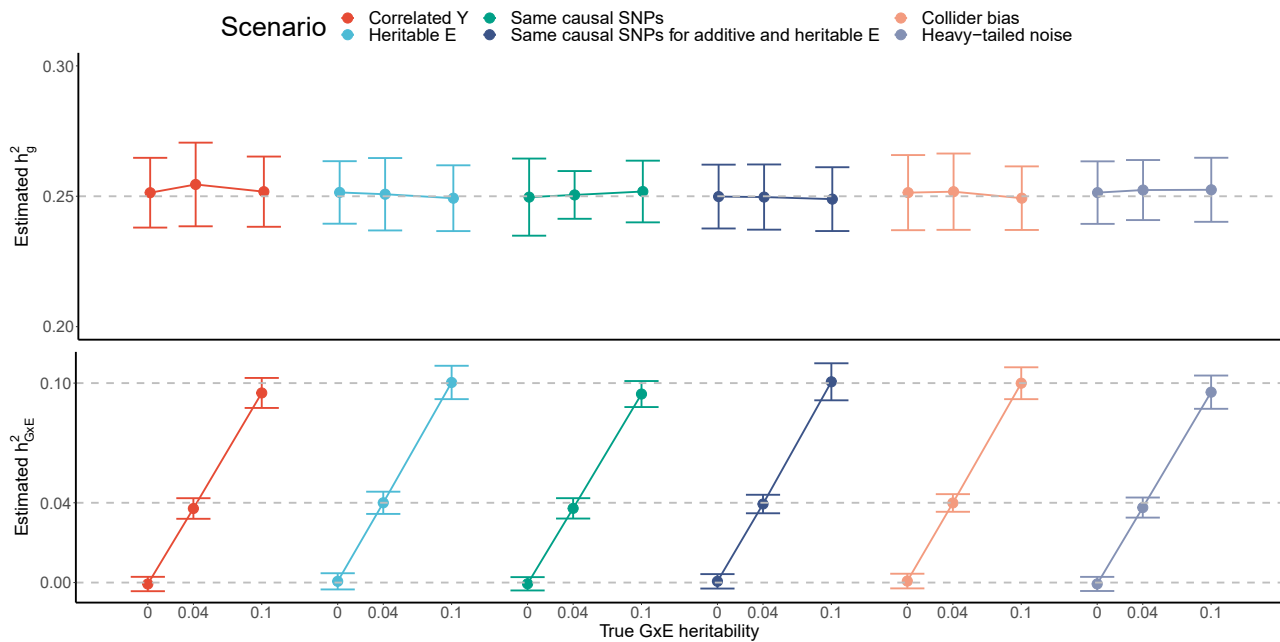


**Figure 3. Estimation of G and GxE heritability in six simulated scenarios**

We investigated the performance of GENIE in estimating G and GxE heritability under six simulated scenarios. (1) Correlated Y: the phenotypes were correlated with the continuous environment exposure, with Pearson's correlation  $r = 0.5$ ; (2) heritable E: the environment exposure E was simulated from the same set of genotype data as in the phenotype simulation, with an additive genetic heritability of 0.1; (3) same causal SNPs: additive genetic causal SNPs completely overlap with GxE causal SNPs; (4) same causal SNPs for additive and heritable E: additive genetic causal SNPs completely overlap with the causal SNPs explaining heritability in E, where E is the same as in scenario (2); (5) collider bias: the phenotype Y and environment exposure E are correlated through an unobserved confounder; we simulated a heritable environment variable with a genetic heritability of 0.1. The phenotypes were then generated to have a Pearson's correlation  $r = 0.2$  with the heritable E. We assumed that the correlation was due to an unobserved confounder.<sup>17</sup> (6) Heavy-tailed noise: we drew the environment noise component from the Student's t-distribution with degrees of freedom = 4. In all scenarios, we simulated 100 replicates of phenotypes with Nx E and varying magnitude of GxE effects across  $N = 291, 273$  individuals genotyped at 454, 207 SNPs. The ground truth GxE heritability was 0, 0.04, and 0.1, with corresponding Nx E variance of 0.04, 0.04, and 0.1. The additive genetic heritability was fixed at 0.25. The x and y axes denote the true GxE heritability and the estimated G and GxE heritability. Points and error bars represent the mean and estimated 95% CI, respectively. Across all simulations where there is no GxE, the mean of  $P(\text{rejection at } p < t)$  are 5.5% and 0% for  $t = 0.05$  and  $t = 0.05/200$ , respectively (5.5% is not significantly different from the nominal rate of 5%).

drawn from a heavy-tailed distribution (see [Note S3](#) for details). In these simulations, we use a continuous environmental exposure (to complement our previous set of simulations that used a discrete environmental exposure, i.e., statin usage). In scenarios where the environmental exposure is heritable, we simulated continuous environmental exposure with specific genetic architecture. In simulations where the environment exposure is not heritable, we use a continuous exposure measured in UKB (cystatin-C). In all simulations, we simulated phenotypes with Nx E and varying GxE effects across  $N = 291, 273$  individuals genotyped at 454, 207 SNPs for 100 replicates. The results summarized in [Figure 3](#) indicate that GENIE obtains accurate estimates across these scenarios.

### Computational efficiency

We evaluated the runtime of GENIE, MonsterLM, MEMMA, and GCTA(HE) (which implements an exact MoM estimator) with increasing sample size ( $N \in \{10000, 50000, 100000, 290000\}$ ) for a fixed number of SNPs ( $M = 454, 207$ ) and a single environmental variable. All methods were run on an Intel(R) Xeon(R) Gold 6140 CPU 2.30GHz,

with 187GB RAM. Ten random vectors are used by GENIE and MEMMA. For GENIE, runtime measurements were obtained for the single component and eight MAF/LD components. All other methods fit a single G and GxE variance component. The runtime of GCTA(HE) includes the computation of the GRM matrix. Our comparison used the CPU implementation of MonsterLM, with runtime calculations excluding the preprocessing step for genotype filtering required by MonsterLM. GENIE is highly scalable and can estimate GxE on about 300,000 individuals and roughly 500,000 SNPs within an hour, with the eight-component model nearly as efficient as the single-component model ([Figure S11](#)).

### Estimating GxE in the UKB

We applied GENIE to estimate additive heritability ( $h_g^2$ ) and GxE heritability ( $h_{GxE}^2$ ) for 50 quantitative phenotypes measured in UKB across unrelated white British individuals. These 50 phenotypes fall into eight broader phenotypic categories (blood biochemistry, kidney biomarkers, anthropometry, lipid metabolism biomarkers, blood pressure, liver biomarkers, lung, and glucose metabolism



biomarkers) that have been analyzed in prior works.<sup>24–26</sup> Following these studies, we applied a rank-based inverse normal transformation to all phenotypes. For certain phenotypes affected by medication usage (systolic/diastolic blood pressure, LDL direct, and total cholesterol), we adopted heuristic adjustments for medication variables.<sup>24,27</sup> We then reevaluated the GxE heritability estimates using GENIE (see [Note S4](#) for details). We considered, in turn, smoking status, sex, age, and statin usage as environmental variables. We included each environmental variable as a fixed effect in the relevant analyses. First, we explored the importance of modeling NxE in real data (building on our simulation results). We then analyzed, in turn, common SNPs genotyped on the UKB array (MAF > 1%) and then common and low-frequency imputed SNPs (MAF ≥ 0.1%). For selected combinations of phenotypes and environmental variables, we also applied GENIE to partition GxE heritability across functional annotations to estimate GxE heritability in genes expressed in specific tissues.

We note that individuals with missing environmental or phenotype data were removed in the implementation of GENIE instead of being imputed by the mean value. We observed that the application of mean imputation to the phenotype results in underestimation of  $h_g^2$  and  $h_{gxe}^2$  while mean imputation of the environment variables affected the estimation of  $h_{gxe}^2$  but not  $h_g^2$  ([Figure S12](#)). We therefore recommend that users leave missing exposure and outcome data as it is when applying GENIE in their analysis based on the simulation results.

### Robustness of GENIE in the UKB

We first assessed the robustness of GENIE by estimating  $h_g^2$  under three different models: G, G + GxE, and G + GxE + NxE, where each model is named by the set of variance components fitted jointly. The additive heritability estimates were highly correlated across the models (Pearson's correlation  $r \geq 0.98$  for every pair of models), leading us to conclude that GENIE provides robust estimates of additive heritability across different models ([Figure S13](#)). We observed a significant difference in  $h_g^2$  for a handful of trait-E pairs when estimated with G + GxE and G + GxE + NxE that include alcohol frequency intake and overall health with smoking status, sex, or age as the environmental variable. In previous work,<sup>21</sup> we compared the additive  $h_g^2$  estimates from RHE with S-LDSC,<sup>28</sup> GRE,<sup>29</sup> SumHer,<sup>30</sup> and LDSC<sup>31</sup> to find that RHE estimates of additive heritability for 22 complex traits are consistent with the existing methods. We additionally compared the additive heritability estimates from GENIE with those obtained using LDSC (run with in-sample LD scores estimated from a subset of 50 K unrelated white British individuals in UKB). The estimates of additive  $h_g^2$  from LDSC were compared against those from GENIE with environmental exposures of smoking status, sex, age, and statin.

The estimates across 50 traits were consistently correlated for the two methods, with Pearson's correlations ranging from 0.87 to 0.93 ([Figure S14](#)).

Our simulations in the previous section revealed the importance of modeling noise heterogeneity ([Figure S7](#)). To investigate the consequences of modeling NxE in real data, we fitted, in turn, models without and with NxE (in addition to G and GxE components). The number of trait-E pairs with significant  $h_{gxe}^2$  ( $p < 0.05/200$ ) decreased from 135 under the G + GxE model to 68 under the G + GxE + NxE model: changing from 40 to 21 for smoking ([Figure 4B](#)), 27 to 28 for sex ([Figure S15B](#)), 28 to 12 for age ([Figure S16B](#)), and 40 to 7 for statin usage ([Figure S17B](#)). For traits with significant  $h_{gxe}^2$ , the magnitudes of the estimates varied across the two models: the ratios of  $h_{gxe}^2$  estimates under the G + GxE + NxE to the G + GxE model were 137% on average (range: 43% – 350%), 110% (70% – 224%), 131% (99% – 166%), and 42% (21% – 72%) for smoking ([Figure 4A](#)), sex ([Figure S15A](#)), age ([Figure S16A](#)), and statin ([Figure S17A](#)), respectively. The magnitude of noise heterogeneity across trait-E pairs can be substantial: 0.05%, 164%, 10%, and 14% of the additive heritability on average for smoking, sex, age, and statin, respectively ([Figures S18–S21](#)). To further investigate the effect of modeling NxE, we performed permutation analyses by randomly shuffling the genotypes while preserving the trait-E relationship (a setting where there is expected to be no GxE by construction while the relationship between phenotype and E is preserved). We applied GENIE under the G + GxE and G + GxE + NxE models to each trait-E pair. The false positive rate of rejecting the null hypothesis of no GxE across the trait-E pairs is substantially inflated under the G + GxE model while being controlled under the G + GxE + NxE model ([Figures 4C, S15C, S16C, and S17C](#) for smoking, sex, age, and statin respectively). These results indicate that modeling NxE is critical to avoid spurious findings of GxE.

### Gene-by-smoking interaction

We applied GENIE to estimate the proportion of phenotypic variance explained by gene-by-smoking interactions ( $h_{gxSmoking}^2$ ) for 50 quantitative phenotypes. We find 21 traits showing statistically significant evidence for  $h_{gxSmoking}^2$  ( $p < 0.05/200$ ) with  $h_{gxSmoking}^2$  about 6.1% of  $h_g^2$  on average ([Figures 5A and 6A](#)). Two of the traits with the largest  $h_{gxSmoking}^2$  were basal metabolic rate and BMI with estimates of 2.4% and 2.3%, respectively (estimates remained significant when we used the binary coding of the smoking status variable obtained by merging the categories of never and previous; [Figures S25 and S28C](#)). Our estimates are consistent with a previous study that analyzed BMI and lifestyle factors in the UKB to find significant GxE for smoking behavior.<sup>5</sup> The  $h_{gxSmoking}^2$  estimates for basal metabolic rate and BMI are about 11% and 7% of their respective  $h_g^2$  estimates.

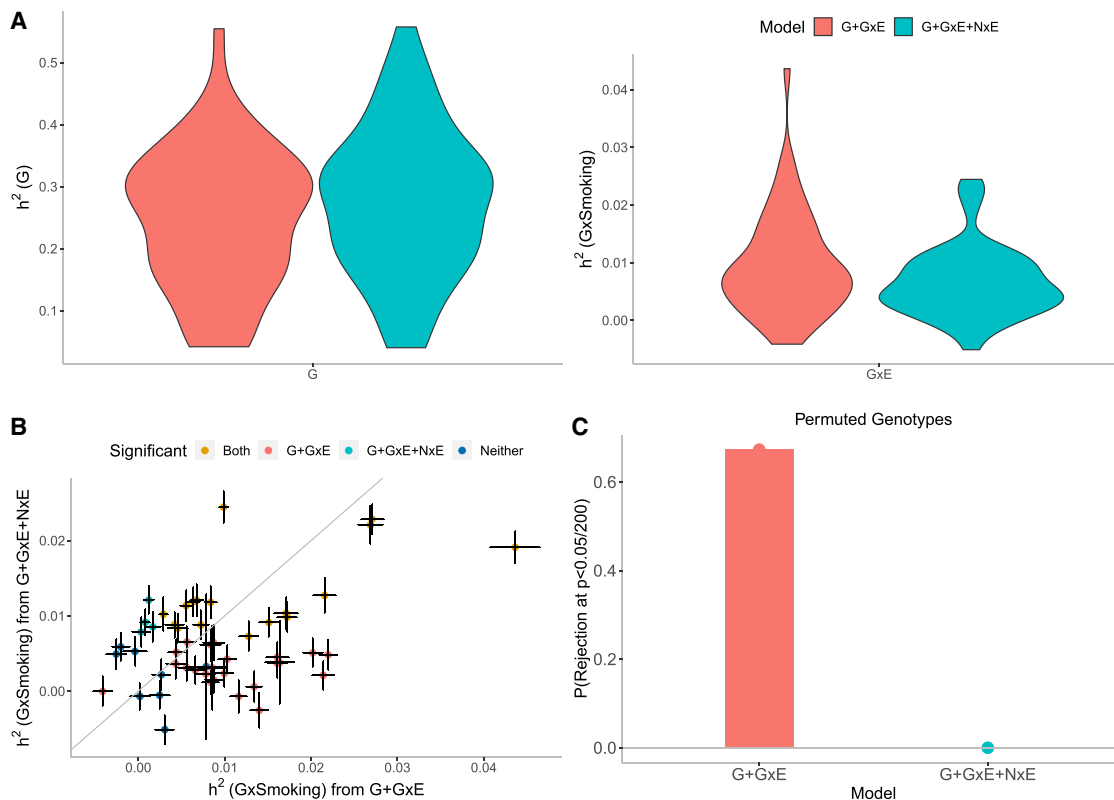


**Figure 4. Effect of noise heterogeneity (Nx) on estimates of heritability associated with GxSmoking across 50 quantitative phenotypes in UKB**

Model G + GxE refers to a model with additive and gene-by-environment interaction components where the environmental variable is smoking status. Model G + GxE + Nx refers to a model with additive, gene-by-environment interaction, and noise heterogeneity (noise-by-environment interaction) components.

(A) We ran GENIE under G + GxE and G + GxE + Nx models to assess the effect of fitting an Nx component on the additive and GxE heritability estimates.

(B) Comparison of GxE heritability estimates obtained from GENIE under a G + GxE + Nx model (x axis) to a G + GxE model (y axis). Black error bars mark  $\pm$  standard errors centered on the estimated GxE heritability. The color of the dots indicates whether estimates of GxE heritability are significant under each model.

(C) We performed permutation analyses by randomly shuffling the genotypes while preserving the trait-E relationship and applied GENIE in each setting under G + GxE and G + GxE + Nx models. We report the fraction of rejections  $P(p \text{ value of a test of the null hypothesis of zero GxE heritability} < \frac{0.05}{200})$  that accounts for the number of phenotypes tested) over 50 UKB phenotypes.

### Gene-by-sex interaction

We find 28 traits with statistically significant  $h^2_{gxSex}$  ( $p < 0.05/200$ ) with  $h^2_{gxSex}/h^2_g$  observed to be 8.7% on average (Figures 5B and 6B). Serum testosterone levels showed the largest  $h^2_{gxSex}$  of 11% with the  $h^2_{gxSex}$  nearly as large as  $h^2_g$  consistent with prior work showing differences in genetic associations<sup>32,33</sup> and heritability<sup>34</sup> across males and females. Beyond testosterone, we observe significant  $h^2_{gxSex}$  for several anthropometric traits, such as waist-hip-ratio (WHR) adjusted for BMI ( $h^2_{gxSex} = 4.3\%$  and  $\frac{h^2_{gxSex}}{h^2_g} = 20\%$ ), and lipid measures (results consistent for binary encoding; Figures S26 and S28B) consistent with previous work documenting sex-specific differences in the genetic architecture of anthropometric traits.<sup>34–39</sup> Consistent with prior GWAS that identified genetic variants with sex-dependent effects,<sup>40,41</sup> our analyses of serum urate levels show substantial point estimates of

$h^2_{gxSex}$ , although these estimates are not statistically significant.

### Gene-by-age interaction

We find 12 traits with statistically significant  $h^2_{gxAge}$  ( $p < 0.05/200$ ) with  $h^2_{gxAge}/h^2_g$  observed to be 4.3% on average (Figures 5C and 6C). Lipid and blood pressure measures show some of the largest  $h^2_{gxAge}$  (about 2.5% for LDL and total cholesterol and 1.9% for diastolic blood pressure). Previous studies have found genetic variants in *SORT1* to have age-dependent effects on LDL cholesterol<sup>42</sup> and nominal evidence for age-dependent genetic effects on blood pressure regulation.<sup>43</sup> We find that BMI shows evidence for significant  $h^2_{gxAge}$  while WHR does not, expanding on prior work that identified age-dependent genetic variants for BMI but not for WHR in genome-wide association studies (GWASs).<sup>36</sup> Interestingly, we used a

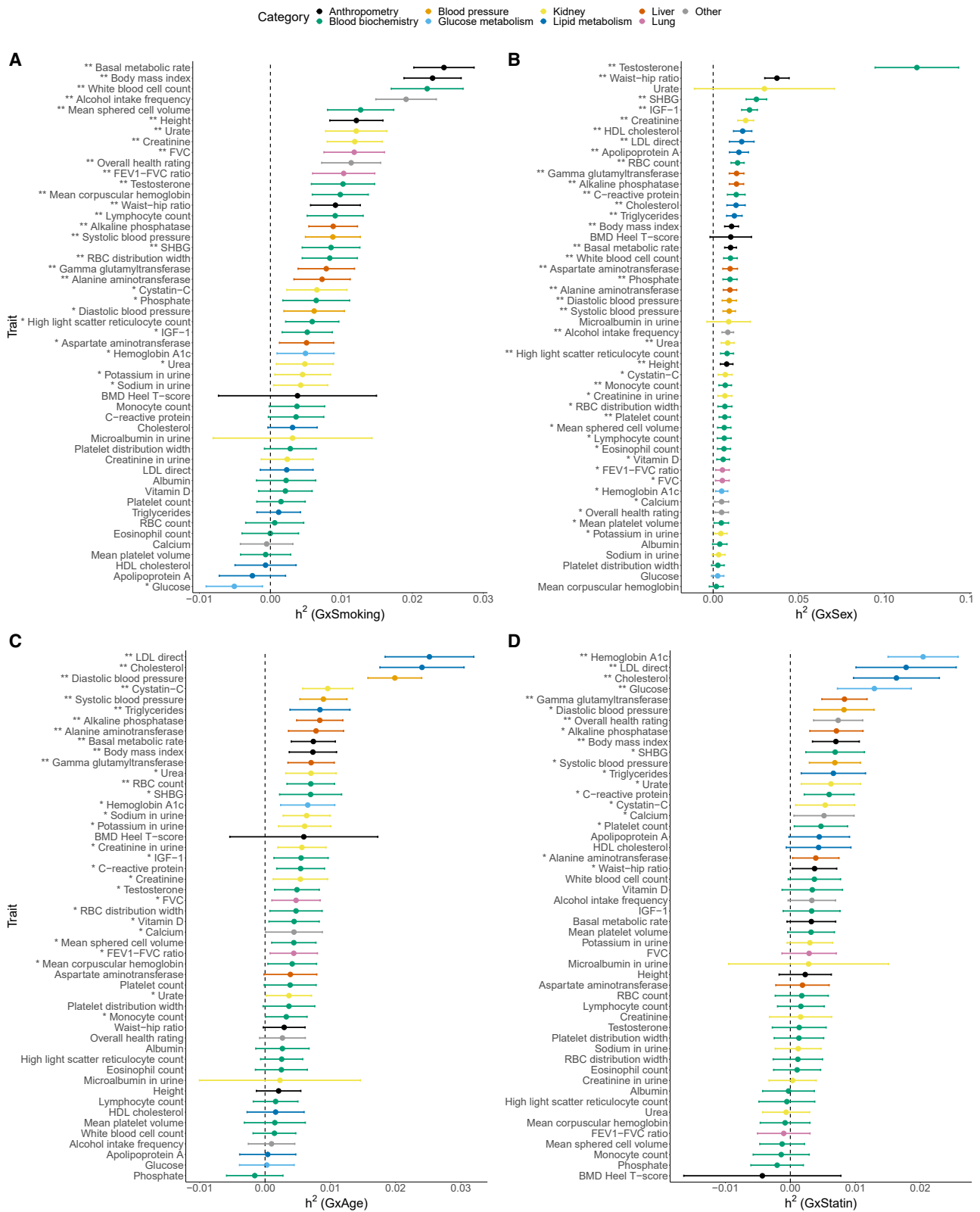


**Figure 5. Estimates of GxE heritability across phenotypes in UKB**

Estimates of (A) GxSmoking, (B) GxSex, (C) GxAge, and (D) GxStatin heritability across 50 UKB phenotypes. We applied GENIE to  $N = 291,273$  unrelated white British individuals and  $M = 454,207$  array SNPs ( $MAF \geq 1\%$ ). Our model includes the environmental variable as a fixed effect and accounts for noise heterogeneity. The environmental variable is standardized in these analyses. Error bars mark  $\pm 2$  standard errors centered on the point estimates. The asterisk and double asterisk correspond to the nominal  $p < 0.05$  and  $p < 0.05/200$ , respectively.

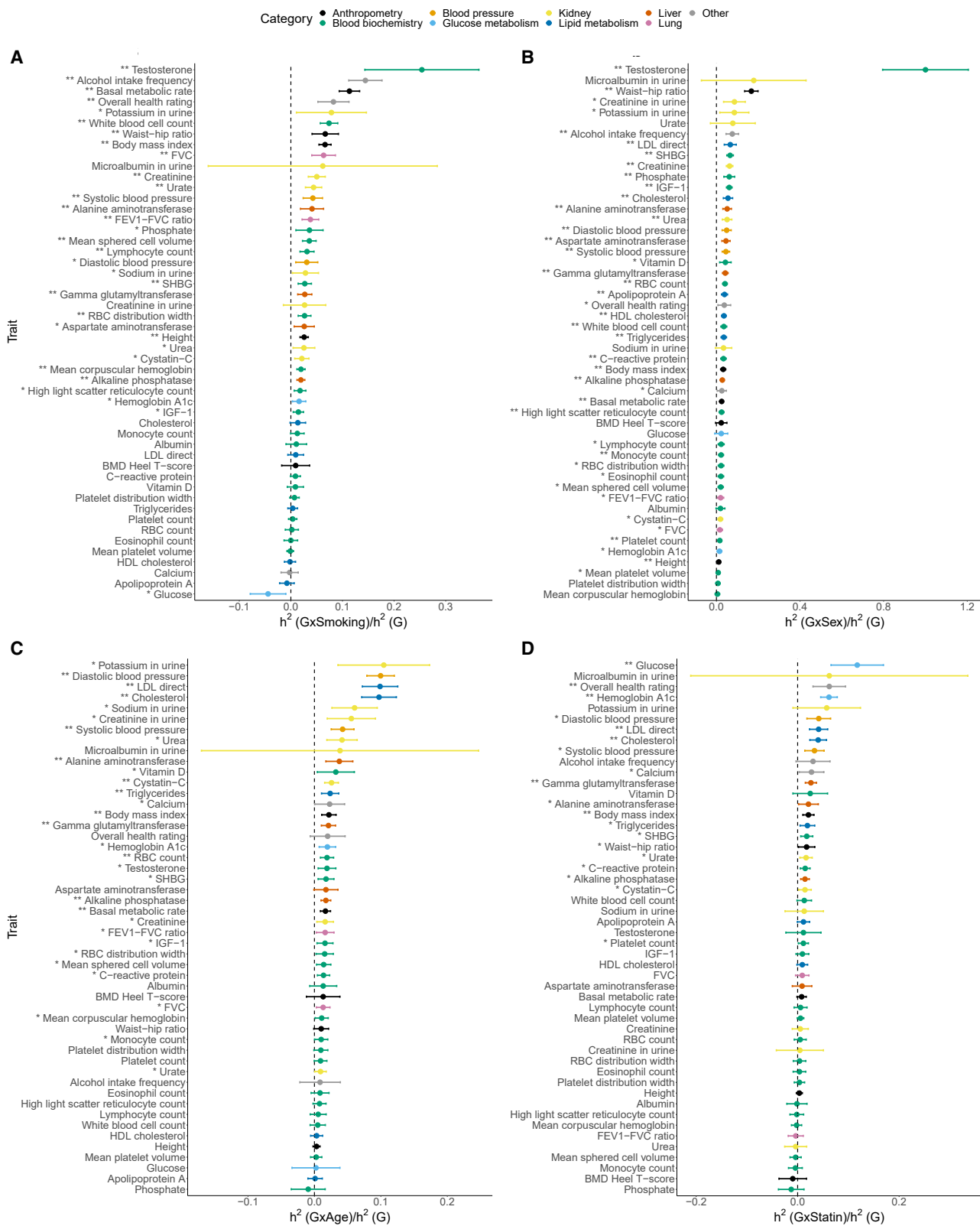


**Figure 6. Estimates of the ratio of GxE to additive heritability across phenotypes in UKB**

Estimates of the ratio of (A) GxSmoking, (B) GxSex, (C) GxAge, and (D) GxStatin to additive heritability across 50 UKB phenotypes. Error bars mark  $\pm 2$  standard errors centered on the point estimates. The asterisk and double asterisk correspond to the nominal  $p < 0.05$  and  $p < 0.05/200$ , respectively.

standardized encoding of age so that GxAge effects capture the interaction of genetic effects on the phenotype as a function of deviation from the mean age in UKB while previous studies typically focus on changes in genetic effects in bins of age. It is plausible that other codings of age, e.g., coding age to measure interactions as a function of older vs. younger individuals, could yield differing results.

### Gene-by-statin interaction

We find seven traits that show statistically significant evidence for  $h_{gxStatin}^2$  ( $p < 0.05/200$ ) with an average ratio of  $h_{gxStatin}^2$  to  $h_g^2$  across traits of 5.2% (Figures S5D and S6D). We find that LDL and total cholesterol show significant  $h_{gxStatin}^2$  (1.7% and 1.6% respectively) while HDL cholesterol with a point estimate of  $h_{gxStatin}^2$  of 0.4% does not (results consistent for binary encoding; Figures S27 and S28A). We observe the largest estimates of  $h_{gxStatin}^2$  for HbA1c and blood glucose measurements (2% and 1.2% respectively), which are interesting in light of statin usage being shown to be associated with a small increase in risk for type 2 diabetes.<sup>44</sup>

### GxE heritability estimates stratified by sex

Quantitative measurements like testosterone concentrations are strongly determined by sex, and therefore, one might be concerned with the possibility of collider bias in  $h_{gxe}^2$  estimates on the whole population for these sex-determined traits. To address this issue, we repeated our previous analyses to estimate GxSmoking, GxAge, and GxStatin in females and males separately across the 50 traits. The results show that the sex-specific GxE heritability estimates are overall consistent with the results on all individuals (Pearson's correlations ranging from 0.67 to 0.80). By comparing GxE heritability estimates between female and male individuals, we noted Pearson's correlations of 0.50, 0.61, and 0.40 for GxSmoking, GxAge, and GxStatin, respectively (Figures S22–S24). In terms of the GxE heritability of testosterone specifically, we see that  $\frac{h_{gxSmoking}^2}{h_g^2}$  is no longer significant for testosterone in female and male individuals (Figure S22) while estimates of  $h_{gxSmoking}^2$  overlap with the previous results: (−0.82%, 0.97%) and (−0.71%, 1.37%) in females and males, respectively, and (0.58%, 1.47%) in the whole population. Hence, the attenuation of our estimates could be explained by the possibility of collider bias or a reduction in power. In general, the phenotypes that have the most significant GxE interactions are in the categories of anthropometry and blood biochemistry for GxSmoking, blood pressure and glucose metabolism for GxAge, and glucose metabolism and lipid metabolism for GxStatin in the sex-stratified analyses. In particular, GxSmoking estimates on BMI, basal metabolic rate, and white blood cell count remain significant for both males and females under  $p < 0.05/200$ . The differences in the GxE estimates between males and females

could suggest the presence of sex-specific GxE interaction effects.

### Comparison with existing methods on significant trait-E pairs

We compared GxE heritability estimates of MEMMA, MonsterLM, and GENIE on real UKB phenotypes. While the consistency of GxE estimates from methods based on different model assumptions can enhance our confidence in the results, such comparisons have inherent limitations—our simulations have revealed variations in false positive rates among different methods. With these caveats, we evaluated GxE heritability using MonsterLM and MEMMA on 68 significant trait-E pairs detected by GENIE ( $p < 0.05/200$ ). We noted Pearson's correlation  $r = 0.91$  between the point estimates of GENIE and MonsterLM and 0.24 between GENIE and MEMMA across the 68 trait-E pairs (Figure S10). The closer alignment between the point estimates by GENIE and MonsterLM can be attributed to the shared consideration of noise heterogeneity within both models.

### Estimating GxE heritability from imputed SNPs

We applied GENIE to estimate  $h_{gxSmoking}^2$ ,  $h_{gxSex}^2$ ,  $h_{gxAge}^2$ , and  $h_{gxStatin}^2$  attributable to  $M = 7,774,235$  imputed SNPs with  $MAF \geq 0.1\%$ . Prior work has shown that analyzing common and low-frequency variants with a single variance component can result in biased estimates of additive heritability.<sup>45,46</sup> A solution to this problem involves fitting multiple variance components obtained by partitioning SNPs based on their frequency and local LD scores (as quantified by the LD scores<sup>31</sup> or the LDK scores<sup>45</sup>).<sup>30,46–48</sup> We follow this approach by partitioning SNPs into eight annotations based on quartiles of the LD scores and two MAF annotations ( $MAF < 5\%$  and  $MAF > 5\%$ ; material and methods).

We performed simulations to show that GENIE applied with SNPs partitioned based on MAF and LD scores can accurately estimate  $h_{gxe}^2$  across varying MAF and LD-dependent genetic architectures while using a single component for all SNPs can lead to substantial biases (Note S2, Figure S29). We applied GENIE using MAF-LD partitions to jointly estimate  $h_g^2$  and  $h_{gxe}^2$  (Figures S30–S33). While estimates of  $h_{gxe}^2$  from imputed SNPs are largely concordant with the estimates obtained from array SNPs, we identify nine trait-E pairs for which the  $h_{gxe}^2$  estimates are significantly different ( $p < 0.05/200$ ). In all these cases,  $h_{gxe}^2$  estimates from imputed SNPs are higher than those from array SNPs. For example, we estimated  $h_{gxSmoking}^2$  for BMI =  $6.5 \pm 0.5\%$ , which is larger than our estimate based on array SNPs as well as a previous estimate of  $4.0 \pm 0.8\%$  based on common HapMap3 SNPs.<sup>5</sup> Across all trait-E pairs, we observed that the average ratio ( $\frac{h_{gxe}^2(\text{imputed})}{h_{gxe}^2(\text{array})}$ ) is 1.17 (1.66, 1.23, 0.71, and 1.17, respectively, for GxSmoking, GxSex,



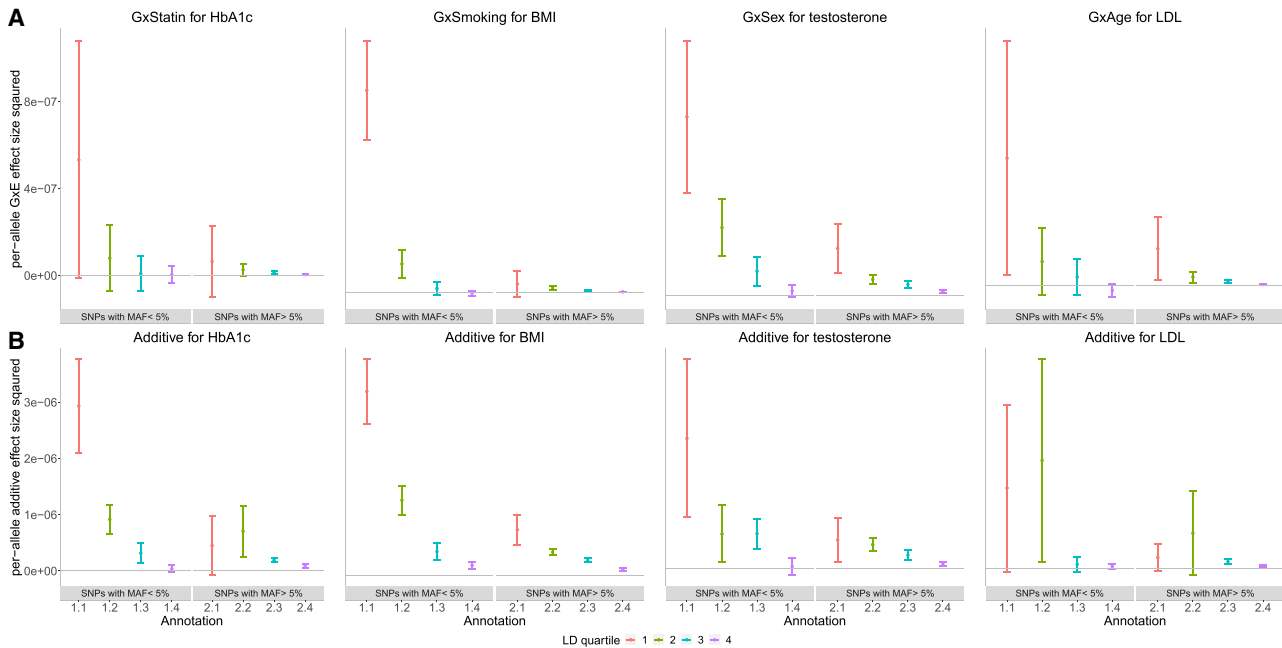


**Figure 7. Per-allele squared GxE and additive effect sizes as a function of MAF and LD**

(A) The squared per-allele GxE effect size for four selected pairs of trait and environment (trait-E pairs).

(B) The squared per-allele additive effect size for the same trait-E pairs. The x axis corresponds to MAF-LD annotations where annotation  $ij$  includes SNPs in MAF bin  $i$  and LD quartile  $j$  where MAF bin 1 and MAF bin 2 correspond to SNPs with  $MAF \leq 5\%$  and  $MAF > 5\%$ , respectively, while the first quartile of LD scores correspond to SNPs with the lowest LD scores respectively). The y axis shows the per-allele GxE (or additive) effect size squared defined as  $\frac{h_k^2}{2M_k f_k (1-f_k)}$  where  $h_k^2$  is the GxE (or additive) heritability attributed to bin  $k$ ,  $M_k$  is the number of SNPs in bin  $k$ , and  $f_k$  is the mean MAF in bin  $k$ . Error bars mark  $\pm 2$  standard errors centered on the estimated effect sizes.

GxAge, and GxStatin; Figure S34). Across trait-E pairs with significant  $h_{gxe}^2$ , the average  $h_{gxe}^2$  is 2.8% on the imputed data compared to 1.5% on array data while the ratio of  $\frac{h_{gxe}^2}{h_s^2}$  is 14.3% on the imputed data compared to 6.8% on the array data (averaged across trait-E pairs, we estimated  $h_{gxe}^2 = 0.9\%$  on imputed vs. 0.7% on array data).

We explored the impact of fitting multiple variance components based on MAF and LD by applying GENIE to fit a single GxE and additive variance component using smoking status as the environmental variable. While ten traits showed significant  $h_{gxSmoking}^2$  in both analyses, five traits were exclusively significant in the MAF-LD model while one was exclusively significant in the single-component model. Restricting to traits with significant GxSmoking in both models,  $h_{gxSmoking}^2$  estimates in the MAF-LD model were about three times those from the single-component model on average (Figure S35). We also investigated whether MAF-LD partitioning affected estimates of  $h_{gxSmoking}^2$  obtained from array SNPs. We find that  $h_{gxSmoking}^2$  estimates are largely concordant whether obtained from a single component or an MAF-LD partitioned model (ratio of 0.99 on average) consistent with the array SNPs being relatively common ( $MAF > 1\%$ ). Our analysis suggests that partitioning by MAF and LD is helpful for estimating  $h_{gxe}^2$  from both common and low-frequency SNPs and the inclusion low-frequency SNPs can increase estimates of  $h_{gxe}^2$  for specific traits.

### Partitioning GxE heritability across MAF and LD annotations

Previous studies have shown that the additive SNP effects increase with decreasing MAF and local levels of LD<sup>21,49–51</sup> likely due to the effects of negative selection. Similar to previous analyses,<sup>15,17</sup> we explored the MAF-LD dependence of SNP effects in the context of specific environmental factors. Our analyses in the preceding section, showing differences in the genome-wide  $h_{gxe}^2$  estimates when partitioning by MAF and LD vs. fitting a single variance component, suggest that GxE effects are expected to vary by MAF and LD in a pattern that is distinct from what would be expected when fitting a single variance component, which assumes that the effect size at a SNP varies with its allele frequency  $f$  as  $\frac{1}{f(1-f)}$  while not varying with local LD (for a fixed value of the allele frequency  $f$ ). To explore the MAF-LD dependence of GxE effects, we used GENIE to partition  $h_{gxe}^2$  across MAF and LD annotations (while simultaneously partitioning additive heritability) of  $M = 7,774,235$  imputed SNPs divided into eight annotations based on quartiles of LD-scores and two MAF bins (low-frequency bins with  $MAF < 5\%$  and high-frequency bins with  $MAF \geq 5\%$ ). Within each of these eight bins, we defined the per-allele squared effect size as  $\beta_k^2 = \frac{h_k^2}{2M_k f_k (1-f_k)}$  where  $h_k^2$  is the GxE (or additive) heritability attributed to bin  $k$ ,  $M_k$  is the number of SNPs in bin  $k$ , and  $f_k$  is the mean MAF in bin  $k$ .

For the sake of presentation, we selected one phenotype with high genome-wide GxE heritability for each of the four environmental variables analyzed (Figure 7; see Table S4 for results on all trait-E pairs). Across bins of MAF and LD, the magnitude of additive allelic effects tends to be larger than those of the GxE effects consistent with the genome-wide results. We observed that the per-allele squared GxE effect size  $\beta_{gxe}^2$  tends to increase with lower MAF within a given quartile of LD score and to increase with lower bins of LD score for a fixed MAF bin (Figure 7A). These trends are analogous to the relationship observed for additive per-allele effect sizes (Figure 7B). Across the trait-E pairs, restricting to the lowest quartile of LD scores, low-frequency SNPs tend to have higher per-allele GxE effect sizes compared to high-frequency SNPs: the ratio of  $\beta_{gxe}^2$  in low vs. high MAF bins is  $8.2 \pm 11.2$ ,  $24.6 \pm 19.7$ ,  $3.4 \pm 2.1$ , and  $3.7 \pm 1.2$  for HbA1c-statin, BMI-smoking, LDL-age, and testosterone-sex, respectively. In the highest quartile of LD scores, we found no statistically significant differences in  $\beta_{gxe}^2$  across low and high MAF SNPs in any of the four trait-E pairs (we also plot the per-standardized genotype additive and GxE heritability,  $\frac{h_g^2}{M_k}$ , in Figure S36).

### Partitioning GxE heritability across tissue-specific genes

The ability of GENIE to simultaneously estimate multiple, potentially overlapping, additive and GxE variance components enables us to explore how  $h_{gxe}^2$  is localized across the genome. Specifically, we set to answer the question of whether  $h_{gxe}^2$  is enriched in genes specifically expressed in a given tissue as a means to identify tissues that are relevant to a trait in a specific environmental context.

We applied GENIE to estimate  $h_g^2$  and  $h_{gxe}^2$  across each of 53 sets of genomic annotations defined as regions around genes that are highly expressed in a specific tissue in the GTEx dataset<sup>18</sup> (Table S3). For each of the four environmental variables, we analyzed only traits with genome-wide significant  $h_{gxe}^2$  based on our prior analyses of the array SNPs. For every set of tissue-specific genes, we followed prior work<sup>18</sup> by jointly modeling the tissue-specific gene annotation as well as 28 genomic annotations that are part of the baseline LDSC annotations that include genic regions, enhancer regions, and conserved regions.<sup>28</sup> Specifically, our model has 29 additive variance components and 29 GxE variance components and estimates the additive and GxE heritability that can be attributed to genes specifically expressed in a tissue while controlling for the effects of the background annotations. A positive  $h_{g,tissue}^2$  represents a positive contribution of genetic effects in a tissue to additive heritability.<sup>18</sup> Analogously, a positive  $h_{gxe,tissue}^2$  represents a positive contribution of genetic effects in this tissue to trait heritability in the context of the specific environment. We test estimates of  $\frac{h_{gxe,tissue}^2/h_{g,tissue}^2}{M_{tissue}/M_{total}}$

$\left(\frac{h_{g,tissue}^2/h_{g,total}^2}{M_{tissue}/M_{total}}\right)$  to answer whether a tissue of interest is en-

riched for GxE (additive) heritability conditional on the remaining genomic annotations included in the model.

We first verified that our approach is able to detect previously reported enrichments for additive effects such as brain-specific enrichment for BMI and adipose-specific enrichment for WHR (Figure 8).<sup>18</sup> Across 68 trait-E pairs with significant genome-wide GxE that we tested, we observed significant enrichment of  $h_{gxe,tissue}^2$  (FDR < 0.10) for at least one tissue in five trait-E pairs (we plot four of these pairs in Figure 8 since the results from the fifth LDL-age are highly correlated with cholesterol-age). Across these trait-E pairs, we documented differential patterns of enrichments for GxE effects compared to additive effects. BMI exhibits brain-specific enrichment of  $h_{gSmoking}^2$  and  $h_g^2$  while WHR exhibits enrichment of  $h_{gSex}^2$  and  $h_g^2$  in adipose and breast tissue (in addition to the enrichment of  $h_g^2$  in the uterus and cardiovascular tissues). The adipose-tissue-specific enrichment of  $h_{gSex}^2$  in WHR is notable in light of known instances of genes associated with WHR in adipose tissue in a sex-dependent manner. *ADAMTS9*, a gene involved in insulin sensitivity,<sup>35</sup> is specifically expressed in adipose tissue and has been shown to be located near GWAS hits for WHR that are specific to females.<sup>35,36,52</sup> The transcription factor, *KLF14*, is located near a sex-dependent GWAS variant for WHR, type 2 diabetes, and multiple other metabolic and anthropometric traits.<sup>53</sup> Further, the expression level of this gene is associated with the GWAS variant in adipose but not with other tissues.<sup>53</sup> We also found instances where tissues that are enriched for  $h_{gxe}^2$  are distinct from those that are enriched for  $h_g^2$ . We observed that the enrichment of  $h_{gSex}^2$  for basal metabolic rate in brain and adipose tissues is distinct from the tissues that are enriched in  $h_g^2$  for the same trait (cardiovascular and digestive tissues) (Figure 8). Finally, we find suggestive evidence that the liver is the most enriched tissue for  $h_{gStatin}^2$  in HbA1c ( $p = 0.02$ ) as well as for  $h_{gSex}^2$  in testosterone ( $p = 0.005$ ), although neither enrichment is significant at FDR of 0.10. These enrichments recapitulate known biology: the liver-specific enrichment of GxStatin effects for HbA1c reflect the tissues in which the target of statins (HMG-CoA-reductase) is expressed<sup>54</sup> while the liver-specific enrichment of GxSex for testosterone is consistent with previous findings implicating *CYP3A7*, a gene involved in testosterone metabolism that is specifically expressed in the liver and lies within a locus that contains one of the strongest GWAS signals for serum testosterone in females.<sup>32</sup>

### Discussion

We have described GENIE, a method that can jointly estimate the proportion of variation in a complex trait that can be attributed to GxE and additive genetic effects. GENIE can also partition GxE heritability across the

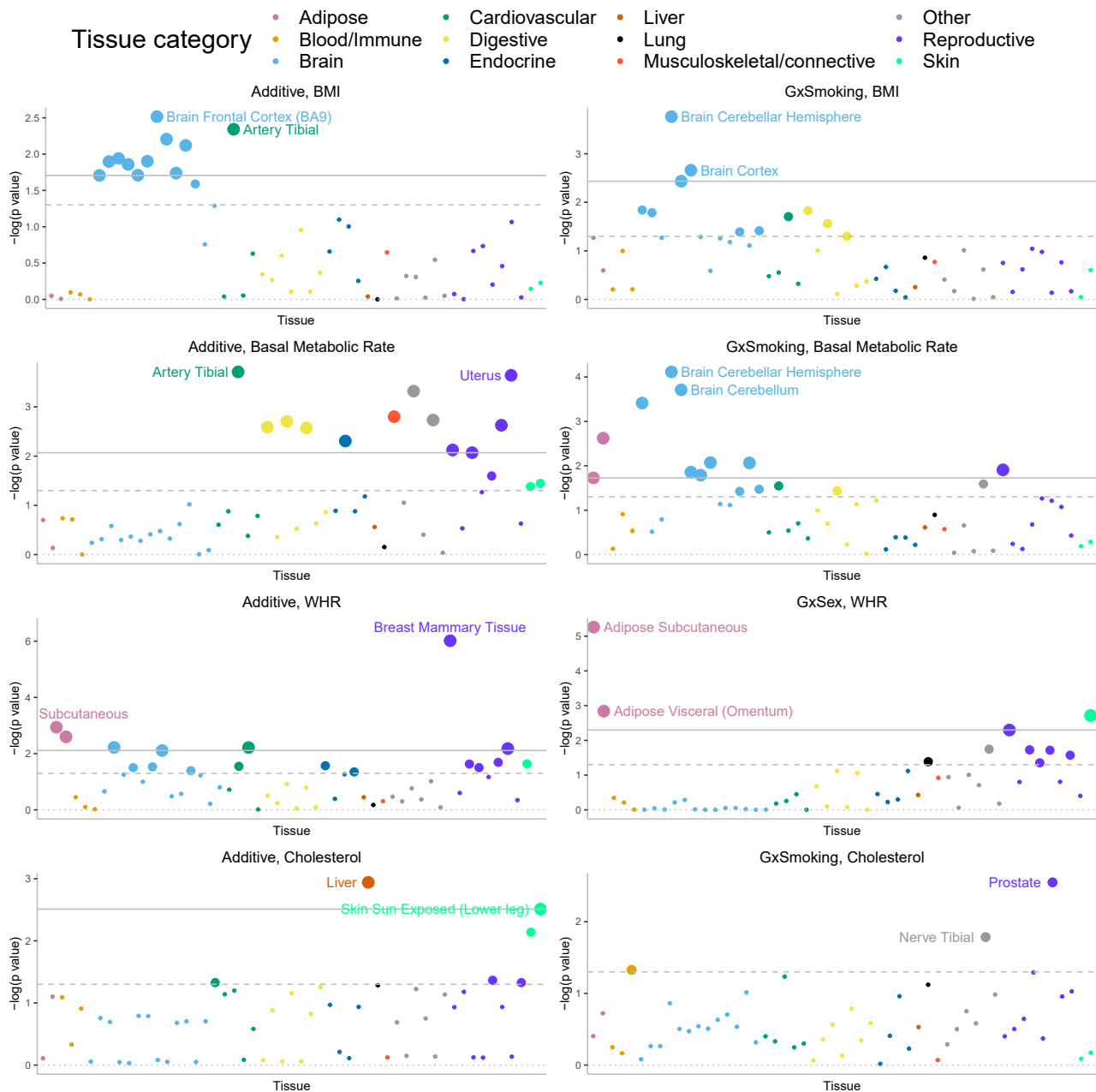


**Figure 8. Partitioning GxE heritability across 53 tissue-specific genes**

We plot  $-\log_{10}(p)$  where  $p$  is the corresponding  $p$  value of the tissue-specific GxE enrichment defined as  $\frac{h^2_{gxe,tissue}/h^2_{gxe,total}}{M_{tissue}/M_{total}}$ . For every tissue-specific annotation, we use GENIE to test whether this annotation is significantly enriched for per-SNP heritability, conditional on 28 functional annotations that are part of the baseline LDSC annotations. The dashed and solid lines correspond to the nominal  $p < 0.05$  and  $FDR < 0.1$  threshold, respectively. We have labeled two tissues with the most significant  $p$  values for each figure.

genome with respect to annotations such as functional and tissue-specific annotations or annotations defined based on the MAF and local LD score of each SNP to localize signals of GxE. GENIE provides well-calibrated tests for the existence of a GxE effect and has high power to detect GxE effects while being scalable to large datasets.

Our simulations and real data analysis results confirm the importance of including noise heterogeneity in GxE models. Simulations comparing the calibration of GENIE to MEMMA and MonsterLM suggest that modeling Nx

does not introduce biases in scenarios without noise heterogeneity. Furthermore, it aids in controlling false positive rates when noise heterogeneity exists. In UKB data analyses, we observed that about half of trait-E pairs with significant  $h^2_{gxe}$  under the  $G + GxE$  model are no longer significant under the  $G + GxE + Nx$  model. Consistent with this observation, we estimated a substantial contribution of noise heterogeneity to trait variation. While our results demonstrated the importance of integrating noise heterogeneity for a more reliable and accurate estimation of GxE

heritability, alternative methods—adjusting the phenotype values of individuals in different quantile bins of the environment variable separately as proposed in Di Scipio et al.<sup>17</sup>—can prove effective under moderate levels of noise heterogeneity.

After accounting for noise heterogeneity, we observe significant genome-wide  $h_{gxe}^2$  across more than a quarter of the trait-E pairs analyzed. Our finding has implications for understanding trait heritability by moving beyond the definition of narrow-sense heritability that only includes additive genetic effects. Based on our analyses, it is conceivable that approaches that can jointly model the hundreds of environmental variables measured in biobank-scale datasets will further increase estimates of  $h_{gxe}^2$ . Additionally, our recovery of additional  $h_{gxe}^2$  from low-frequency SNPs ( $0.1\% \leq \text{MAF} < 1\%$ ) point to traits where an understanding of GxE effects can benefit from whole-exome and whole-genome studies. Our analyses of common and low-frequency SNPs lead us to recommend that SNPs should be partitioned based on MAF and LD when estimating GxE heritability (while such partitioning does not qualitatively affect results for common SNPs). Further, our results point to traits where GxE has the potential to improve genome-wide polygenic scores (GPSs) of complex traits (since  $h_{gxe}^2$  quantifies the maximum predictive accuracy that is achievable by a linear predictor based on GxE effects). In the context of sex as an environmental variable, sex-specific GPS has been shown to provide improved accuracy over agnostic scores.<sup>34,39,55,56</sup> GxE has also been recently proposed as a possible explanation for why GPS may not generalize beyond the cohort on which these predictors were trained<sup>6</sup> so that modeling GxE in relevant traits could improve their transferability. Our finding that allelic effects for GxE increase with decreasing MAF and LD analogous to the relationship observed for additive allelic effects motivates an evolutionary understanding of these trends and can inform what we expect to learn from studies of rare genetic variation. Finally, our identification of sets of genes that are enriched for GxE can offer clues on trait-relevant tissues and pathways and has the potential to inform functional genomic studies.<sup>57,58</sup>

We discuss the limitations of our work as well as directions for future research. First, GENIE does not explicitly model G-E correlations.<sup>13</sup> While such correlations can lead to biases in estimates of GxE in the fixed-effect setting,<sup>59</sup> it has been shown that, in the polygenic setting, the GxE variance component estimates remain unbiased when G-E correlations are independent of the polygenic GxE effects.<sup>14</sup> Further, our simulations suggest that GENIE is robust in the presence of G-E correlations. Nevertheless, there are plausible settings, where such correlations can lead to false positive or biased estimates of GxE, e.g., where the phenotype directly affects the environmental variable. Developing scalable methods that are accurate in these settings is an important direction for future work. Second, estimates of GxE heritability are sensitive to the scale on which traits and environmental variables are

measured and how environmental variables are encoded. In this work, we analyze quantile-normalized traits (following prior studies) and encode discrete environmental variables using a univariate parameterization (either as a 0–1 vector for each environmental variable or as a standardized version). It might be preferable to work with traits measured on their original scale and to encode each level of discrete environmental variables by a separate 0–1 covariate (leading to  $k$  environmental covariates for a  $k$ -valued environmental variable). While such choices would necessarily be guided by domain knowledge and interpretability, GENIE supports easy-to-use and rapid exploration of the consequences of these choices and can aid in assessing the robustness of these choices (we have explored a limited space of these choices here). Third, the environmental variable relevant for GxE may not be measured directly or accurately, so the environmental variable that is measured in a dataset is best viewed as a proxy for the relevant latent environmental covariate. It is essential to acknowledge that the missingness patterns of phenotypes in biobanks frequently display structure that is more intricate than random missingness.<sup>60,61</sup> Consequently, removing individuals with missing data on Es can potentially affect GxE and other heritability estimates. One approach to tackle this complexity involves accurate imputation of missing data while mitigating the introduction of additional biases as observed in the mean imputation simulations (Figure S12). We view this as an important direction for future work. Fourth, the model underlying GENIE is not applicable to binary traits (either with or without ascertainment). GENIE can be extended to be applicable to binary traits (e.g., disease status) along the lines proposed in the context of additive<sup>62,63</sup> and GxE estimation.<sup>14</sup>

Apart from the constraints inherent to the GENIE model, we stress the need for cautious interpretations of the results of this study due to several limitations. While GENIE can model the impact of heterogeneous noise resulting from observed environmental variables by introducing NxG components, it is important to note that the heterogeneous noise may also arise due to non-observed environmental variables. Several recent works have tried to test for GxE when the environmental variables are not observed.<sup>10,64</sup> These issues along with the possibility of reverse causality, i.e., where the phenotype affects the environmental variable, warrant caution in any causal interpretation of our results (although it might be possible to overcome some of these limitations in specific analyses such as GxSex). Moreover, while the primary focus of our work is on the methodological aspects of GxE heritability estimation, our application of GENIE to medication-sensitive traits highlights the complexities arising in this setting that warrant care in interpreting the results. To explore these issues, we repeated our previous analyses after performing heuristic adjustments of phenotypes for relevant medications. Our additional analyses of GxE estimates on measurements adjusted for medication usage suggest that, while most of our results are robust to these issues

(e.g., GxE for systolic and diastolic blood pressure, GxStatin on HbA1c), some are less so (e.g., GxAge on LDL and cholesterol) (see [Note S4](#) for details). Finally, while analyses in this work were based on a cohort of self-identified white British individuals, it is valuable to investigate GxE effects using GENIE across a broader range of populations for stronger and more comprehensive results.

## Data and code availability

GENIE software is an open-source software freely available at <https://github.com/sriramlab/GENIE>. The software requires `g++`, `cmake`, and `make` to compile the `C++` code on a Linux machine. Please see the documentation in the GitHub repository for further information.

## Supplemental information

Supplemental information can be found online at <https://doi.org/10.1016/j.ajhg.2024.05.015>.

## Acknowledgments

This research was conducted using the UK Biobank Resource under application 331277. We thank the participants of UK Biobank for making this work possible. This work was funded by NIH grants R35GM125055 (A.P. and S.S.), HG006399 (S.S.), and NSF grant CAREER-1943497 (A.P. and S.S.).

The authors would like to thank Alkes Price and Arbel Harpak for their feedback on the manuscript. The authors would also like to acknowledge the stimulating discussions at the UCLA Computational Genomics Summer Institute (supported by NIH grants GM135043 and GM112625) and the 2018 Bertinoro workshop in Statistical and Computational Genomics that enabled this work.

## Declaration of interests

The authors declare no competing interests.

Received: September 20, 2023

Accepted: May 15, 2024

Published: June 11, 2024

## Web resources

GCTA (v1.94.1), <https://yanglab.westlake.edu.cn/software/gcta>

LDSC (v1.0.1), <https://github.com/bulik/ldsc>

LEMMA (v1.0.4), <https://github.com/mkerin/LEMMA>

MonsterLM (v0.1.1), <https://github.com/GMELab/MonsterLM>

PLINK (v1.90), <https://www.cog-genomics.org/plink>

## References

1. Yang, J., Loos, R.J., Powell, J.E., Medland, S.E., Speliotes, E.K., Chasman, D.I., Rose, L.M., Thorleifsson, G., Steinthorsdottir, V., Mägi, R., et al. (2012). FTO genotype is associated with phenotypic variability of body mass index. *Nature* 490, 267–272.
2. Gagneur, J., Stegle, O., Zhu, C., Jakob, P., Tekkedil, M.M., Aiyar, R.S., Schuon, A.-K., Pe'er, D., and Steinmetz, L.M. (2013). Genotype-environment interactions reveal causal pathways that mediate genetic effects on phenotype. *PLoS Genet.* 9, e1003803.
3. Virolainen, S.J., VonHandorf, A., Viel, K.C.M.F., Weirauch, M.T., and Kottyan, L.C. (2023). Gene-environment interactions and their impact on human health. *Genes Immun.* 24, 1–11.
4. Khoury, M.J., and Wagener, D.K. (1995). Epidemiological evaluation of the use of genetics to improve the predictive value of disease risk factors. *Am. J. Hum. Genet.* 56, 835–844.
5. Robinson, M.R., English, G., Moser, G., Lloyd-Jones, L.R., Triplett, M.A., Zhu, Z., Nolte, I.M., van Vliet-Ostapchouk, J.V., Snieder, H., et al.; LifeLines Cohort Study (2017). Genotype-covariate interaction effects and the heritability of adult body mass index. *Nat. Genet.* 49, 1174–1181.
6. Mostafavi, H., Harpak, A., Agarwal, I., Conley, D., Pritchard, J.K., and Przeworski, M. (2020). Variable prediction accuracy of polygenic scores within an ancestry group. *Elife* 9, e48376.
7. Laville, V., Majarian, T., Sung, Y.J., Schwander, K., Feitosa, M.F., Chasman, D.I., Bentley, A.R., Rotimi, C.N., Cupples, L.A., de Vries, P.S., et al. (2022). Gene-lifestyle interactions in the genomics of human complex traits. *Eur. J. Hum. Genet.* 30, 730–739.
8. Bycroft, C., Freeman, C., Petkova, D., Band, G., Elliott, L.T., Sharp, K., Motyer, A., Vukcevic, D., Delaneau, O., O'Connell, J., et al. (2018). The UK Biobank resource with deep phenotyping and genomic data. *Nature* 562, 203–209.
9. Moore, R., Casale, F.P., Jan Bonder, M., Horta, D., BIOS Consortium, Franke, L., Barroso, I., and Stegle, O. (2019). A linear mixed-model approach to study multivariate gene-environment interactions. *Nat. Genet.* 51, 180–186.
10. Young, A.I., Wauthier, F.L., and Donnelly, P. (2018). Identifying loci affecting trait variability and detecting interactions in genome-wide association studies. *Nat. Genet.* 50, 1608–1614.
11. Yang, J., Lee, S.H., Goddard, M.E., and Visscher, P.M. (2011). GCTA: a tool for genome-wide complex trait analysis. *Am. J. Hum. Genet.* 88, 76–82.
12. Lee, S.H., and van der Werf, J.H.J. (2016). MTG2: an efficient algorithm for multivariate linear mixed model analysis based on genomic information. *Bioinformatics* 32, 1420–1422.
13. Ni, G., Van Der Werf, J., Zhou, X., Hyppönen, E., Wray, N.R., and Lee, S.H. (2019). Genotype-covariate correlation and interaction disentangled by a whole-genome multivariate reaction norm model. *Nat. Commun.* 10, 2239.
14. Dahl, A., Nguyen, K., Cai, N., Gandal, M.J., Flint, J., and Zaitlen, N. (2020). A robust method uncovers significant context-specific heritability in diverse complex traits. *Am. J. Hum. Genet.* 106, 71–91.
15. Kerin, M., and Marchini, J. (2020a). Inferring Gene-by-Environment Interactions with a Bayesian Whole-Genome Regression Model. *Am. J. Hum. Genet.* 107, 698–713.
16. Kerin, M., and Marchini, J. (2020b). A non-linear regression method for estimation of gene-environment heritability. *Bioinformatics* 36, 5632–5639.
17. Di Scipio, M., Khan, M., Mao, S., Chong, M., Judge, C., Pathan, N., Perrot, N., Nelson, W., Lali, R., Di, S., et al. (2023). A versatile, fast and unbiased method for estimation of gene-by-environment interaction effects on biobank-scale datasets. *Nat. Commun.* 14, 5196.
18. Finucane, H.K., Reshef, Y.A., Anttila, V., Slowikowski, K., Guisev, A., Byrnes, A., Gazal, S., Loh, P.-R., Lareau, C., Shores, H., et al. (2015). Partitioning multiethnic and admixed population genetic structure. *Nat. Genet.* 47, 1287–1295.



- N., et al. (2018). Heritability enrichment of specifically expressed genes identifies disease-relevant tissues and cell types. *Nat. Genet.* *50*, 621–629.
19. Hutchinson, M. (1989). A stochastic estimator of the trace of the influence matrix for laplacian smoothing splines. *Commun. Stat. Simulat. Comput.* *18*, 1059–1076.
  20. Liberty, E., and Zucker, S.W. (2009). The mailman algorithm: A note on matrix–vector multiplication. *Inf. Process. Lett.* *109*, 179–182.
  21. Pazokitoroudi, A., Wu, Y., Burch, K.S., Hou, K., Zhou, A., Pasaniuc, B., and Sankararaman, S. (2020). Efficient variance components analysis across millions of genomes. *Nat. Commun.* *11*, 4020.
  22. Sudlow, C., Gallacher, J., Allen, N., Beral, V., Burton, P., Danesh, J., Downey, P., Elliott, P., Green, J., Landray, M., et al. (2015). UK Biobank: An Open Access Resource for Identifying the Causes of a Wide Range of Complex Diseases of Middle and Old Age. *PLoS Med.* *12*, e1001779.
  23. Sul, J.H., Bilow, M., Yang, W.-Y., Kostem, E., Furlotte, N., He, D., and Eskin, E. (2016). Accounting for population structure in gene-by-environment interactions in genome-wide association studies using mixed models. *PLoS Genet.* *12*, e1005849.
  24. Sinnott-Armstrong, N., Tanigawa, Y., Amar, D., Mars, N., Benner, C., Aguirre, M., Venkataraman, G.R., Wainberg, M., Ollila, H.M., Kiiskinen, T., et al. (2021). Genetics of 35 blood and urine biomarkers in the UK Biobank. *Nat. Genet.* *53*, 185–194.
  25. Pazokitoroudi, A., Chiu, A.M., Burch, K.S., Pasaniuc, B., and Sankararaman, S. (2021). Quantifying the contribution of dominance deviation effects to complex trait variation in biobank-scale data. *Am. J. Hum. Genet.* *108*, 799–808.
  26. Wei, X., Robles, C.R., Pazokitoroudi, A., Ganna, A., Gusev, A., Durvasula, A., Gazal, S., Loh, P.-R., Reich, D., and Sankararaman, S. (2023). The lingering effects of Neanderthal introgression on human complex traits. *Elife* *12*, e80757.
  27. Warren, H.R., Evangelou, E., Cabrera, C.P., Gao, H., Ren, M., Mifsud, B., Ntalla, I., Surendran, P., Liu, C., Cook, J.P., et al. (2017). Genome-wide association analysis identifies novel blood pressure loci and offers biological insights into cardiovascular risk. *Nat. Genet.* *49*, 403–415.
  28. Finucane, H.K., Bulik-Sullivan, B., Gusev, A., Trynka, G., Reshef, Y., Loh, P.-R., Anttila, V., Xu, H., Zang, C., Farh, K., et al. (2015a). Partitioning heritability by functional annotation using genome-wide association summary statistics. *Nat. Genet.* *47*, 1228–1235.
  29. Hou, K., Burch, K.S., Majumdar, A., Shi, H., Mancuso, N., Wu, Y., Sankararaman, S., and Pasaniuc, B. (2019). Accurate estimation of SNP-heritability from biobank-scale data irrespective of genetic architecture. *Nat. Genet.* *51*, 1244–1251.
  30. Speed, D., and Balding, D.J. (2019). Sumher better estimates the SNP heritability of complex traits from summary statistics. *Nat. Genet.* *51*, 277–284.
  31. Bulik-Sullivan, B.K., Loh, P.-R., Finucane, H.K., Ripke, S., Yang, J., Schizophrenia Working Group of the Psychiatric Genomics Consortium, Patterson, N., Daly, M.J., Price, A.L., Neale, B.M., et al. (2015). LD Score regression distinguishes confounding from polygenicity in genome-wide association studies. *Nat. Genet.* *47*, 291–295.
  32. Sinnott-Armstrong, N., Naqvi, S., Rivas, M., and Pritchard, J.K. (2021b). GWAS of three molecular traits highlights core genes and pathways alongside a highly polygenic background. *Elife* *10*, e58615.
  33. Ruth, K.S., Day, F.R., Tyrrell, J., Thompson, D.J., Wood, A.R., Mahajan, A., Beaumont, R.N., Wittmans, L., Martin, S., Busch, A.S., et al. (2020). Using human genetics to understand the disease impacts of testosterone in men and women. *Nat. Med.* *26*, 252–258.
  34. Zhu, C., Ming, M.J., Cole, J.M., Edge, M.D., Kirkpatrick, M., and Harpak, A. (2023). Amplification is the primary mode of gene-by-sex interaction in complex human traits. *Cell Genom.* *3*, 100297.
  35. Randall, J.C., Winkler, T.W., Kutalik, Z., Berndt, S.I., Jackson, A.U., Monda, K.L., Kilpeläinen, T.O., Esko, T., Mägi, R., Li, S., et al. (2013). Sex-stratified genome-wide association studies including 270,000 individuals show sexual dimorphism in genetic loci for anthropometric traits. *PLoS Genet.* *9*, e1003500.
  36. Winkler, T.W., Justice, A.E., Graff, M., Barata, L., Feitosa, M.F., Chu, S., Czajkowski, J., Esko, T., Fall, T., Kilpeläinen, T.O., et al. (2015). The influence of age and sex on genetic associations with adult body size and shape: a large-scale genome-wide interaction study. *PLoS Genet.* *11*, e1005378.
  37. Pulit, S.L., Stoneman, C., Morris, A.P., Wood, A.R., Glastonbury, C.A., Tyrrell, J., Yengo, L., Ferreira, T., Marouli, E., Ji, Y., et al. (2019). Meta-analysis of genome-wide association studies for body fat distribution in 694 649 individuals of European ancestry. *Hum. Mol. Genet.* *28*, 166–174.
  38. Rask-Andersen, M., Karlsson, T., Ek, W.E., and Johansson, Å. (2019). Genome-wide association study of body fat distribution identifies adiposity loci and sex-specific genetic effects. *Nat. Commun.* *10*, 339.
  39. Bernabeu, E., Canela-Xandri, O., Rawlik, K., Talenti, A., Prendergast, J., and Tenesa, A. (2021). Sex differences in genetic architecture in the UK Biobank. *Nat. Genet.* *53*, 1283–1289.
  40. Döring, A., Gieger, C., Mehta, D., Gohlke, H., Prokisch, H., Coassin, S., Fischer, G., Henke, K., Klopp, N., Kronenberg, F., et al. (2008). SLC2A9 influences uric acid concentrations with pronounced sex-specific effects. *Nat. Genet.* *40*, 430–436.
  41. Kolz, M., Johnson, T., Sanna, S., Teumer, A., Vitart, V., Perola, M., Mangino, M., Albrecht, E., Wallace, C., Farrall, M., et al. (2009). Meta-analysis of 28,141 individuals identifies common variants within five new loci that influence uric acid concentrations. *PLoS Genet.* *5*, e1000504.
  42. Shirts, B.H., Hasstedt, S.J., Hopkins, P.N., and Hunt, S.C. (2011). Evaluation of the gene–age interactions in HDL cholesterol, LDL cholesterol, and triglyceride levels: the impact of the SORT1 polymorphism on ldl cholesterol levels is age dependent. *Atherosclerosis* *217*, 139–141.
  43. Simino, J., Shi, G., Bis, J.C., Chasman, D.I., Ehret, G.B., Gu, X., Guo, X., Hwang, S.-J., Sijbrands, E., Smith, A.V., et al. (2014). Gene-age interactions in blood pressure regulation: a large-scale investigation with the CHARGE, Global BPgen, and ICBP consortia. *Am. J. Hum. Genet.* *95*, 24–38.
  44. Sattar, N., Preiss, D., Murray, H.M., Welsh, P., Buckley, B.M., de Craen, A.J.M., Seshasai, S.R.K., McMurray, J.J., Freeman, D.J., Jukema, J.W., et al. (2010). Statins and risk of incident diabetes: a collaborative meta-analysis of randomised statin trials. *Lancet* *375*, 735–742.
  45. Speed, D., Hemani, G., Johnson, M.R., and Balding, D.J. (2012). Improved heritability estimation from genome-wide snps. *Am. J. Hum. Genet.* *91*, 1011–1021.
  46. Evans, L.M., Tahmasbi, R., Vrieze, S.I., Abecasis, G.R., Das, S., Gazal, S., Bjelland, D.W., de Candia, T.R., Haplotype Reference Consortium, and Goddard, M.E., et al. (2018). Comparison of methods that use whole genome data to estimate the

- heritability and genetic architecture of complex traits. *Nat. Genet.* *50*, 737–745.
47. Speed, D., Cai, N., UCLEB Consortium, Johnson, M.R., Nejentsev, S., Balding, D.J., et al. (2017). Reevaluation of SNP heritability in complex human traits. *Nat. Genet.* *49*, 986–992.
  48. Gazal, S., Loh, P.-R., Finucane, H.K., Ganna, A., Schoech, A., Sunyaev, S., and Price, A.L. (2018). Functional architecture of low-frequency variants highlights strength of negative selection across coding and non-coding annotations. *Nat. Genet.* *50*, 1600–1607.
  49. Gazal, S., Finucane, H.K., Furlotte, N.A., Loh, P.-R., Palamara, P.F., Liu, X., Schoech, A., Bulik-Sullivan, B., Neale, B.M., Gusev, A., and Price, A.L. (2017). Linkage disequilibrium-dependent architecture of human complex traits shows action of negative selection. *Nat. Genet.* *49*, 1421–1427.
  50. Schoech, A.P., Jordan, D.M., Loh, P.-R., Gazal, S., O'Connor, L.J., Balick, D.J., Palamara, P.F., Finucane, H.K., Sunyaev, S.R., and Price, A.L. (2019). Quantification of frequency-dependent genetic architectures in 25 UK Biobank traits reveals action of negative selection. *Nat. Commun.* *10*, 790.
  51. Zeng, J., De Vlaming, R., Wu, Y., Robinson, M.R., Lloyd-Jones, L.R., Yengo, L., Yap, C.X., Xue, A., Sidorenko, J., McRae, A.F., et al. (2018). Signatures of negative selection in the genetic architecture of human complex traits. *Nat. Genet.* *50*, 746–753.
  52. Shungin, D., Winkler, T.W., Croteau-Chonka, D.C., Ferreira, T., Locke, A.E., Mägi, R., Strawbridge, R.J., Pers, T.H., Fischer, K., Justice, A.E., et al. (2015). New genetic loci link adipose and insulin biology to body fat distribution. *Nature* *518*, 187–196.
  53. Small, K.S., Todorčević, M., Civelek, M., El-Sayed Moustafa, J.S., Wang, X., Simon, M.M., Fernandez-Tajes, J., Mahajan, A., Horikoshi, M., Hugill, A., et al. (2018). Regulatory variants at *KLF14* influence type 2 diabetes risk via a female-specific effect on adipocyte size and body composition. *Nat. Genet.* *50*, 572–580.
  54. Stancu, C., and Sima, A. (2001). Statins: mechanism of action and effects. *J. Cell Mol. Med.* *5*, 378–387.
  55. Rawlik, K., Canela-Xandri, O., and Tenesa, A. (2016). Evidence for sex-specific genetic architectures across a spectrum of human complex traits. *Genome Biol.* *17*, 166.
  56. Flynn, E., Tanigawa, Y., Rodriguez, F., Altman, R.B., Sinnott-Armstrong, N., and Rivas, M.A. (2021). Sex-specific genetic effects across biomarkers. *Eur. J. Hum. Genet.* *29*, 154–163.
  57. Dixit, A., Parnas, O., Li, B., Chen, J., Fulco, C.P., Jerby-Arnon, L., Marjanovic, N.D., Dionne, D., Burks, T., Raychowdhury, R., et al. (2016). Perturb-Seq: dissecting molecular circuits with scalable single-cell RNA profiling of pooled genetic screens. *Cell* *167*, 1853–1866.e17.
  58. Findley, A.S., Monziani, A., Richards, A.L., Rhodes, K., Ward, M.C., Kalita, C.A., Alazizi, A., Pazokitoroudi, A., Sankararaman, S., Wen, X., et al. (2021). Functional dynamic genetic effects on gene regulation are specific to particular cell types and environmental conditions. *Elife* *10*, e67077.
  59. Dudbridge, F., and Fletcher, O. (2014). Gene-environment dependence creates spurious gene-environment interaction. *Am. J. Hum. Genet.* *95*, 301–307.
  60. Mitra, R., McGough, S.F., Chakraborti, T., Holmes, C., Copping, R., Hagenbuch, N., Biedermann, S., Noonan, J., Lehmann, B., Shenvi, A., et al. (2023). Learning from data with Structured Missingness. *Nat. Mach. Intell.* *5*, 13–23.
  61. An, U., Pazokitoroudi, A., Alvarez, M., Huang, L., Bacanu, S., Schork, A.J., Kendler, K., Pajukanta, P., Flint, J., Zaitlen, N., et al. (2023). Deep learning-based phenotype imputation on population-scale Biobank data increases genetic discoveries. *Nat. Genet.* *55*, 2269–2276.
  62. Golan, D., Lander, E.S., and Rosset, S. (2014). Measuring missing heritability: inferring the contribution of common variants. *Proc. Natl. Acad. Sci. USA* *111*, E5272–E5281.
  63. Weissbrod, O., Flint, J., and Rosset, S. (2018). Estimating snp-based heritability and genetic correlation in case-control studies directly and with summary statistics. *Am. J. Hum. Genet.* *103*, 89–99.
  64. Marderstein, A.R., Davenport, E.R., Kulm, S., Van Hout, C.V., Elemento, O., and Clark, A.G. (2021). Leveraging phenotypic variability to identify genetic interactions in human phenotypes. *Am. J. Hum. Genet.* *108*, 49–67.

**The American Journal of Human Genetics, Volume 111**

**Supplemental information**

**A scalable and robust variance components method  
reveals insights into the architecture of  
gene-environment interactions underlying complex traits**

**Ali Pazokitoroudi, Zhengtong Liu, Andrew Dahl, Noah Zaitlen, Saharon Rosset, and Sriram Sankararaman**

# Supplemental Notes

## Note S1

We can extend each of our models to include covariates as follows:

$$\mathbf{y} = \mathbf{W}\boldsymbol{\alpha} + \sum_k \mathbf{Z}_k \boldsymbol{\beta}_k + \boldsymbol{\epsilon} \quad (1)$$

Here  $\mathbf{W}$  is a  $N \times C$  matrix of covariates while  $\boldsymbol{\alpha}$  is a vector of fixed effects of length  $C$ . Matrix  $\mathbf{Z}_k$  can represent genotype or GxE matrices. In this setting, we need to solve the following normal equations to estimate the variance components.

$$\begin{bmatrix} \mathbf{T} & \mathbf{b} \\ \mathbf{b}^T & N - C \end{bmatrix} \begin{bmatrix} \sigma_1^2 \\ \vdots \\ \sigma_K^2 \\ \sigma_e^2 \end{bmatrix} = \begin{bmatrix} \mathbf{c} \\ \mathbf{y}^T \mathbf{V} \mathbf{y} \end{bmatrix} \quad (2)$$

Here  $\mathbf{V} = \mathbf{I}_N - \mathbf{W}(\mathbf{W}^T \mathbf{W})^{-1} \mathbf{W}^T$  and  $\mathbf{T}$  is a  $K \times K$  matrix where  $T_{k,l} = \text{tr}(\mathbf{K}_k \mathbf{V} \mathbf{K}_l \mathbf{V})$ , and  $\mathbf{b}$  is a vector of length  $K$  where  $b_k = \text{tr}(\mathbf{V} \mathbf{K}_k)$ , and  $\mathbf{c}$  is a vector of length  $K$  where  $c_k = \mathbf{y}^T \mathbf{V} \mathbf{K}_k \mathbf{V} \mathbf{y}$ ,  $\mathbf{K}_k = \frac{\mathbf{Z}_k \mathbf{Z}_k^T}{M}$  where  $M$  is the number of column in  $\mathbf{Z}_k$ . Commonly, the number of covariates  $C$  is small (tens to hundreds) so including covariates does not significantly affect the computational cost. The cost of computing the elements of the normal equations 2 includes the cost of inverting  $\mathbf{W}^T \mathbf{W}$  which is a  $C \times C$  matrix and multiplying  $\mathbf{W}$  by a real-valued vector of length  $N$  can be computed in  $\mathcal{O}(C^3 + NC)$ .

## Note S2

To simulate MAF and LD-dependent architectures, we simulated phenotypes from genotypes using the following model that extends prior models of additive genetic architecture<sup>1,2</sup> to include GxE effects:

$$\begin{aligned} \sigma_{g,m}^2 &= S c_m w_m^b [f_m (1 - f_m)]^a \\ (\boldsymbol{\beta}_1, \boldsymbol{\beta}_2, \dots, \boldsymbol{\beta}_m)^T &\sim \mathcal{N}(\mathbf{0}, \text{diag}(\sigma_{g,1}^2, \sigma_{g,2}^2, \dots, \sigma_{g,m}^2)) \\ \sigma_{gxe,m}^2 &= S' c'_m w_m^b [f_m (1 - f_m)]^a \\ (\boldsymbol{\alpha}_1, \boldsymbol{\alpha}_2, \dots, \boldsymbol{\alpha}_m)^T &\sim \mathcal{N}(\mathbf{0}, \text{diag}(\sigma_{gxe,1}^2, \sigma_{gxe,2}^2, \dots, \sigma_{gxe,m}^2)) \\ \mathbf{y} | \boldsymbol{\beta}, \boldsymbol{\alpha} &\sim \mathcal{N}(\mathbf{X}\boldsymbol{\beta} + (\mathbf{X} \odot \mathbf{E})\boldsymbol{\alpha}, (1 - h_g^2 - h_{gxe}^2 - h_{nxe}^2) \mathbf{I}_N + h_{nxe}^2 (\mathbf{I}_N \odot \mathbf{E})) \end{aligned} \quad (3)$$

where  $h_g^2, h_{gxe}^2, h_{nxe}^2 \in [0, 1]$ ,  $a \in \{0, 0.75\}$ ,  $b \in \{0, 1\}$ . Here  $S$  and  $S'$  are normalizing constants chosen so that  $\sum_{m=1}^M \sigma_{g,m}^2 = h_g^2$ ,  $\sum_{m=1}^M \sigma_{gxe,m}^2 = h_{gxe}^2$ . Additive and GxE effect sizes are denoted by  $\boldsymbol{\beta}$  and  $\boldsymbol{\alpha}$  respectively.  $f_m$  and  $w_m$  are the minor allele frequency and LD score of  $m^{\text{th}}$  SNP respectively. In this model,  $c_m, c'_m \in \{0, 1\}$  are indicator variables for the causal status of SNP  $m$  ( $c_m = 1$  and  $c'_m = 1$  for all SNPs). The LD score of a SNP is defined to be the sum of the squared correlation of the SNP with all other SNPs that lie within a specific distance. Setting  $a = 0, b = 0$  for additive effects results in the GCTA model where the per-standardized genotypic effect sizes at a SNP do not vary with MAF or LD score<sup>3,4</sup> while setting  $a = 0.75, b = 1$  results in the LDAK model<sup>5</sup>. Our simulations assume that the GxE effects follow the same coupling as the additive effects. We used phenotypes from  $N = 40,000$  individuals genotyped at  $M = 454,207$  SNPs on the UKB array.

## Note S3

We described simulation details of several scenarios in the section **Robustness of GENIE in simulations**. To simulate Y correlated with E, we first generated  $\mathbf{y}' = \mathbf{X}\boldsymbol{\beta} + (\mathbf{X} \odot \mathbf{E})\boldsymbol{\alpha} + (\mathbf{I}_N \odot \mathbf{E})\boldsymbol{\delta} + \boldsymbol{\epsilon}$  as in the GENIE model and then let  $\mathbf{y} = \frac{r}{1-r^2}\mathbf{E} + \mathbf{y}'$  be the simulated phenotype, where  $r$  is the simulated correlation. Since the environment variables are also included in the covariates as a fixed effect, we expected that the correlation between Y and E would not bias the estimates. The heritable E was simulated as  $\mathbf{E} = \mathbf{X}\boldsymbol{\beta} + \boldsymbol{\epsilon}$ , where  $\boldsymbol{\beta} \sim \mathcal{N}(\mathbf{0}, \sigma_g^2 \mathbf{I})$  and  $\boldsymbol{\epsilon} \sim \mathcal{N}(\mathbf{0}, (1 - \sigma_g^2)\mathbf{I})$ , with  $\sigma_g^2$  denoting the variance component associated with additive genetic effects, and  $M$  the number of SNPs. We simulated the collider bias scenario: the phenotypes were simulated to be correlated with a heritable environmental variable through an unobserved confounder<sup>6</sup>. Finally, we drew the environment noise component ( $\boldsymbol{\epsilon}$  in the model) from the Student's  $t$ -distribution with a degree of freedom = 4 to simulate the heavy-tailed noise.

## Note S4

In our additional investigation of GxE heritability of phenotypes likely affected by medication, we repeated our previous analysis using GENIE after performing heuristic adjustments of SBP, DBP<sup>7</sup>, LDL, and cholesterol<sup>8</sup> for relevant medication usage. Our results were broadly consistent with and without the heuristic adjustments though there are notable exceptions. Specifically,  $h_{gxe}^2$  estimates for all four exposures remained significant using the adjusted SBP/DBP values (Figure S37) while  $h_{gxe}^2$  estimates for LDL and cholesterol were about the same for smoking, sex, and statin usage. However,  $h_{gxAge}^2$  estimates decreased substantially after the adjustment for statin although the estimates for cholesterol remained statistically significant (Figure S38). The differences in  $h_{gxAge}^2$  estimates for cholesterol also appeared in the downstream tissue-specific enrichment analysis. While the additive genetic effects were concordant with previous results,  $h_{gxAge}^2$  estimates were weakly correlated after the adjustment (Figure S39, S40). After statin adjustment, we found that none of the tissue-specific gene sets were enriched for  $h_{gxAge}^2$  at FDR < 0.1 (consistent with the attenuation of the genome-wide estimates). To directly account for the effects of statin usage on baseline LDL/cholesterol levels, we also estimated  $h_{gxStatin}^2$  for HbA1c while also including GxLDL and GxTC in the model (with these cholesterol traits treated as environment exposures). We observed that  $h_{gxStatin}^2$  estimates remained significant and consistent with estimates from our previous analyses. Further, there was no substantial difference in the total  $h_{gxe}^2$  estimates across the three exposures (Figure S41).



## Supplemental Figures

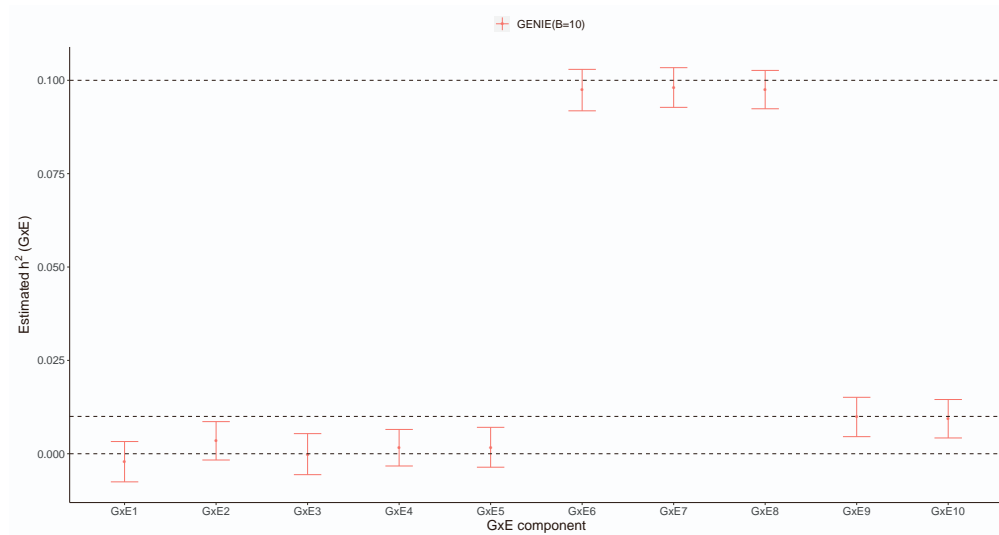


Figure S1: **Accuracy of GENIE when applied to multiple environmental variables.** We evaluated  $h_{gxe}^2$  estimates of GENIE for different values of  $\sigma_{gxe}^2$ . We simulated phenotypes with 10 environmental variables where  $\sigma_g^2 = 0.2$ ,  $\sigma_{ge1}^2 = \sigma_{ge2}^2 = \sigma_{ge3}^2 = \sigma_{ge4}^2 = \sigma_{ge5}^2 = 0$ ,  $\sigma_{ge6}^2 = \sigma_{ge7}^2 = \sigma_{ge8}^2 = 0.10$  and  $\sigma_{ge9}^2 = \sigma_{ge10}^2 = 0.01$ . Points and error bars represent the mean and  $\pm 2$  SE. Mean and SE are computed from 100 replicates. Here  $B$  is the number of random vectors used by GENIE with  $B = 10$  the value that we use as default (we reported values of means, SEs, and  $p$ -values of a test of the null hypothesis of no bias in the estimates of variance components in Table S1).

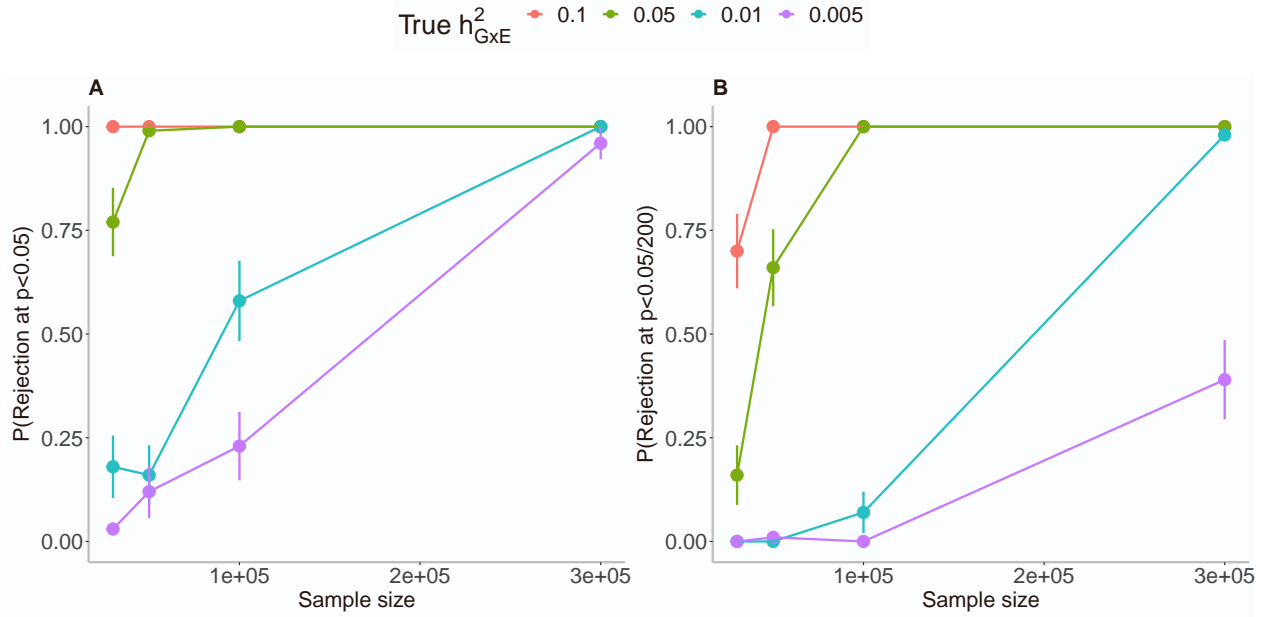


Figure S2: **The power of GENIE as a function of sample size in the absence of noise heterogeneity.** The power of GENIE under different GxE heritability as a function of sample size in the absence of noise heterogeneity at the significance level of (A) 0.05 and (B) 0.05/200. We evaluated the power of GENIE to detect GxE heritability across 0.005, 0.01, 0.05, and 0.1 on 100 simulated phenotypes. The phenotypes were simulated with varying GxE effects on  $M = 454,207$  SNPs and  $N = 30K, 50K, 100K,$  or  $290K$  individuals. The additive genetic heritability was fixed to be 0.25 across all simulations. The power calculated as  $P(\text{Rejection at } p < t)$  for  $t \in \{0.05, 0.05/200\}$  along with the 95% binomial confidence interval using the normal approximation was reported for each simulation.

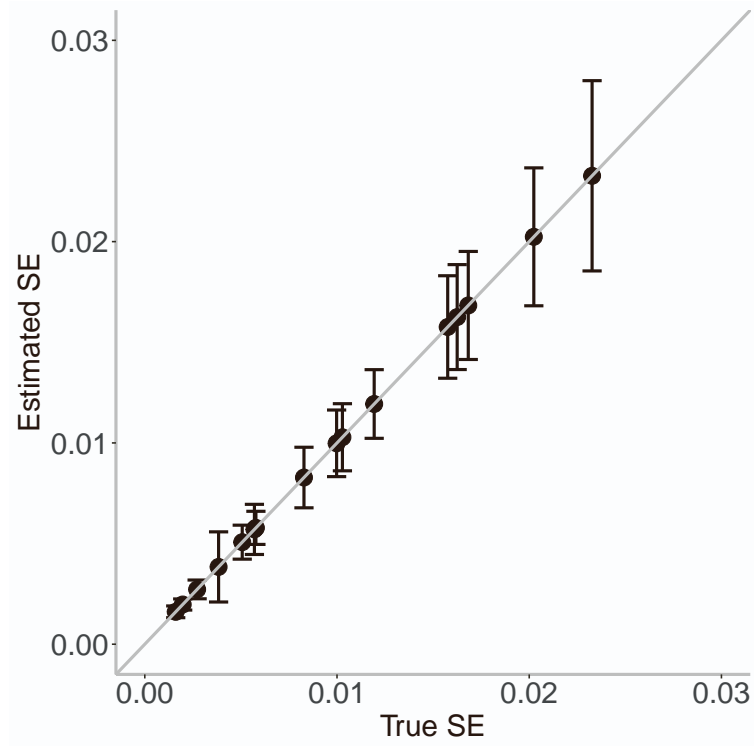


Figure S3: **Comparison between the estimated standard errors with the true standard errors for GxE heritability estimates in simulations.** Comparison of the estimated SEs using the block jackknife method against the true SEs of the point estimates for varying magnitudes of sample sizes under different true GxE heritability levels. The sample size ranged across 30K, 50K, 100K, and 290K, and true GxE heritability varied across 0.005, 0.01, 0.05, and 0.1. The average of estimated SE with 2 standard errors was shown, and the true SE was calculated based on the GxE heritability point estimates across 100 replicates in each simulation.

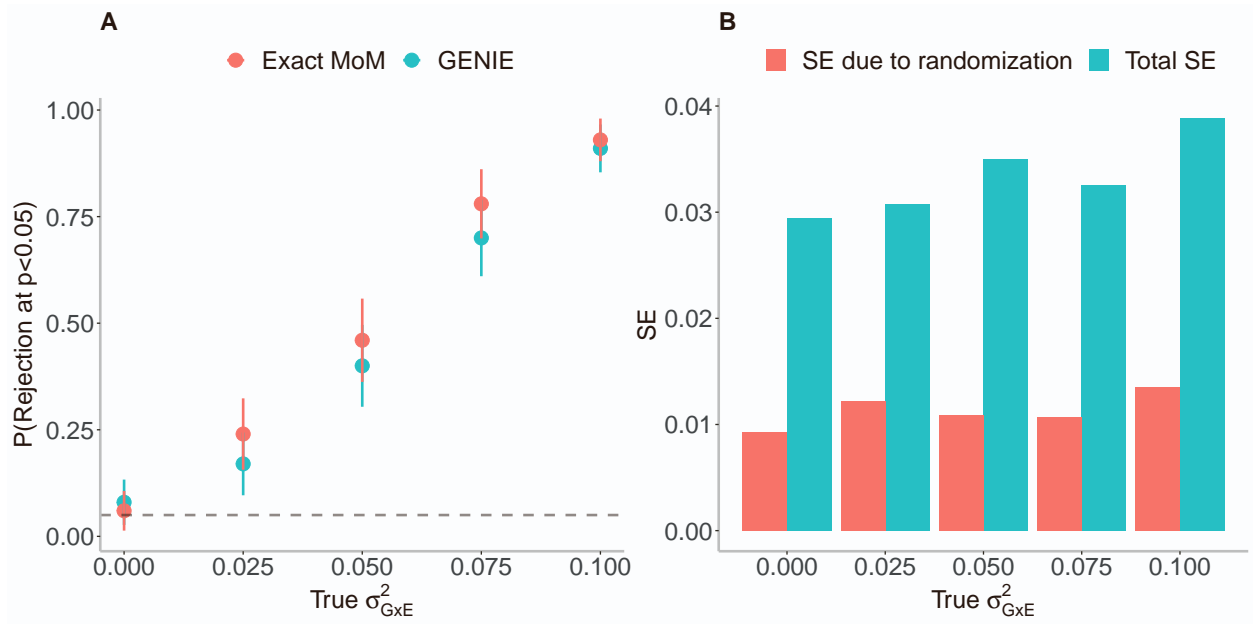


Figure S4: **Investigation of the power decrease of GENIE due to randomization on small-scale datasets in simulations.** (A) Comparison of the power and false positive rate (FPR) between exact MoM (as implemented in GCTA-HE) and GENIE. The FPR/Power is defined as the fraction of rejections of the null:  $\sigma_{GxE}^2 = 0$  at  $p < 0.05$ . The error bars correspond to the estimated 95% CI of the rejection rate. (B) Comparison of total SE and the SE due to randomization in simulations with nonzero  $\sigma_{GxE}^2$ . The total SE was calculated as the standard deviation of estimated GxE heritability over 100 replicates while the SE due to randomization was derived as the standard deviation of estimated GxE over 100 runs on a specific replicate.

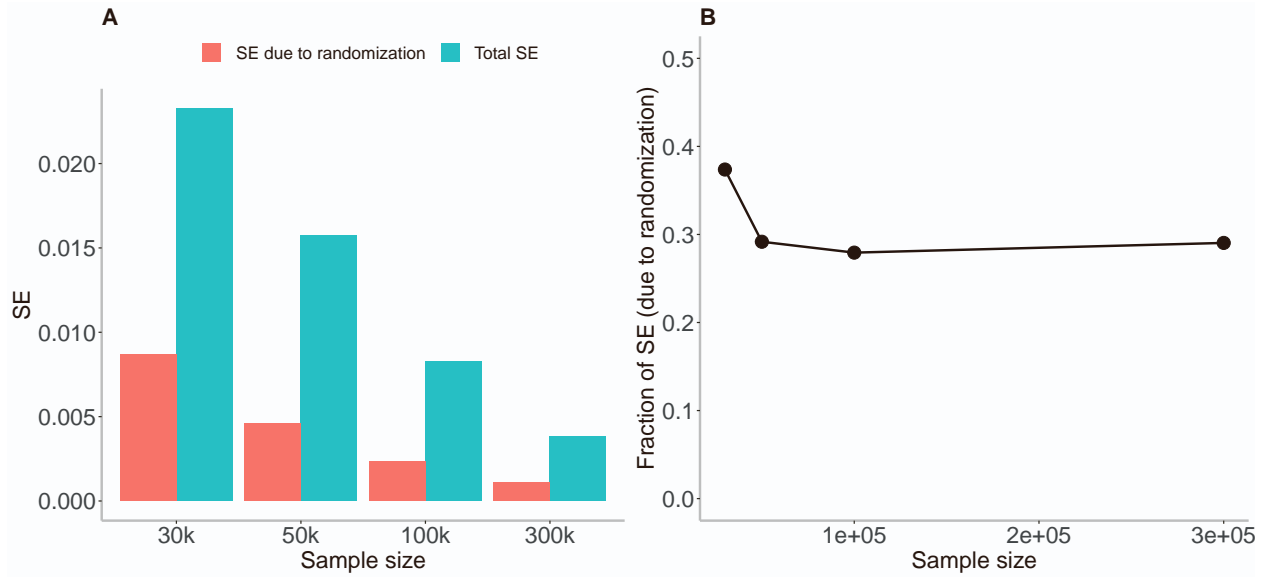


Figure S5: **Contribution of randomization to the standard error of GxE estimates.** (A) The mean of SEs due to randomization and total SE and (B) the fraction of SE due to randomization across different sample sizes. The SE due to randomization was calculated as the mean of SEs over 100 runs with different random seeds on a specific replicate, and the total SE was the true SE calculated over 100 replicates. The fraction of SE due to randomization is around 30% to 40% across different sample sizes.



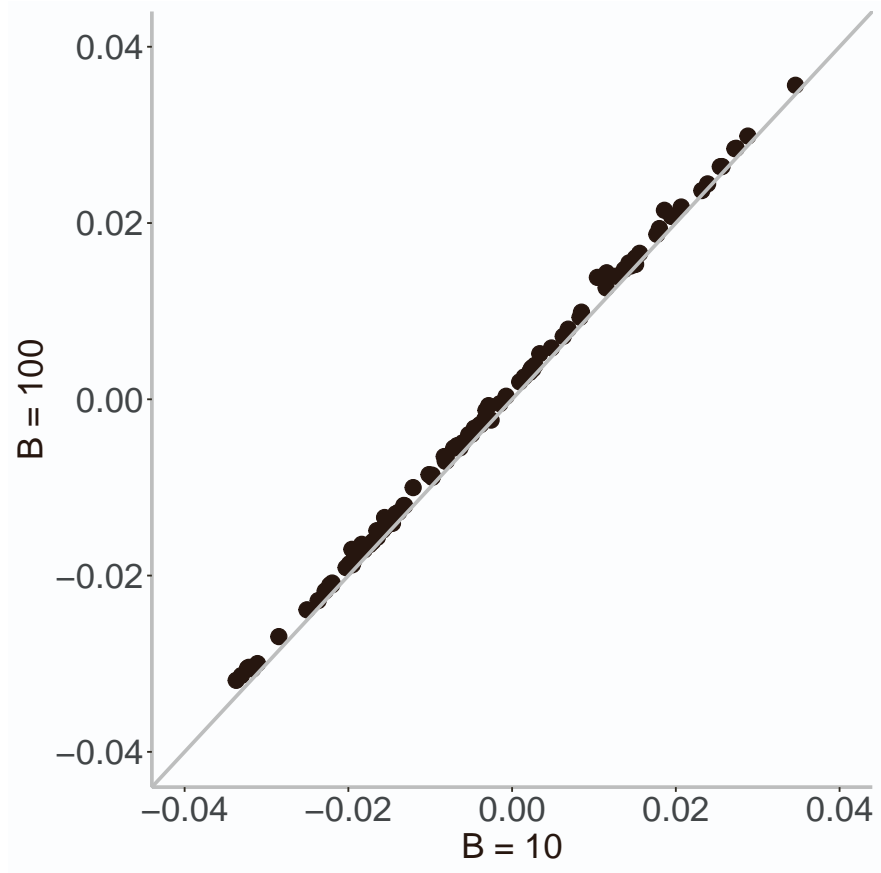


Figure S6: **Comparison of  $h_{gxe}^2$  estimates with  $B = 10$  and  $B = 100$ .** We simulated phenotypes from  $M = 60,000$  array SNPs and  $N = 10,000$  individuals where  $h_g^2 = 0.1$ ,  $h_{gxe}^2 = 0$  and the causal ratio is 10% .

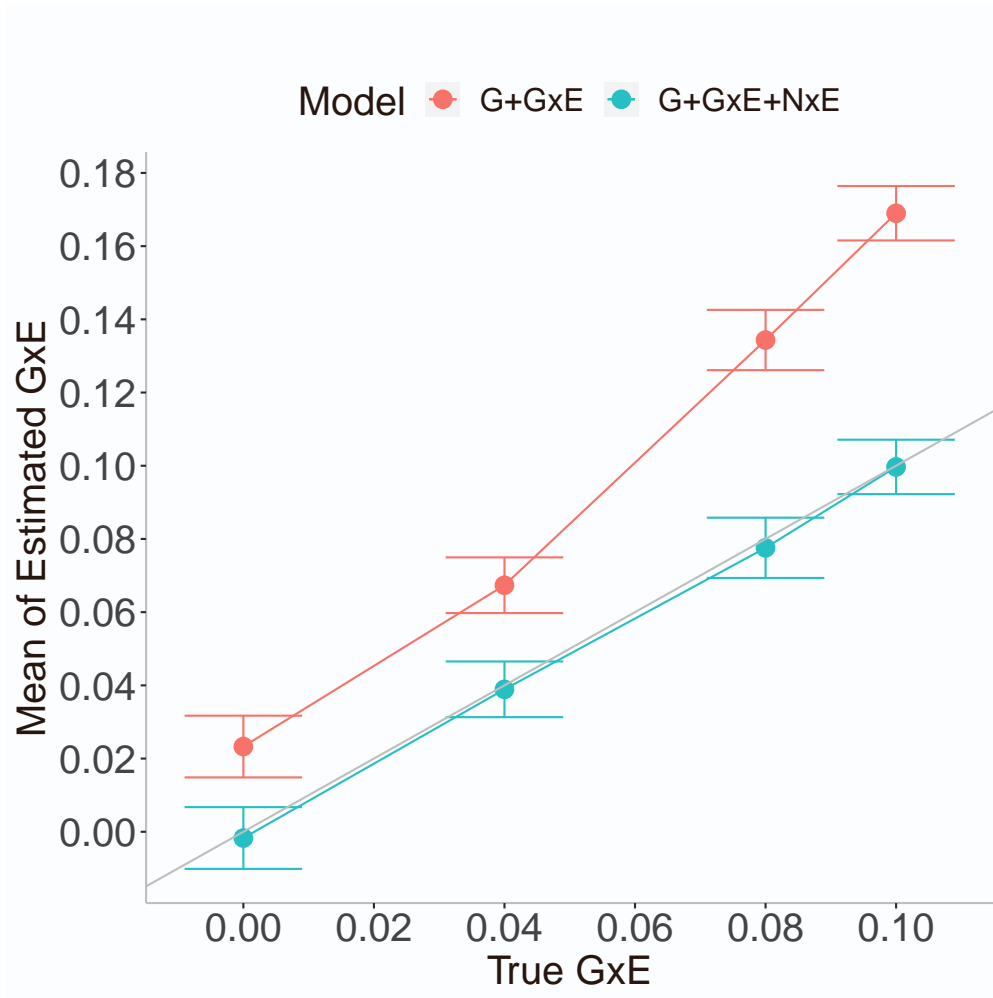


Figure S7: **Effect of noise heterogeneity (NxE) on the accuracy of estimates of GxE heritability in simulations.** Comparison of GxE heritability estimates from GENIE under a G+GxE model to those from a G+GxE+NxE model. Model G+GxE refers to a model with additive and gene-by-environment interaction components. Model G+GxE+NxE refers to a model with additive, gene-by-environment interaction, and noise heterogeneity (noise-by-environment interaction) components. We simulated phenotypes with NxE effects and GxE effects across  $N = 291,273$  individuals genotyped at  $M = 454,207$  SNPs. The  $x$ -axis and  $y$ -axis correspond to the true GxE and the mean of the estimated GxE (from 100 replicates), respectively. Points and error bars represent the mean and  $\pm$  SE, respectively.

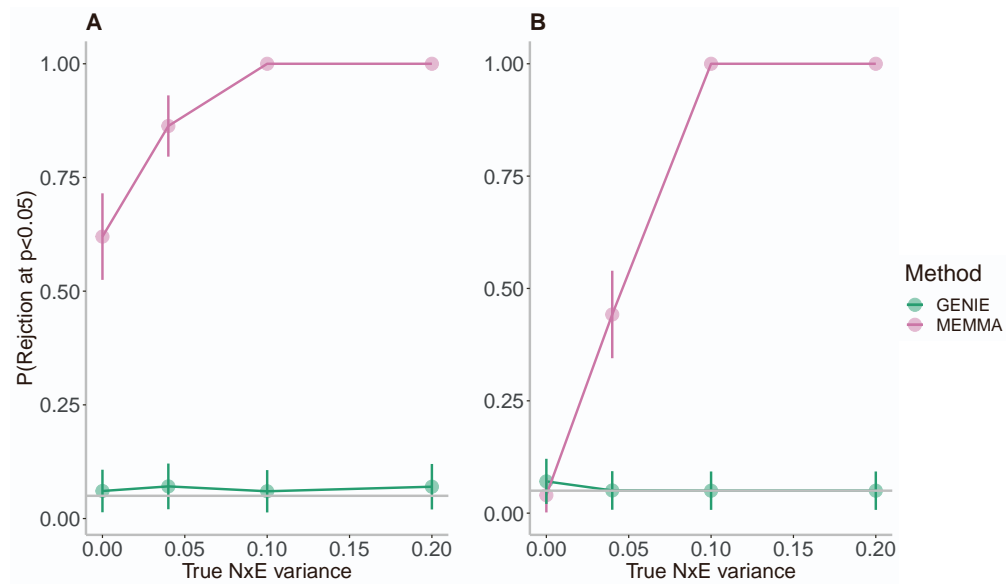


Figure S8: **Comparisons with MEMMA with the presence of noise heterogeneity in simulations.** We assessed the calibration of GENIE and MEMMA using (A) estimated SEs and (B) true SEs in simulations. We performed simulations with no GxE heritability but with varying magnitudes of the variance of the NxE effect. We computed the false positive rate as the fraction of rejections  $P(p\text{-value of a test of the null hypothesis of zero GxE heritability} < 0.05)$  over 100 replicates of phenotypes. The phenotypes were simulated from  $N = 40,000$  individuals and  $M = 454,207$  SNPs. MEMMA has biased estimates of SE, and the false positive rate is calibrated in the absence of a NxE effect using the true SEs. Error bars correspond to the estimated 95% CI of the rejection rate.

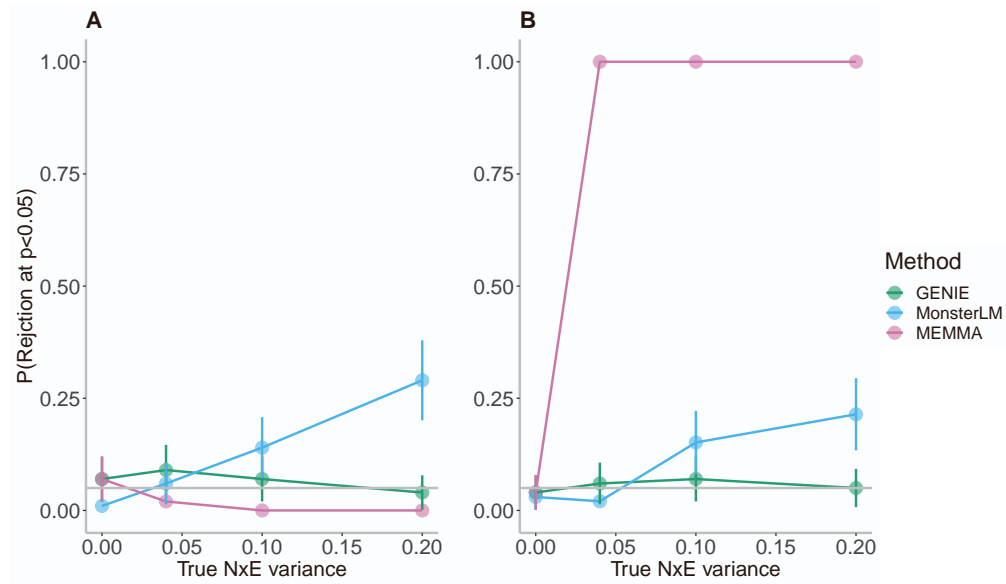


Figure S9: **Effects of estimated standard errors on controlling the false positive rate.** We assessed the calibration of GENIE and existing methods using their true SE instead of the estimation of SE in simulations with (A) continuous and (B) discrete environment exposures. The phenotypes were simulated from  $N = 40,000$  individuals and  $M = 223,591$  SNPs filtered from  $M = 454,207$  SNPs with the genotype QC steps in MonsterLM. Error bars correspond to the estimated 95% CI of the rejection rate.

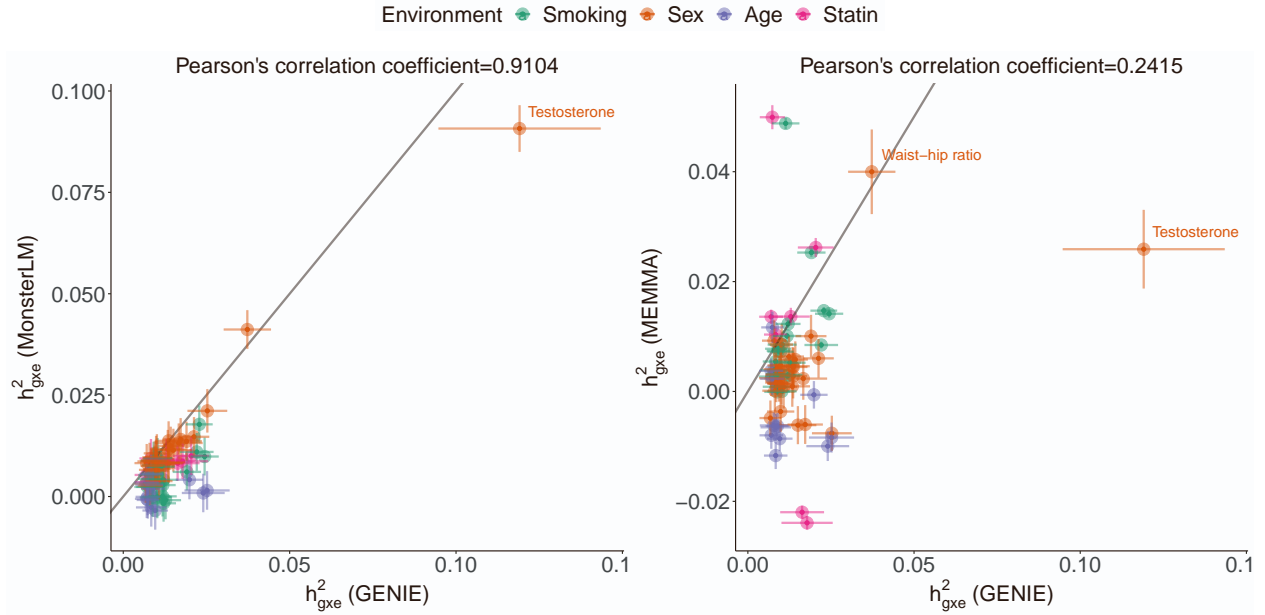


Figure S10: **Estimates of GxE heritability from GENIE, MonsterLM, and MEMMA for 68 trait-environment pairs in the UK Biobank.** We applied GENIE and MEMMA to a cohort of  $N = 291,273$  unrelated white British individuals genotyped at  $M = 454,207$  SNPs. Subsequent to required genotype QC procedures, which involved excluding SNPs with LD  $r^2 > 0.9$  and SNPs with MAF  $< 0.05$ , a total of 223,584 SNPs for  $M = 291,273$  individuals were retained for estimating GxE heritability using MonsterLM. We included age, sex, age<sup>2</sup>, age $\times$ sex, age<sup>2</sup> $\times$ sex, and the top genetic PCs as covariates for each trait-E pair in all methods. The dots and error bars represent the point estimates and standard errors, and the diagonal line denotes the  $y = x$  curve for each plot. We labeled the traits' names for the most extreme outliers (Cook's distance ten times larger than the mean).



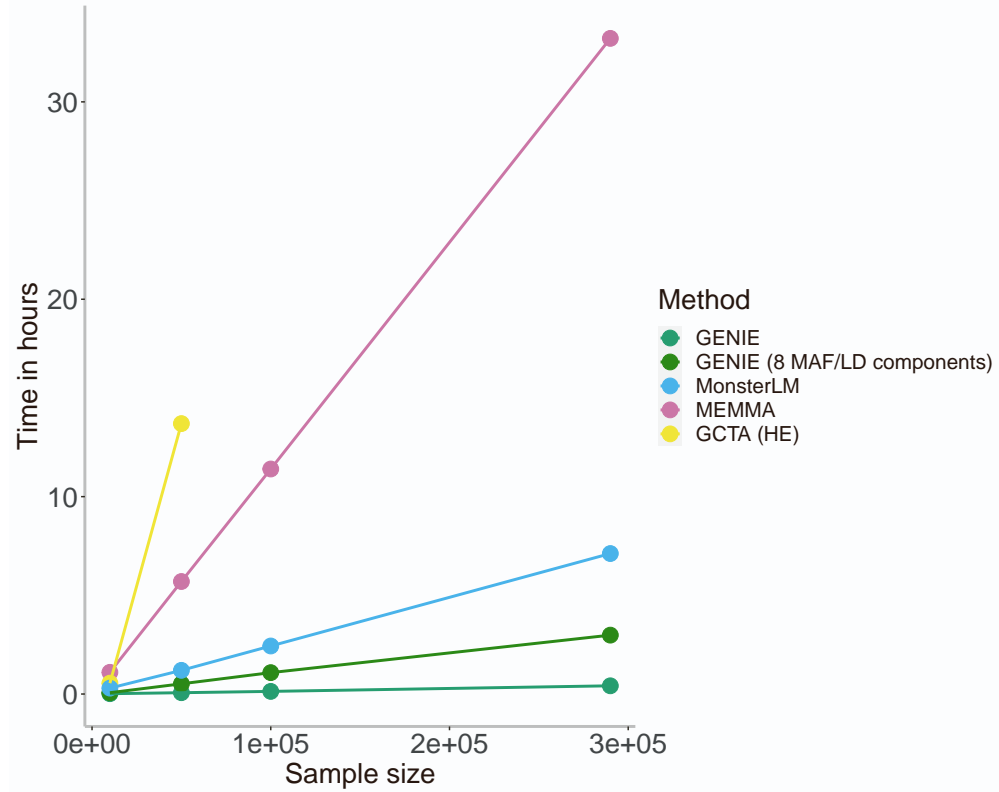


Figure S11: **Comparison of runtimes.** We evaluated the runtime of GENIE, MonsterLM, MEMMA, and GCTA (HE) with increasing sample size  $N$  (for a fixed number of SNPs  $M = 454,207$  and single environmental variable). All methods were run on an Intel(R) Xeon(R) Gold 6140 CPU 2.30 GHz with 187 GB RAM. Ten random vectors are used by GENIE and MEMMA. For GENIE, runtime measurements were obtained for both the single component and eight MAF/LD components (labeled as “GENIE” and “GENIE (8 MAF/LD annotations)”, respectively). All other methods fit a single G and Gx $E$  variance component. The runtime of GCTA (HE) includes the computation of the GRM matrix. Our comparison used the CPU implementation of MonsterLM, with runtime calculations excluding the preprocessing step for genotype filtering required by MonsterLM.

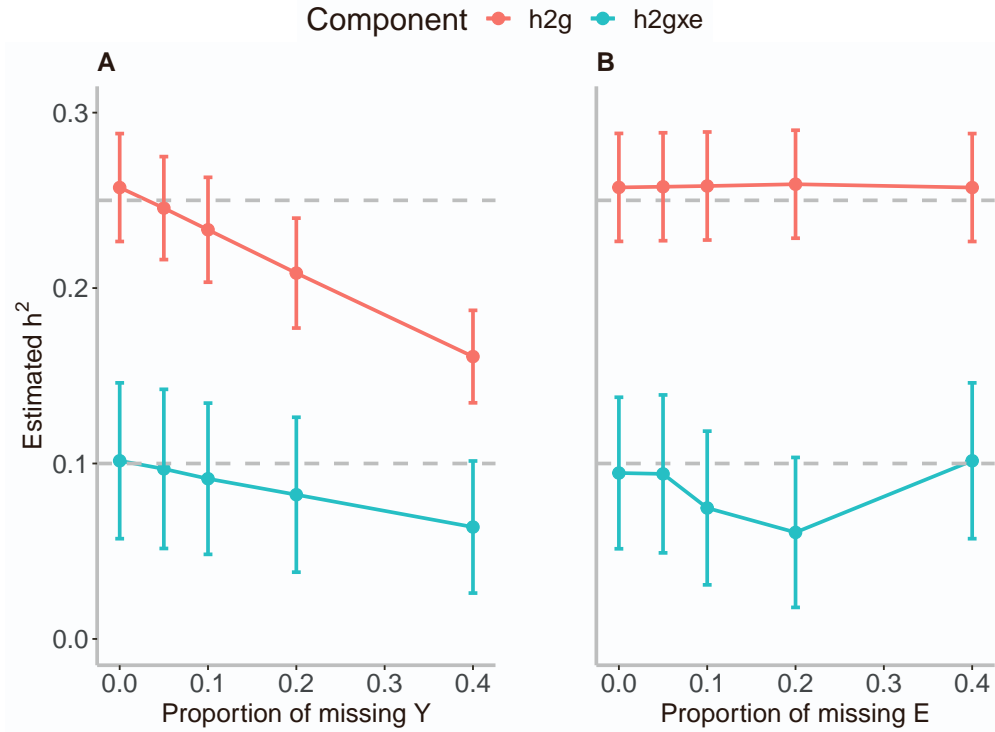


Figure S12: **Impact of mean imputation on the estimation of G and GxE heritability in simulations.** (A) Missing phenotypes and (B) missing environment variables were imputed by mean imputation. We simulated phenotypes with GxE and NxE effects with variance explained by the G, GxE, and NxE components to be 0.25, 0.1, and 0.1, respectively. We varied the proportion of missing phenotypes across 0, 0.05, 0.1, 0.2, and 0.4 over 100 replicates of simulated phenotypes of  $N = 40,000$  individuals genotyped at 454,207 SNPs. The randomly masked phenotypes were replaced with the mean of those unmasked values. Statin usage was used as the environmental variable in the experiment. To test the performance of the missing environment, we randomly masked and mean-imputed E in a similar manner while keeping the phenotypes as all observed. The  $x$ -axis shows the proportion of missing and mean-imputed Y or E, and the  $y$ -axis represents the estimated heritability by GENIE. The dots and error bars indicate the mean of estimated G and GxE heritability and 95% CI.

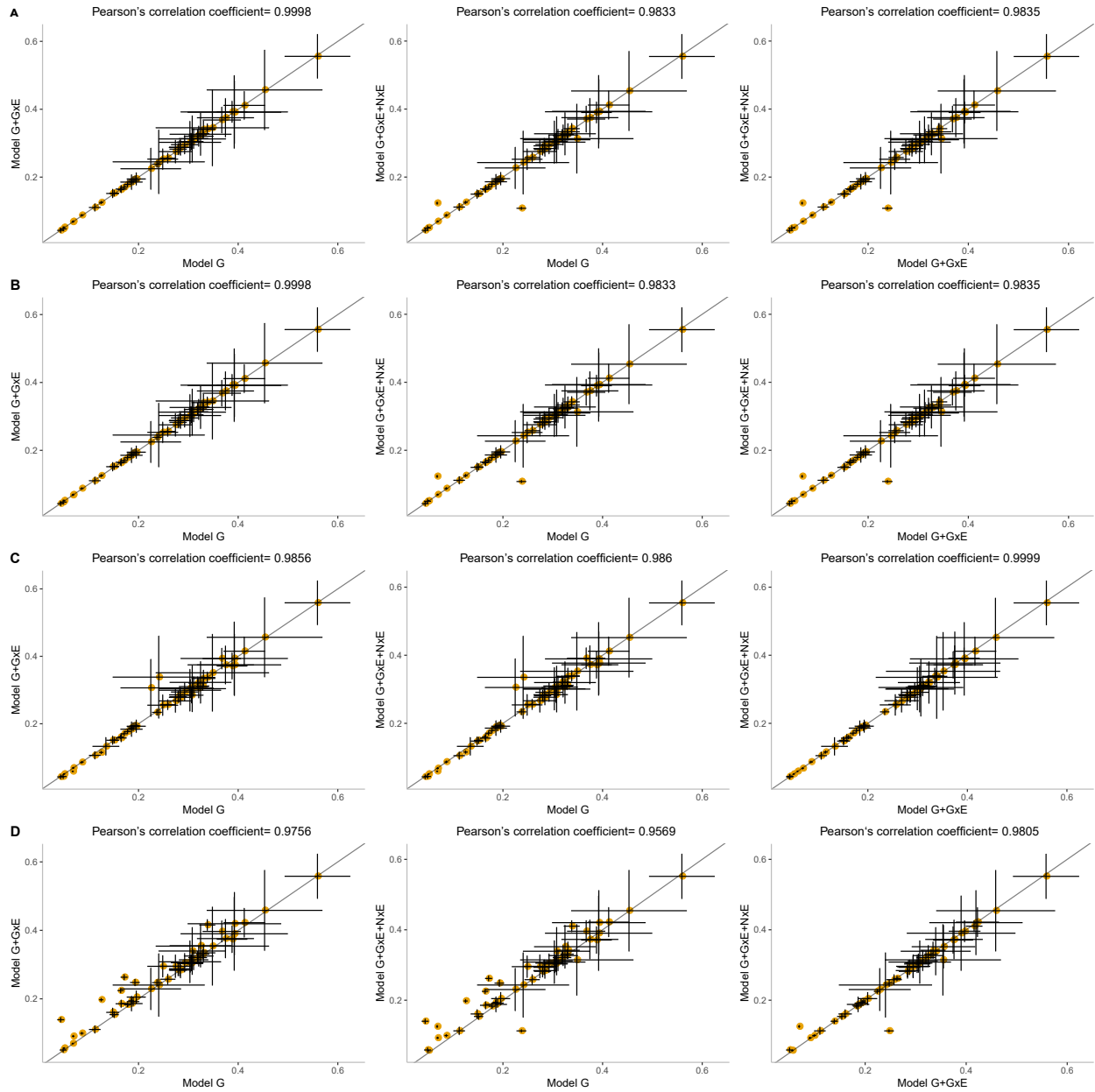


Figure S13: **Estimated additive heritability from three different models.** In this figure, G, GxE, and NxE refer to additive, gene-by-environment, and noise-by-environment components, respectively. Every model is named by a set of variance components fitted jointly under that model. Estimates of additive components under the three models where the environmental variable is (A) smoking status, (B) sex, (C) statin usage, and (D) age. The estimates of additive heritability obtained by GENIE are consistent under these three models across environmental variables.

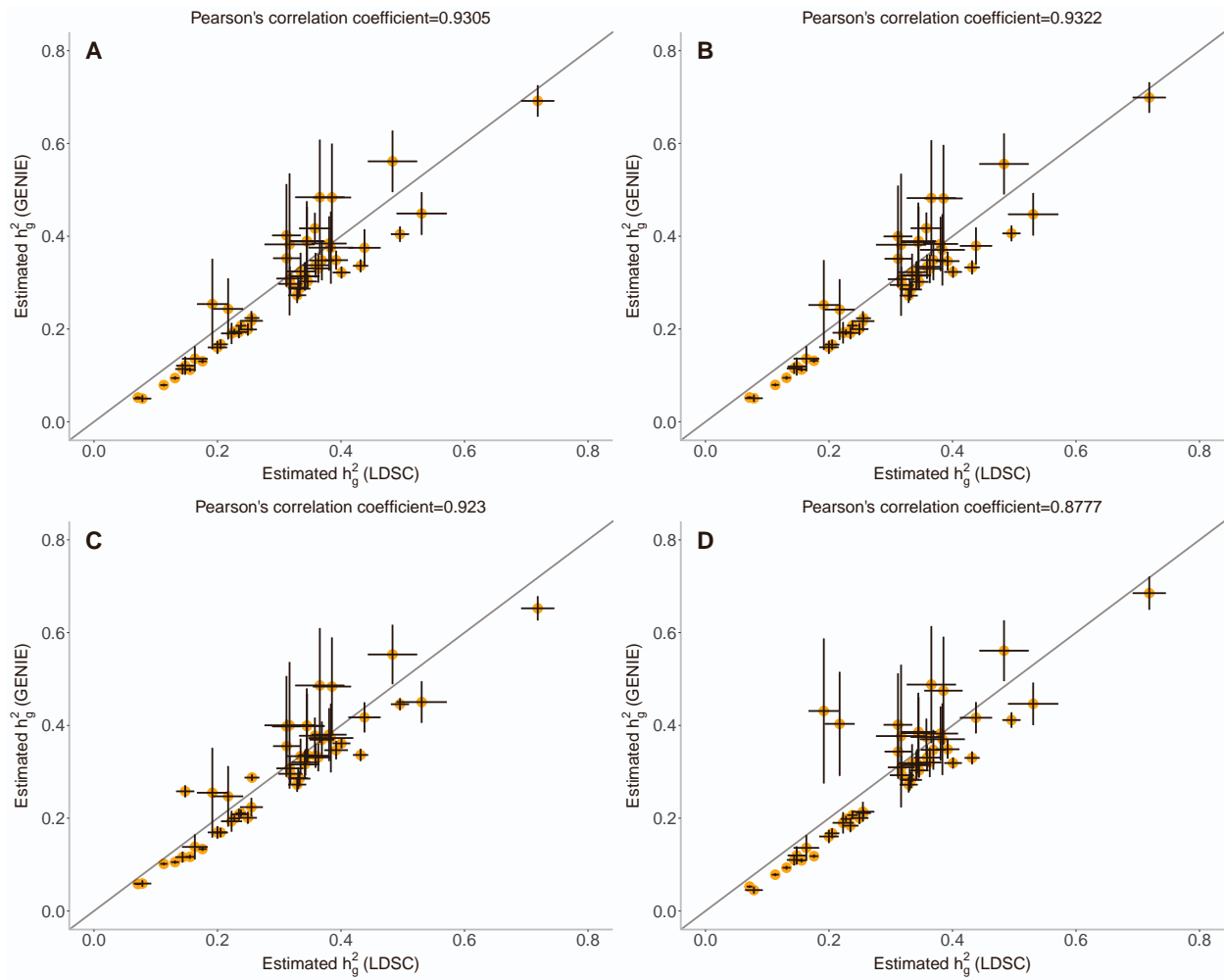


Figure S14: **Comparison of estimated additive heritability with LDSC.** Estimates of additive  $h_g^2$  by LDSC compared with those of GENIE with environment exposures (A) smoking status, (B) sex, (C) age, and (D) statin. Both methods estimated additive  $h_g^2$  on  $N = 291,273$  individuals and  $M = 454,207$  array SNPs and 50 quantitative traits from the UK Biobank. We fitted a single component in LDSC regression to enable a direct comparison with GENIE (which was also applied with a single component in this case). The dots and error bars denote the point estimates and corresponding SEs. GENIE showed consistent and highly correlated estimates compared with LDSC estimates across four environment variables.

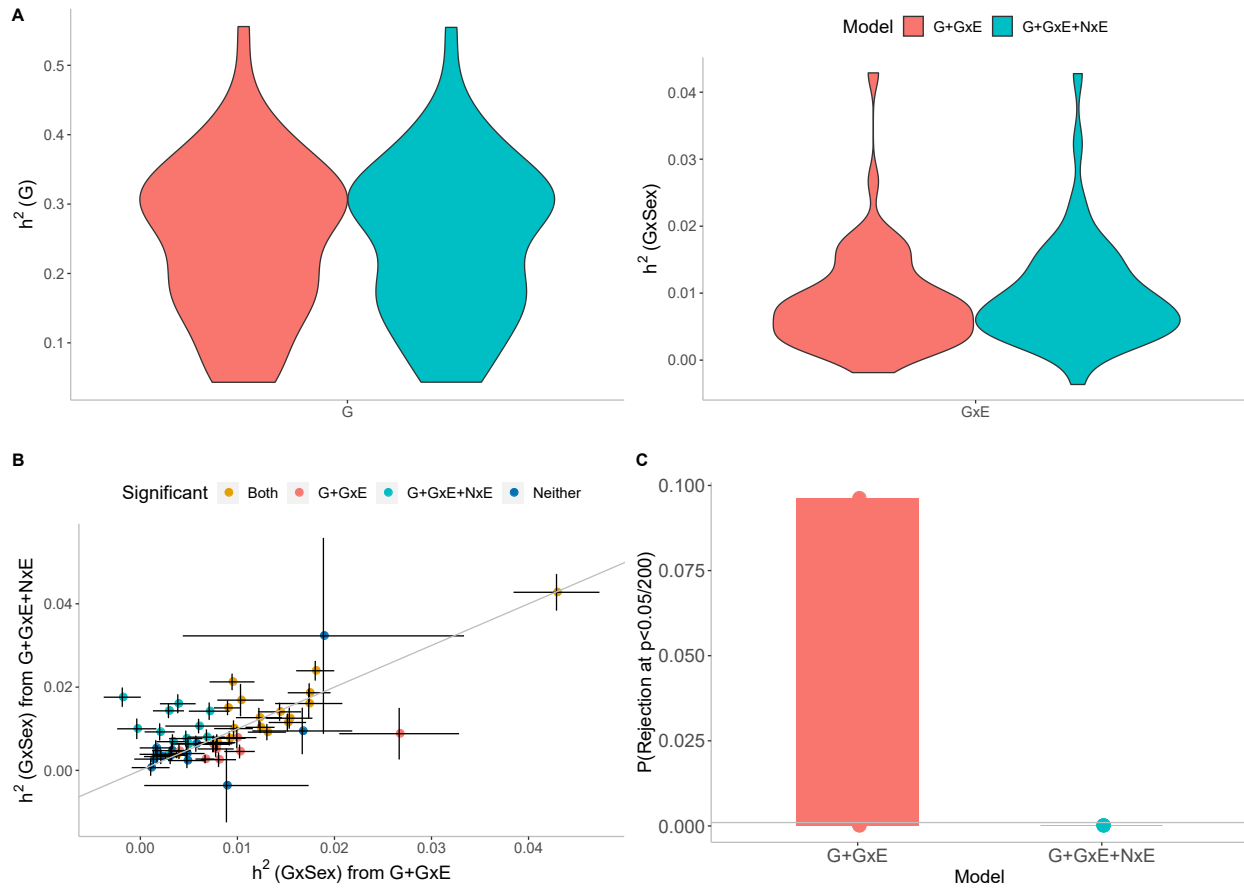


Figure S15: **Effect of Noise heterogeneity (Nx E) on estimates of heritability associated with GxSex across 50 quantitative phenotypes in UKB.** Model G+GxE refers to a model with additive and gene-by-environment interaction components. Model G+GxE+NxE refers to a model with additive, gene-by-environment interaction, and noise heterogeneity (noise-by-environment interaction) components. (A) We ran GENIE under G+GxE and G+GxE+NxE models to assess the effect of fitting an Nx E component on the GxE and additive heritability estimates. (B) Comparison of GxE heritability estimates obtained from GENIE under a G+GxE+NxE model ( $x$ -axis) to a G+GxE model ( $y$ -axis). Black error bars mark  $\pm$  standard errors centered on the estimated GxE heritability. The color of the dots indicates whether estimates of GxE heritability are significant under each model. (C) We performed permutation analyses by randomly shuffling the genotypes while preserving the trait-E relationship and applied GENIE in each setting under G+GxE and G+GxE+NxE models. We report the fraction of rejections  $P(p\text{-value of a test of the null hypothesis of zero GxE heritability} < \frac{0.05}{200} \text{ that accounts for the number of phenotypes tested})$  over 50 UKB phenotypes.



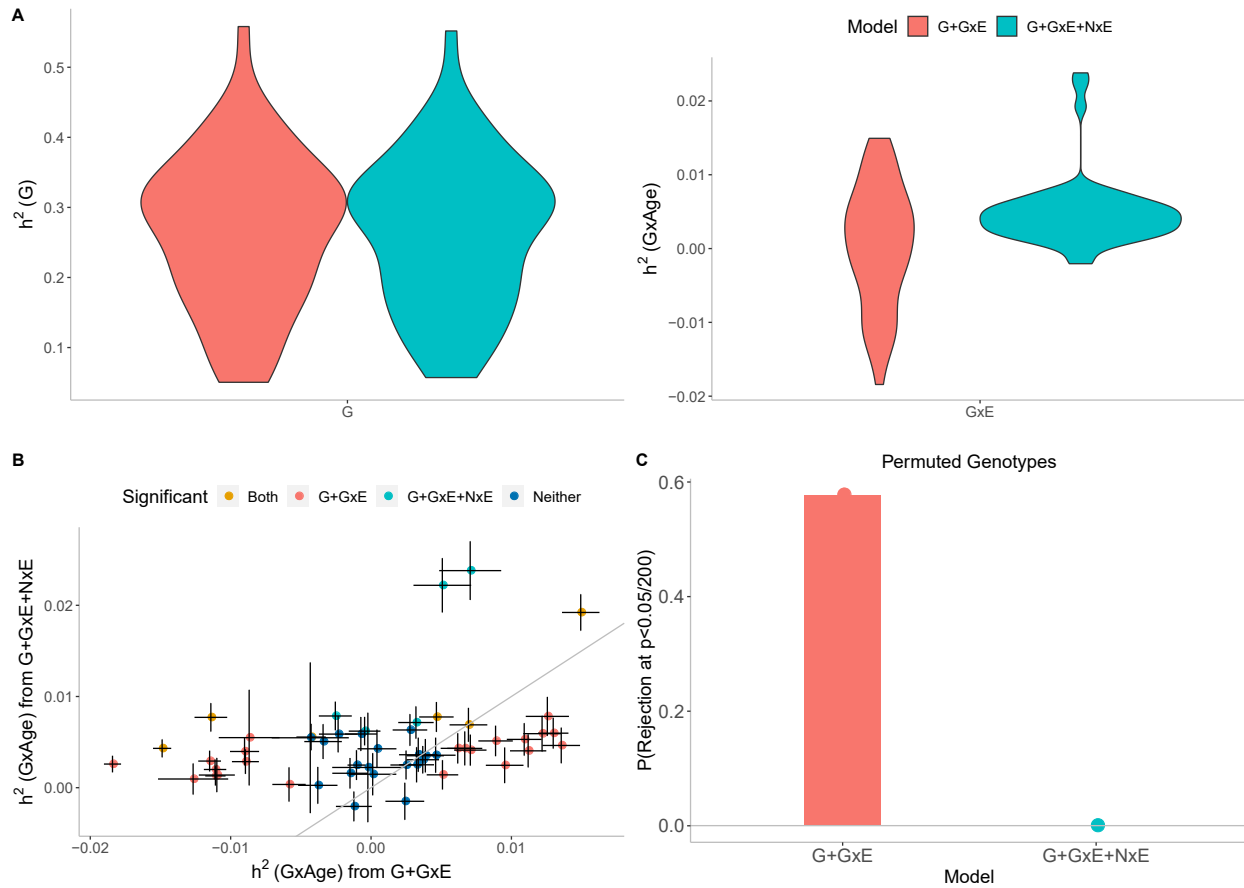


Figure S16: **Effect of Noise heterogeneity (Nx E) on estimates of heritability associated with GxAge across 50 quantitative phenotypes in UKB.** Model G+GxE refers to a model with additive and gene-by-environment interaction components. Model G+GxE+NxE refers to a model with additive, gene-by-environment interaction, and noise heterogeneity (noise-by-environment interaction) components. (A) We ran GENIE under G+GxE and G+GxE+NxE models to assess the effect of fitting an Nx E component on the GxE and additive heritability estimates. (B) Comparison of GxE heritability estimates obtained from GENIE under a G+GxE+NxE model (x-axis) to a G+GxE model (y-axis). Black error bars mark  $\pm$  standard errors centered on the estimated GxE heritability. The color of the dots indicates whether estimates of GxE heritability are significant under each model. (C) We performed permutation analyses by randomly shuffling the genotypes while preserving the trait-E relationship and applied GENIE in each setting under G+GxE and G+GxE+NxE models. We report the fraction of rejections  $P(p\text{-value of a test of the null hypothesis of zero GxE heritability} < \frac{0.05}{200})$  that accounts for the number of phenotypes tested) over 50 UKB phenotypes.

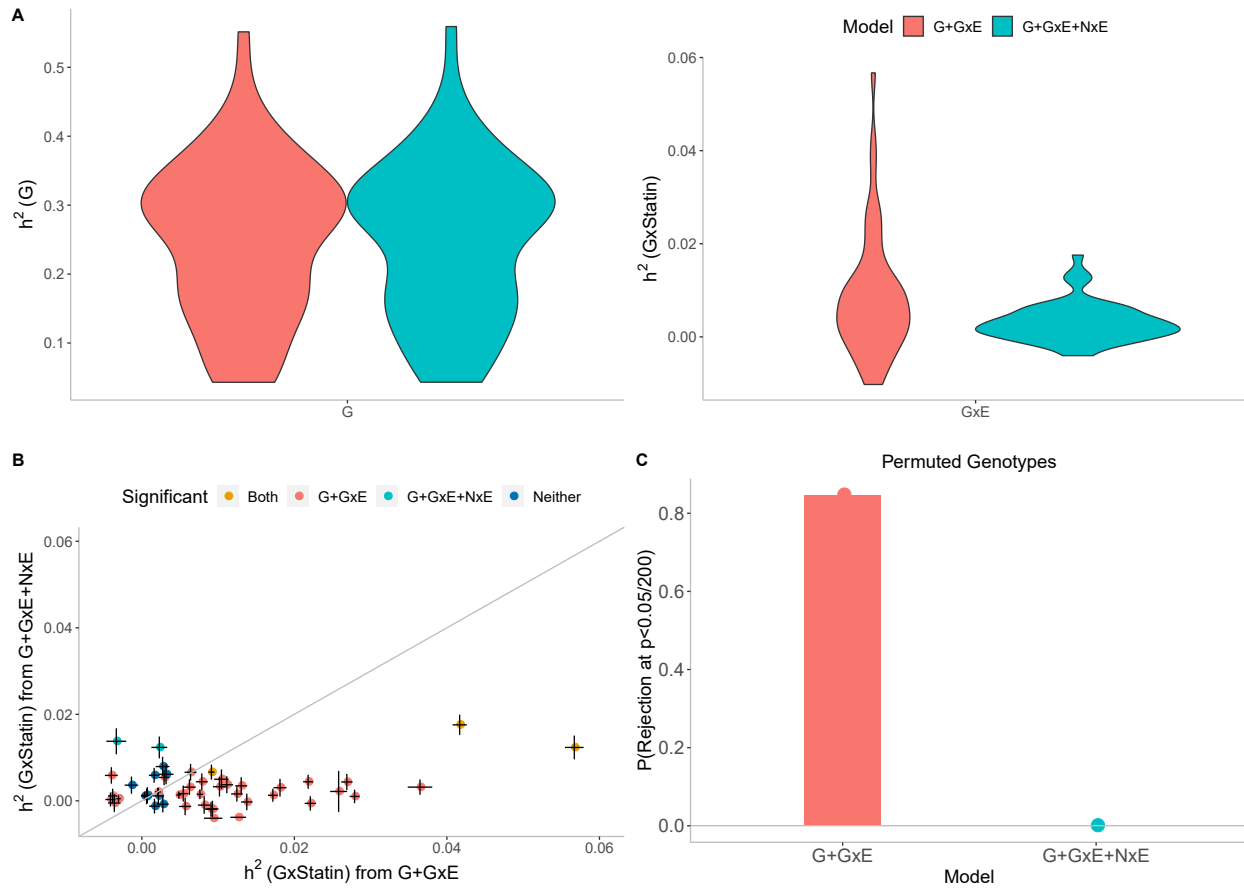


Figure S17: **Effect of Noise heterogeneity (Nx E) on estimates of heritability associated with GxStatin across 50 quantitative phenotypes in UKB.** Model G+GxE refers to a model with additive and gene-by-environment interaction components. Model G+GxE+NxE refers to a model with additive, gene-by-environment interaction, and noise heterogeneity (noise-by-environment interaction) components. (A) We ran GENIE under G+GxE and G+GxE+NxE models to assess the effect of fitting an Nx E component on the GxE and additive heritability estimates. (B) Comparison of GxE heritability estimates obtained from GENIE under a G+GxE+NxE model (x-axis) to a G+GxE model (y-axis). Black error bars mark  $\pm$  standard errors centered on the estimated GxE heritability. The color of the dots indicates whether estimates of GxE heritability are significant under each model. (C) We performed permutation analyses by randomly shuffling the genotypes while preserving the trait-E relationship and applied GENIE in each setting under G+GxE and G+GxE+NxE models. We report the fraction of rejections  $P(p\text{-value of a test of the null hypothesis of zero GxE heritability} < \frac{0.05}{200})$  that accounts for the number of phenotypes tested) over 50 UKB phenotypes.

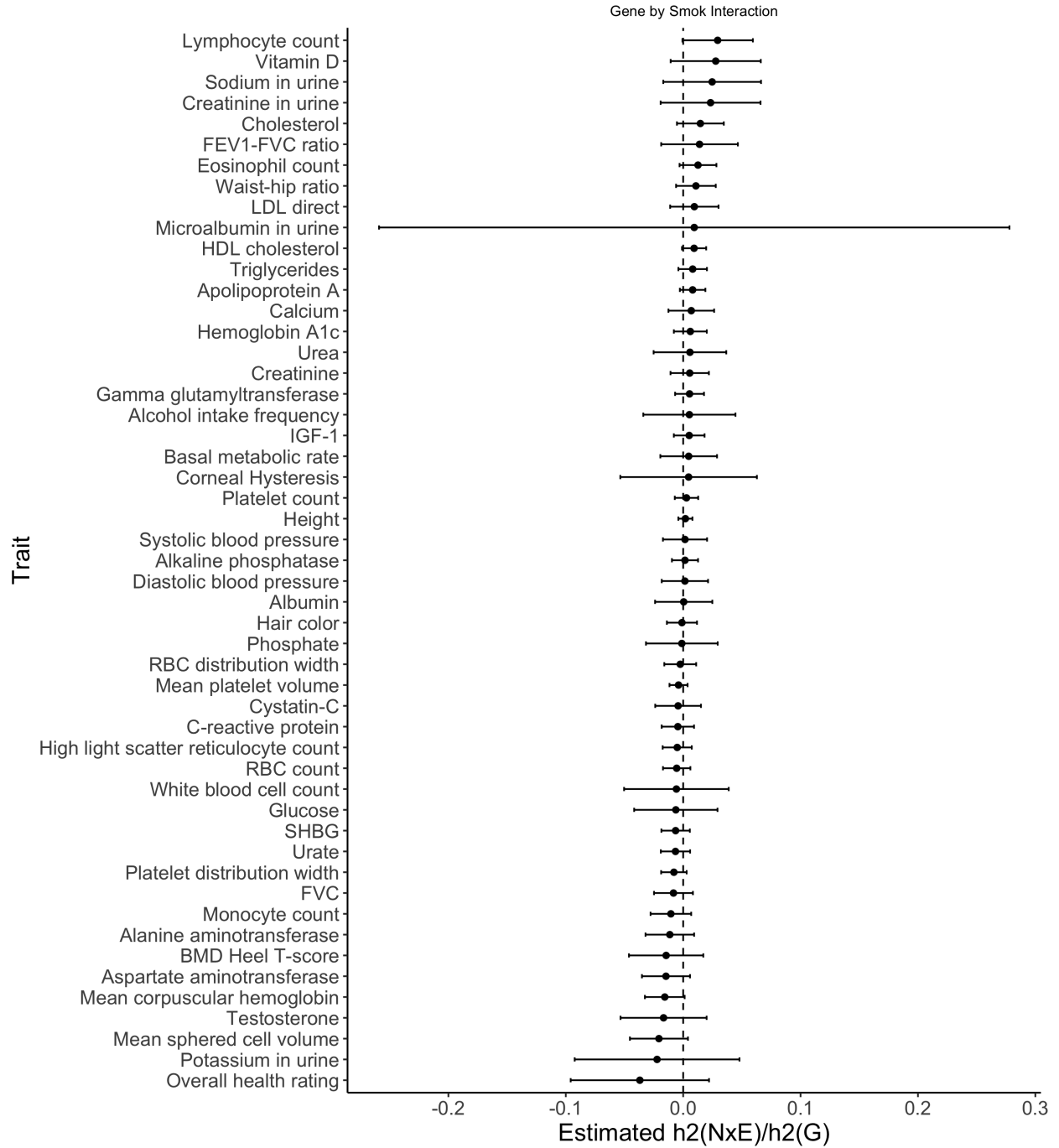


Figure S18: **Estimated ratio of variance attributed to noise heterogeneity over additive heritability for Smoking.** Black error bars mark  $\pm 2$  standard errors centered on the estimated ratio.

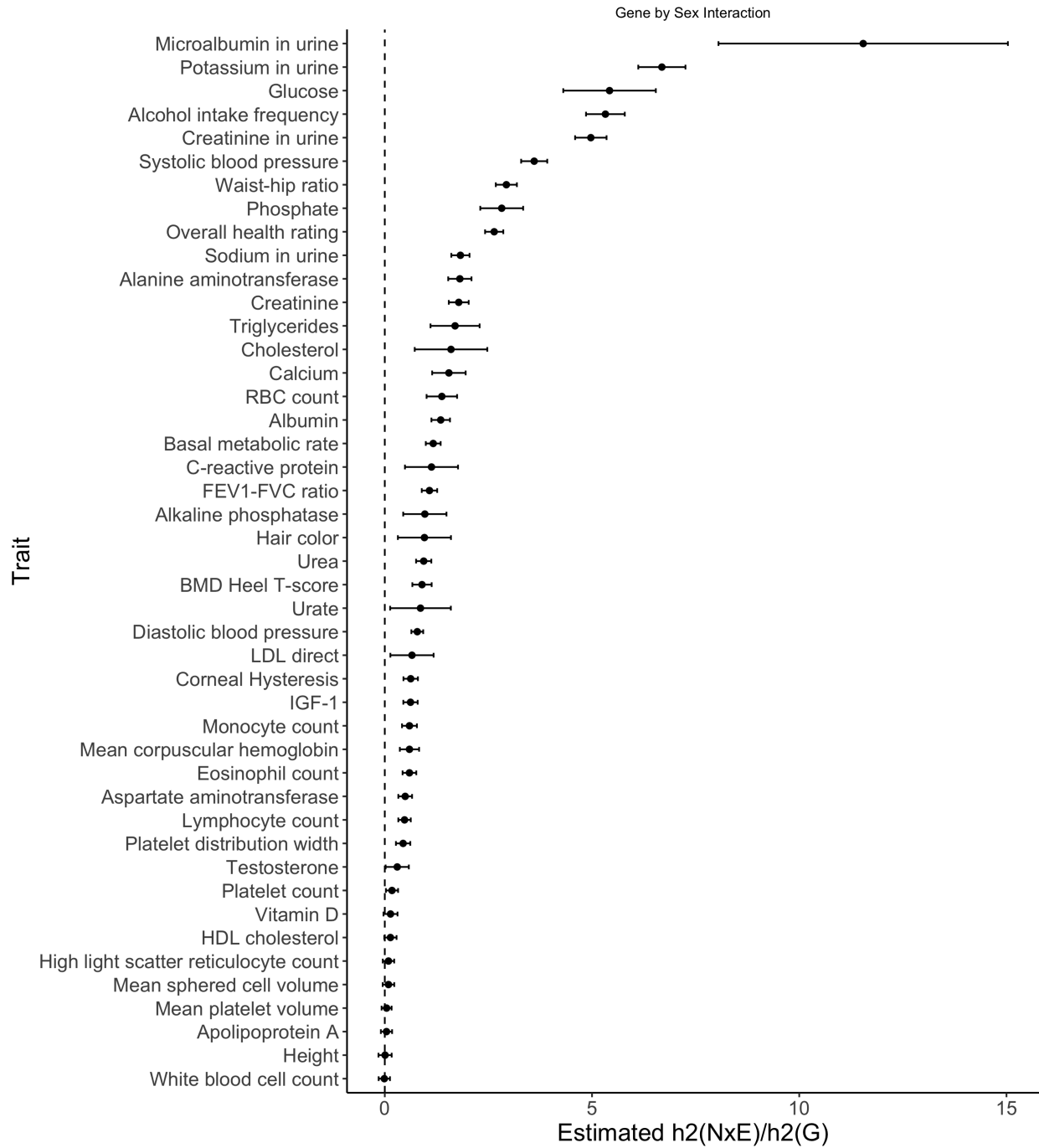


Figure S19: **Estimated ratio of variance attributed to noise heterogeneity over additive heritability for Sex.** Black error bars mark  $\pm 2$  standard errors centered on the estimated ratio.

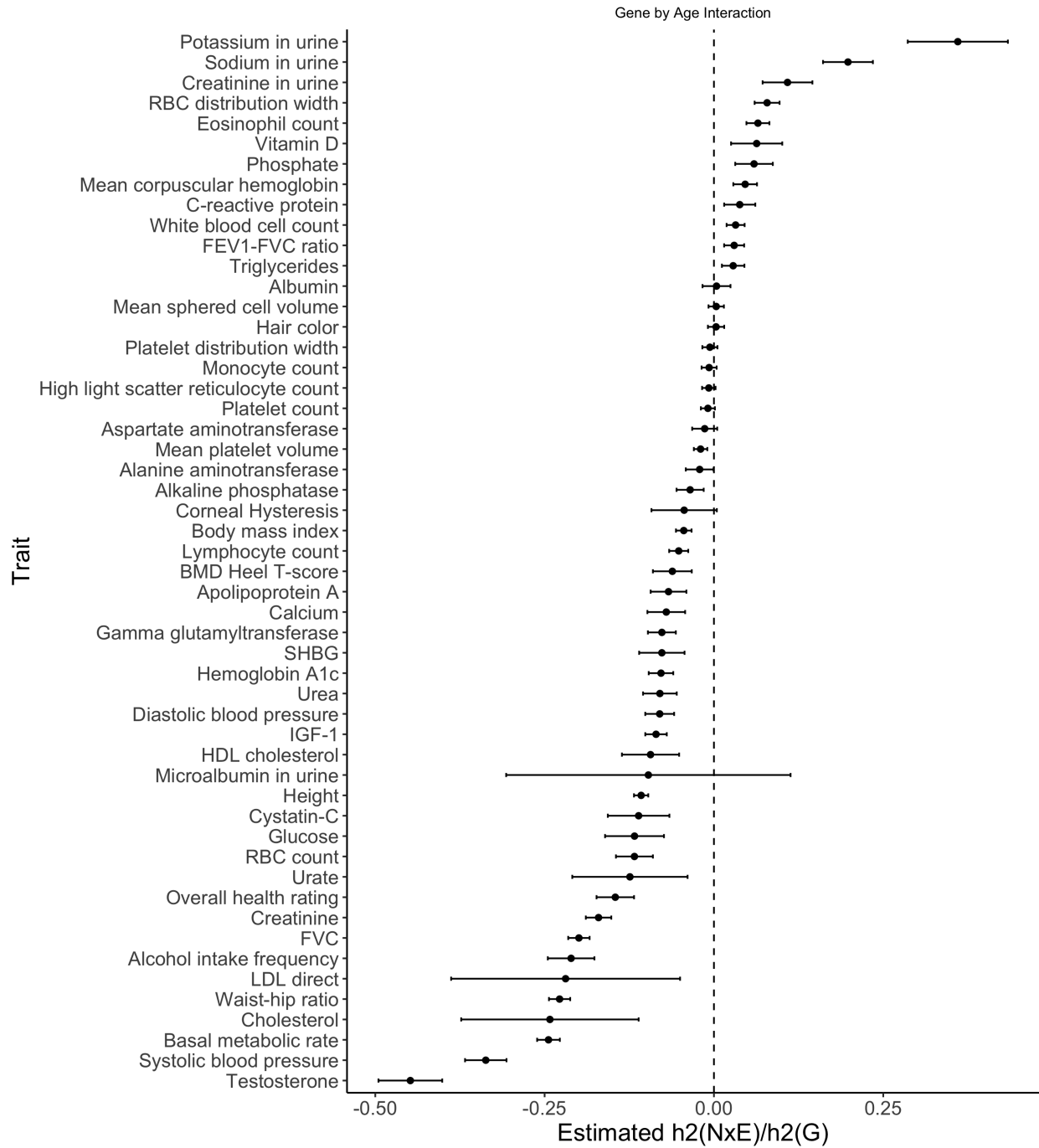


Figure S20: **Estimated ratio of variance attributed to noise heterogeneity over additive heritability for Age.** Black error bars mark  $\pm 2$  standard errors centered on the estimated ratio.



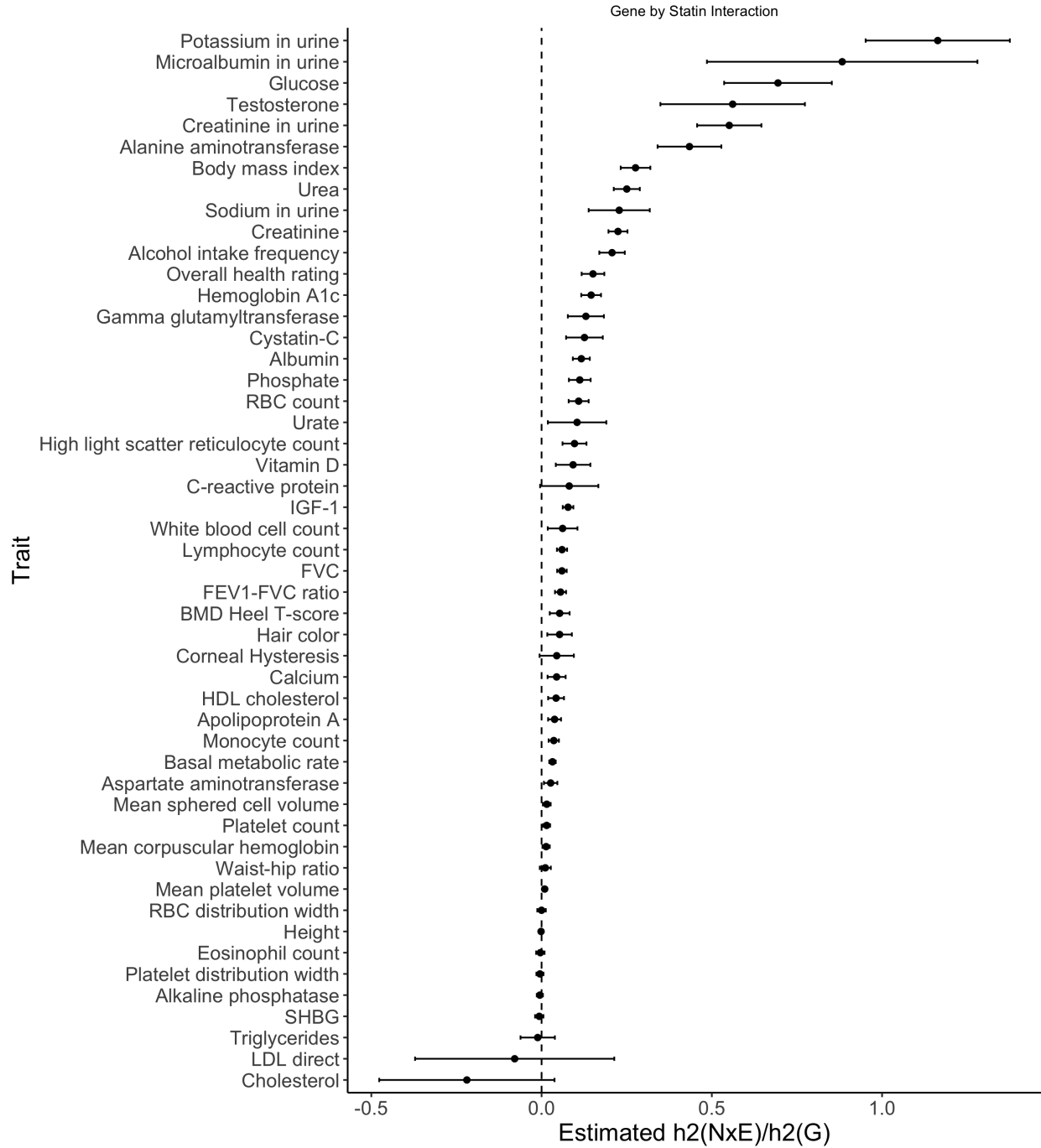


Figure S21: **Estimated ratio of variance attributed to noise heterogeneity over additive heritability for Statin usage.** Black error bars mark  $\pm 2$  standard errors centered on the estimated ratio.

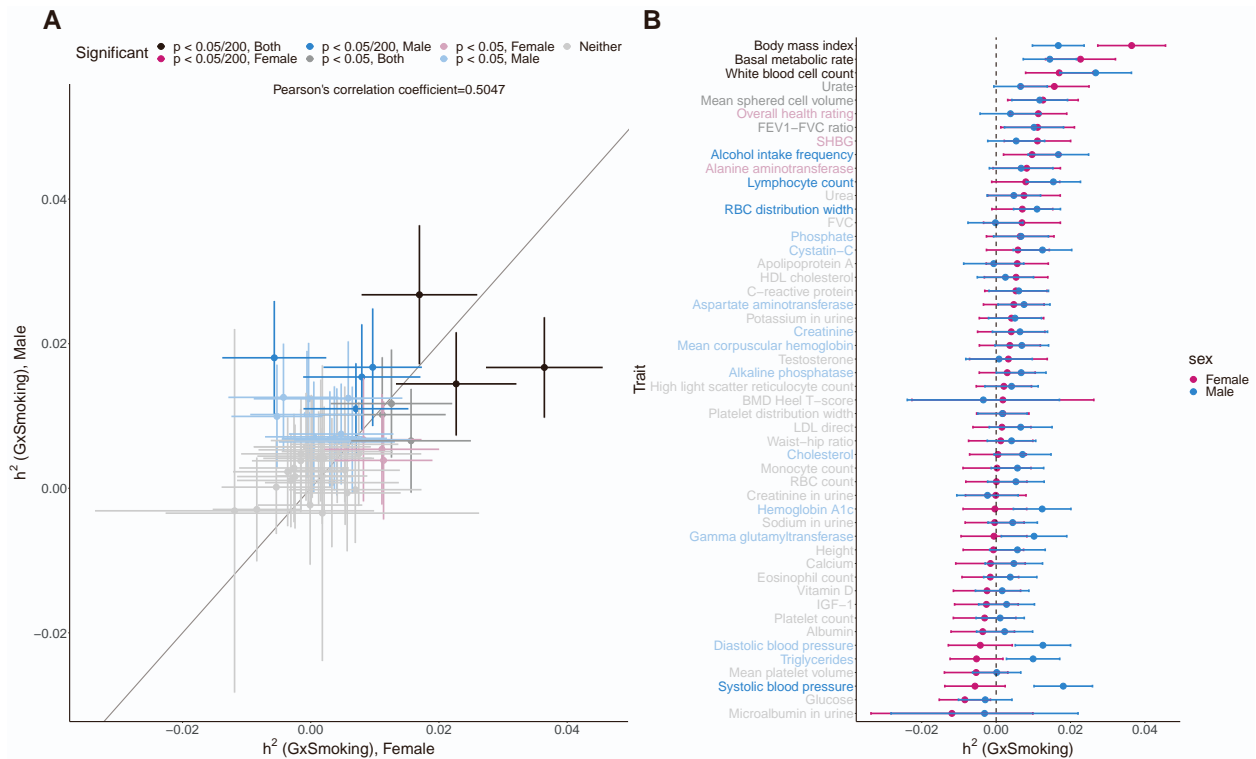


Figure S22: **Estimates of GxSmoking heritability across phenotypes in UK Biobank stratified by sex.** We applied GENIE to  $N = 291,273$  unrelated white British individuals and  $M = 454,207$  array SNPs, with 155,469 male and 135,804 female individuals. The phenotype vectors were masked such that only the measurements of female/male individuals remained. **(A)** The comparison of GxSmoking heritability estimates in female and male individuals across fifty traits. Error bars mark  $\pm 2$  standard errors centered on the point estimates. We grouped the results into seven significant levels based on the  $p$ -values in males and females. **(B)** Estimates of GxSmoking heritability across fifty traits stratified by sex. The trait labels were colored based on the defined significance levels.

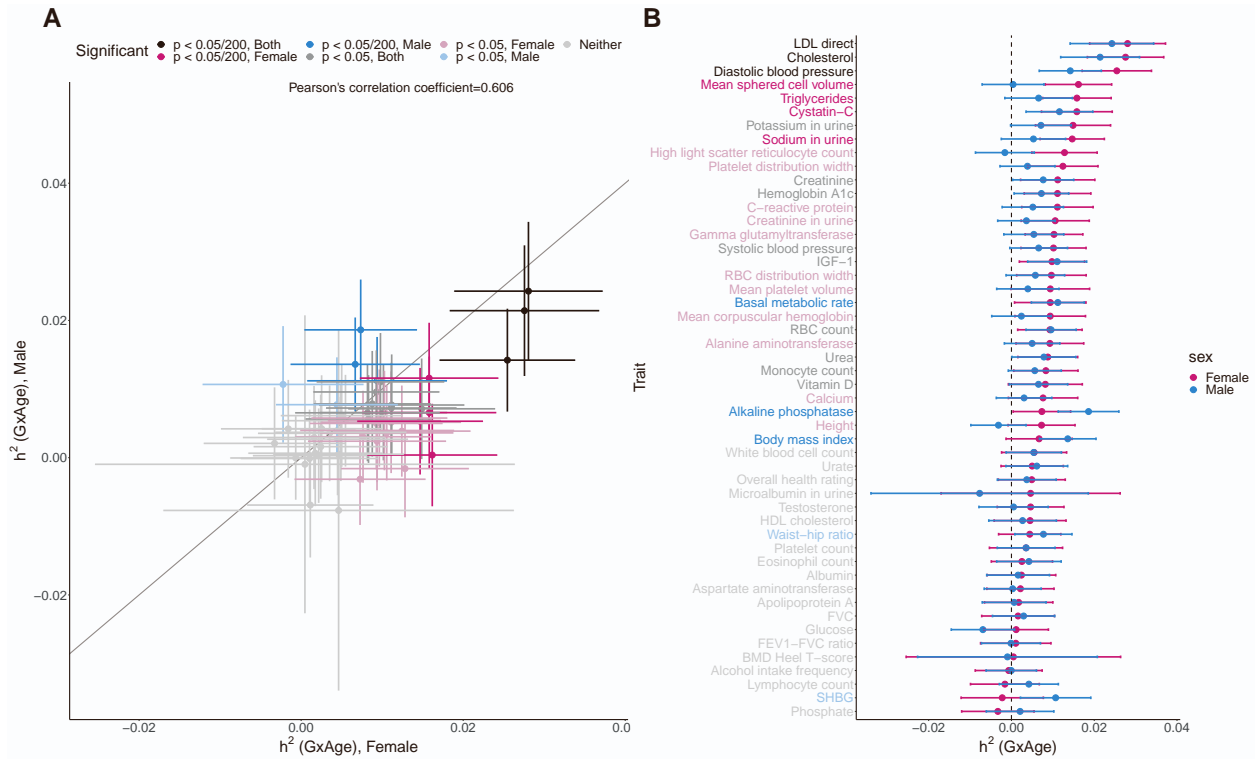


Figure S23: **Estimates of GxAge heritability across phenotypes in UK Biobank stratified by sex.** We applied GENIE to  $N = 291,273$  unrelated white British individuals and  $M = 454,207$  array SNPs, with 155,469 male and 135,804 female individuals. The phenotype vectors were masked such that only the measurements of female/male individuals remained. **(A)** The comparison of GxAge heritability estimates in female and male individuals across fifty traits. Error bars mark  $\pm 2$  standard errors centered on the point estimates. We grouped the results into seven significant levels based on the  $p$ -values in males and females. **(B)** Estimates of GxAge heritability across fifty traits stratified by sex. The trait labels were colored based on the defined significance levels.

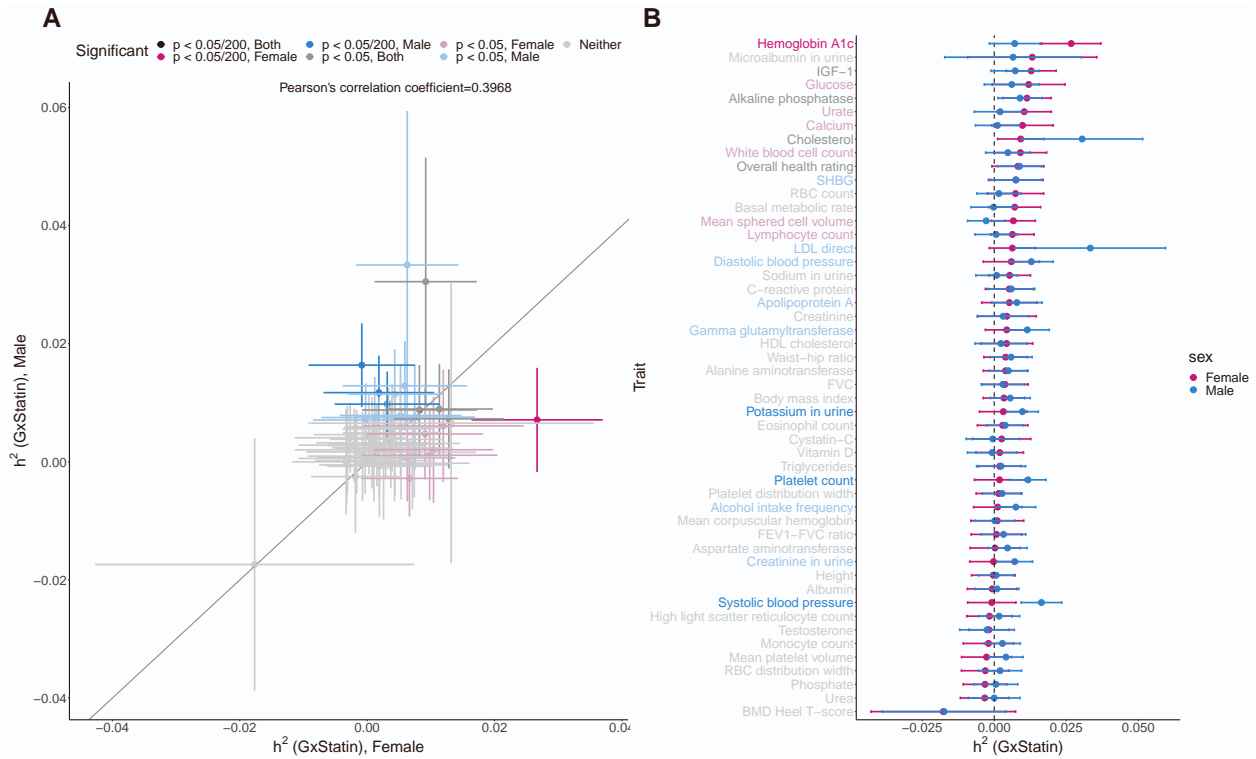


Figure S24: **Estimates of GxStatin heritability across phenotypes in UK Biobank stratified by sex.** We applied GENIE to  $N = 291,273$  unrelated white British individuals and  $M = 454,207$  array SNPs, with 155,469 male and 135,804 female individuals. The phenotype vectors were masked such that only the measurements of female/male individuals remained. **(A)** The comparison of GxStatin heritability estimates in female and male individuals across fifty traits. Error bars mark  $\pm 2$  standard errors centered on the point estimates. We grouped the results into seven significant levels based on the  $p$ -values in males and females. **(B)** Estimates of GxStatin heritability across fifty traits stratified by sex. The trait labels were colored based on the defined significance levels.

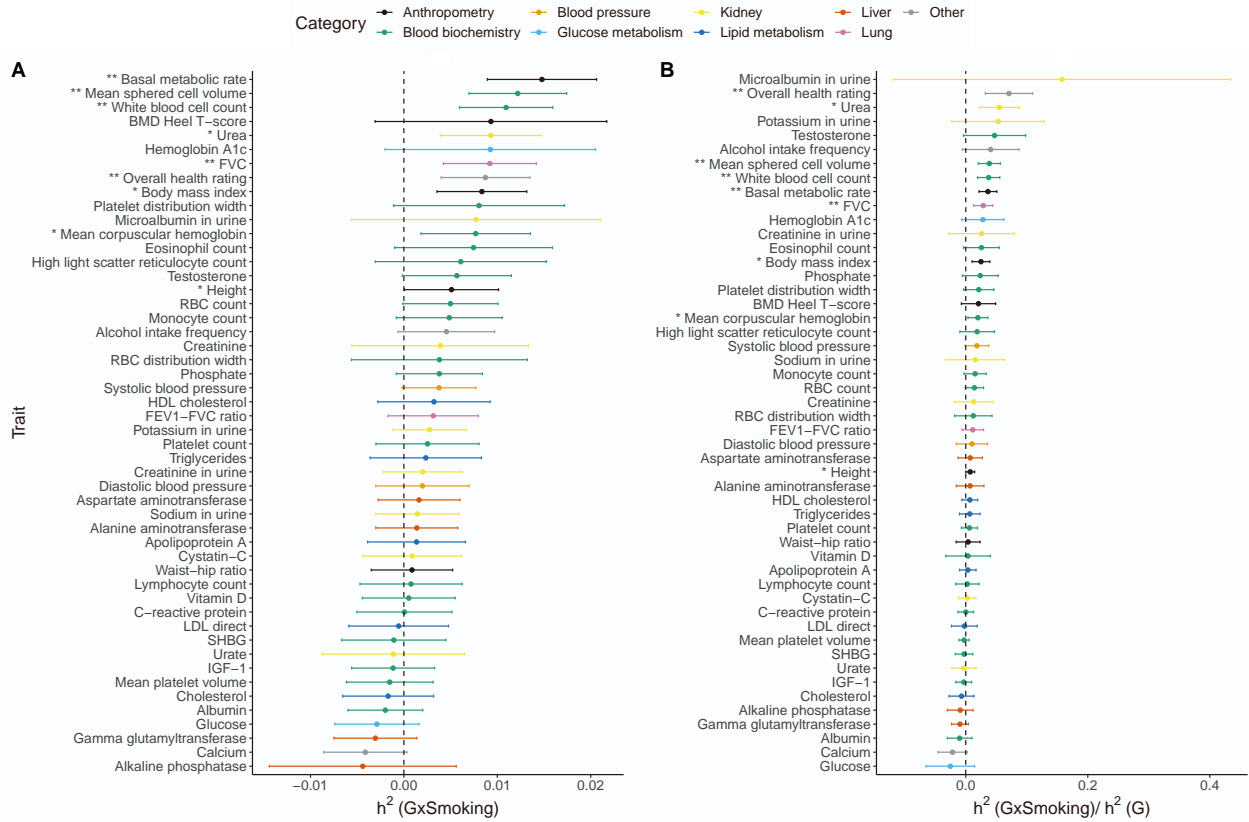


Figure S25: **GxSmoking** across phenotypes in UK Biobank with the environmental variable coded as **binary**. (A) GxSmoking heritability and (B) the ratio of GxSmoking to additive heritability. Our model includes the environmental variable as a fixed effect and accounts for noise heterogeneity. Black error bars mark  $\pm 2$  standard errors. The asterisk and double asterisk correspond to the nominal  $p < 0.05$  and  $p < 0.05/200$  respectively.

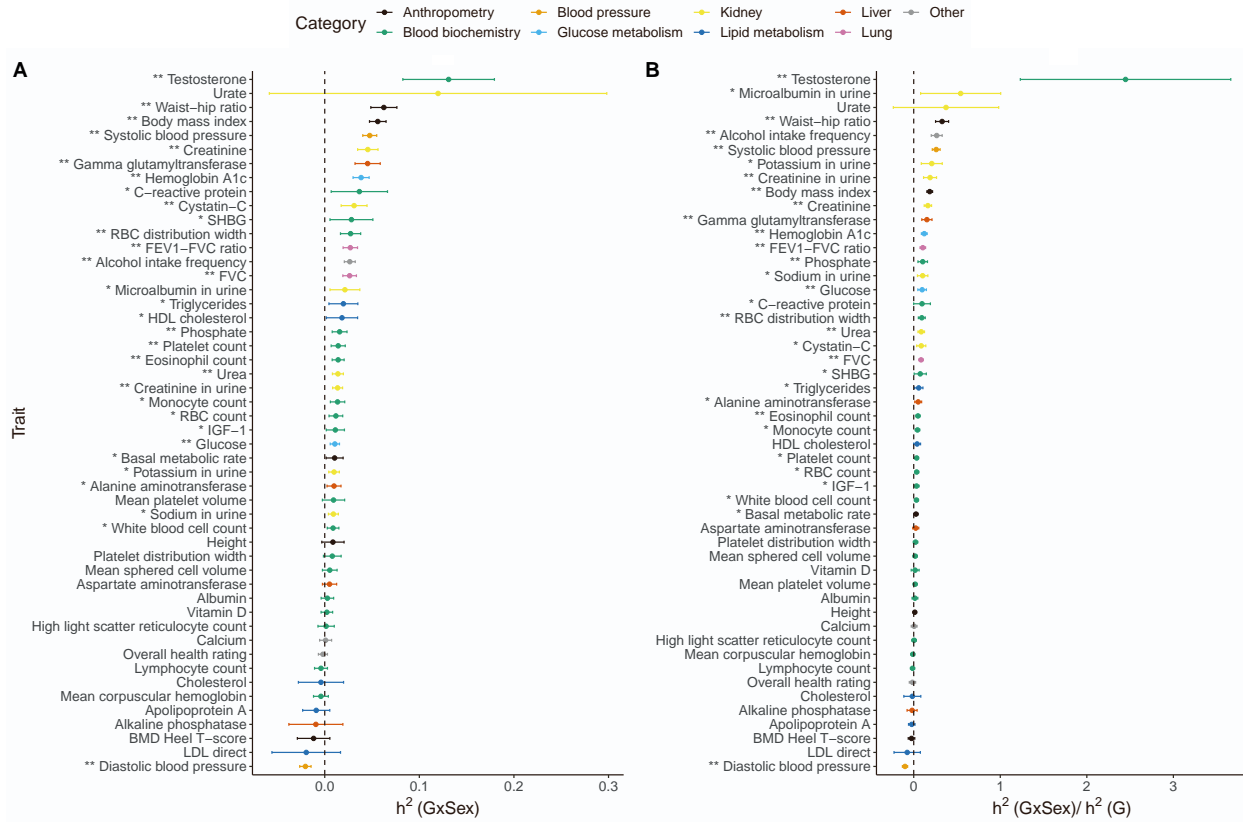


Figure S26: GxSex across phenotypes in UK Biobank with the environmental variable coded as binary. (A) GxSex heritability and (B) the ratio of GxSex to additive heritability. Our model includes the environmental variable as a fixed effect and accounts for noise heterogeneity. Black error bars mark  $\pm 2$  standard errors. The asterisk and double asterisk correspond to the nominal  $p < 0.05$  and  $p < 0.05/50$  respectively.

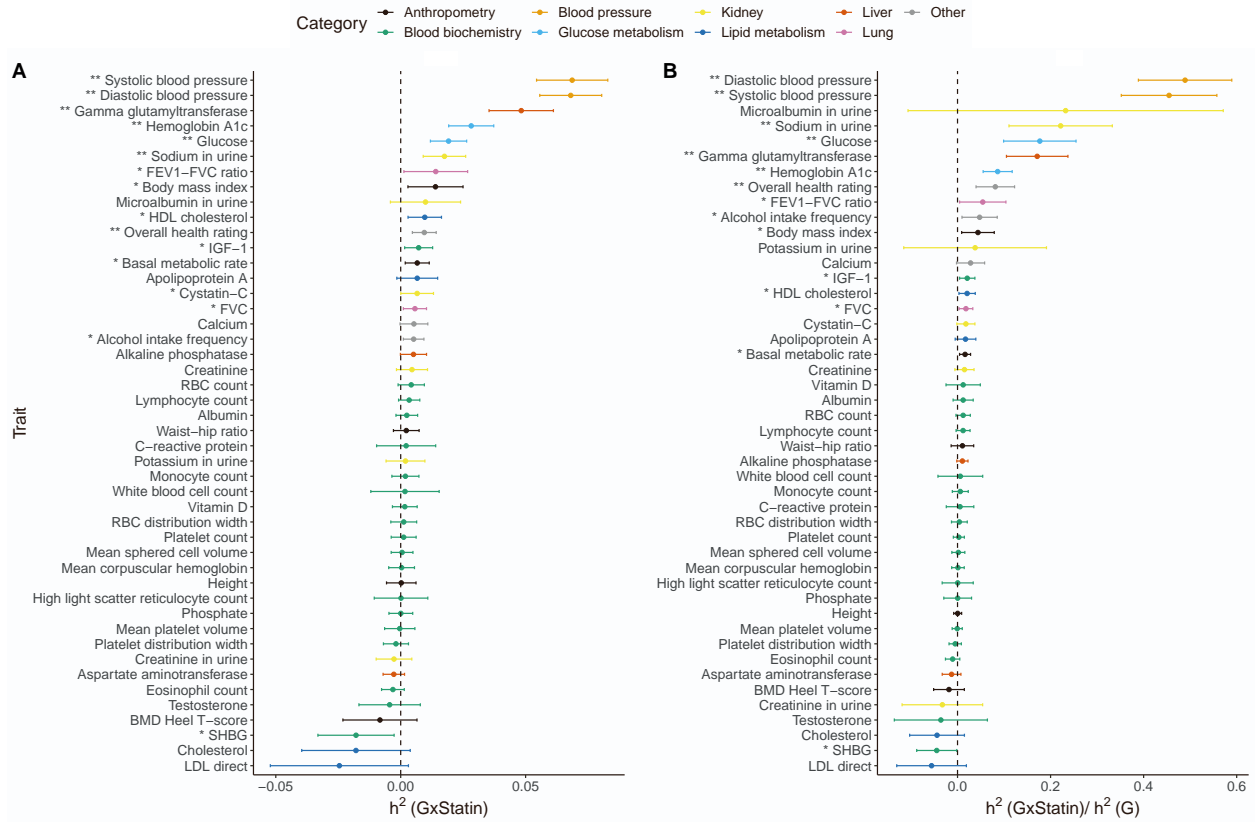


Figure S27: **GxStatin across phenotypes in UK Biobank with the environmental variable coded as binary.** (A) GxStatin heritability and (B) the ratio of GxStatin to additive heritability. Our model includes the environmental variable as a fixed effect and accounts for noise heterogeneity. Black error bars mark  $\pm 2$  standard errors. The asterisk and double asterisk correspond to the nominal  $p < 0.05$  and  $p < 0.05/50$ , respectively.



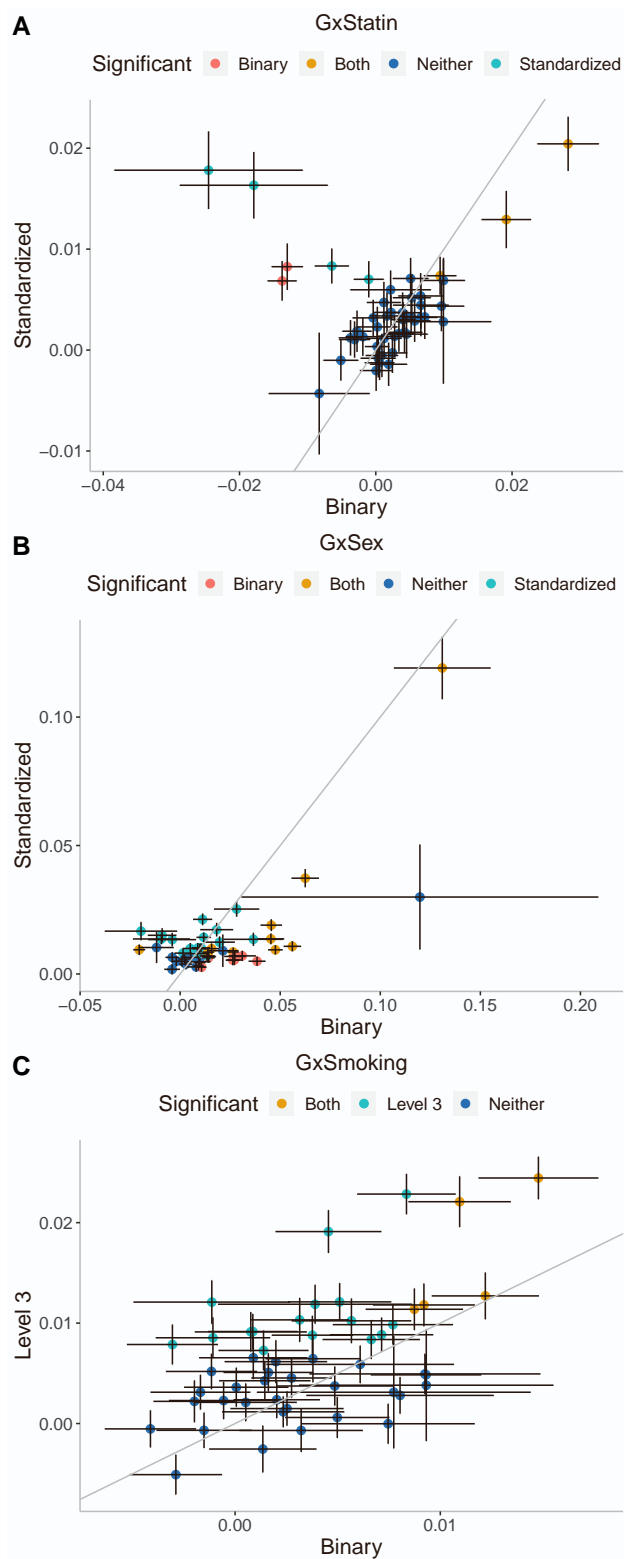


Figure S28: **Comparisons of GxE estimates using standardized or binary encodings of the environment.** We compared (A) GxStatin, (B) GxSex and (C) GxSmoking estimates on  $N = 291,273$  individuals genotyped at 454,207 SNPs for 50 traits using standardized or binary encodings. The traits are significant at  $p < 0.05/200$  using standardized encoding and/or binary encoding (or neither) are labeled with different colors. The standardized encodings of binary variables statin usage and sex and ternary variable smoking status (denoted as “level 3”) were plotted on the  $y$ -axis. The points and error bars represent the point estimates and estimated SEs respectively, and the  $y = x$  curve was drawn in gray.

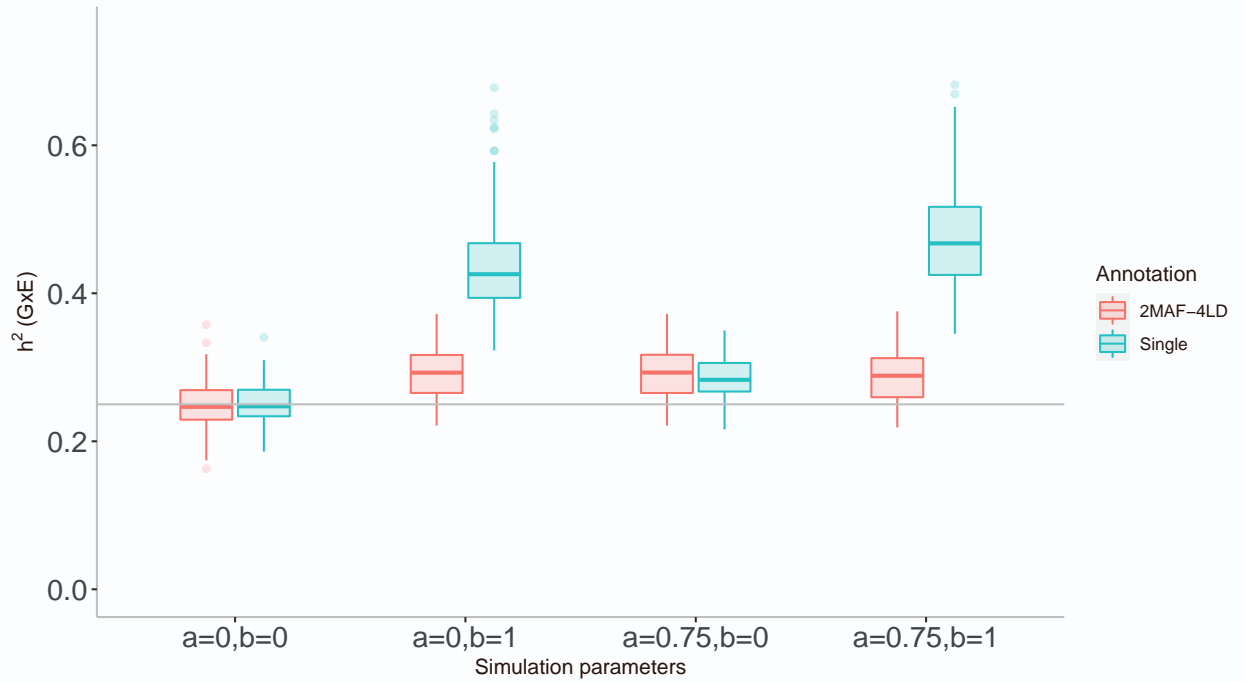


Figure S29: **Effect of MAF-LD partitioning on estimated GxE heritability in simulation.** We assessed the effect of MAF-LD partitioning on estimates of  $h_{gxe}^2$  in simulations. We ran GENIE in two settings: 1) fitting a model with a single additive and a single GxE variance component, and 2) fitting a model with eight additive and eight GxE components defined based on four LD annotations (quartiles of LD scores) and two MAF annotations. We simulated phenotypes with GxE effects and G effects from a subset of  $N = 40,000$  individuals genotyped at array SNPs  $M = 459,792$  by varying the coupling of MAF with effect size ( $a$ ) and the effect of local LD on effect size ( $b$ ). The per-SNP variance component  $\sigma_{g,m}^2 \propto w_m^b [f_m(1-f_m)]^a$  in simulations, where  $f_m$  and  $w_m$  are the minor allele frequency and LD score of  $m^{th}$  SNP respectively (see Note S2 for details). Here we have  $h_g^2 = h_{gxe}^2 = 0.25$ ,  $h_{nxe}^2 = 0.05$ , and all SNPs are causal for both additive and GxE effects. Each box plot represents estimates from 100 simulations.

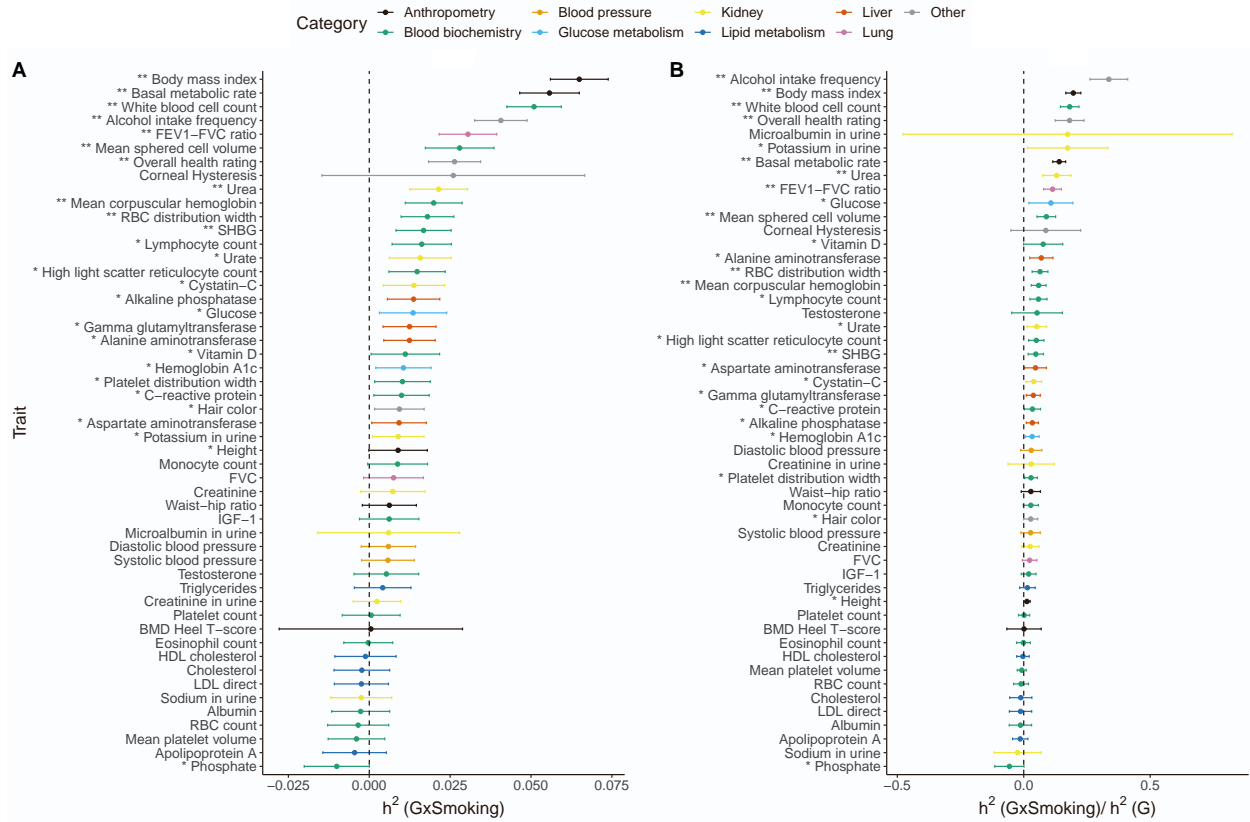


Figure S30: **GxSmoking across phenotypes from imputed SNPs in UK Biobank by MAF-LD partitioning.** (A) GxSmoking heritability and (B) the ratio of GxSmoking to additive heritability. Our model includes the environmental variable as a fixed effect and accounts for noise heterogeneity. Black error bars mark  $\pm 2$  standard errors. The asterisk and double asterisk correspond to the nominal  $p < 0.05$  and  $p < 0.05/200$ , respectively.

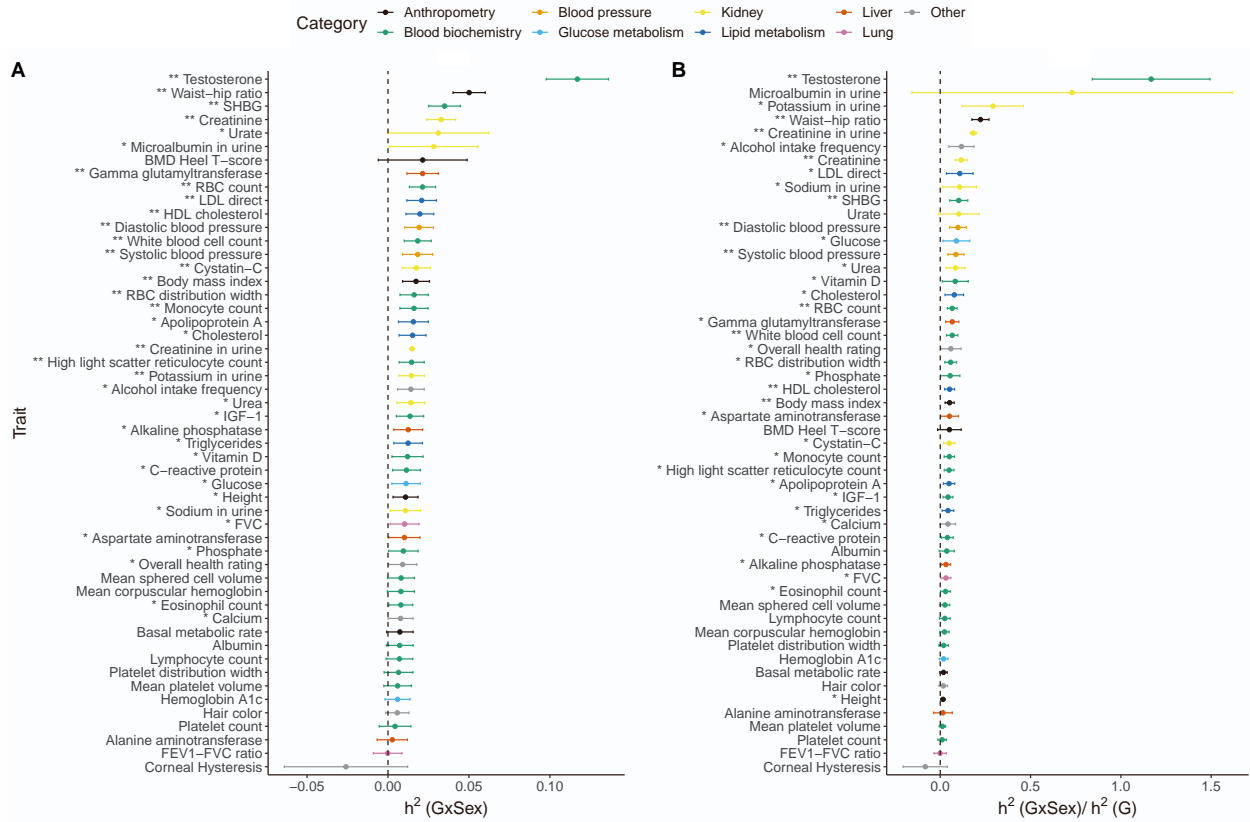


Figure S31: **GxSex across phenotypes from imputed SNPs in UK Biobank by MAF-LD partitioning.** (A) GxSex heritability and (B) the ratio of GxSex to additive heritability. Our model includes the environmental variable as a fixed effect and accounts for noise heterogeneity. Error bars mark  $\pm 2$  standard errors. The asterisk and double asterisk correspond to the nominal  $p < 0.05$  and  $p < 0.05/200$ , respectively.

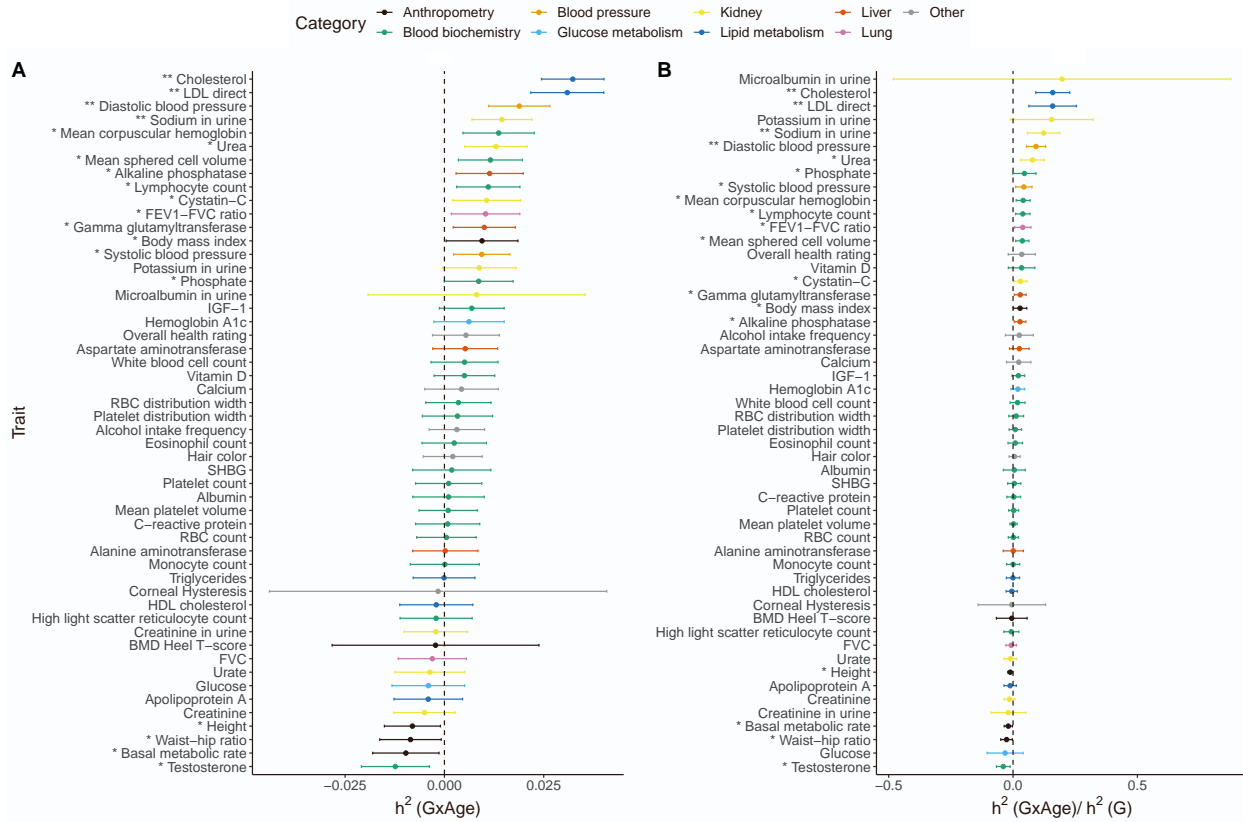


Figure S32: **GxAge across phenotypes from imputed SNPs in UK Biobank by MAF-LD partitioning.** (A) GxAge heritability and (B) the ratio of GxAge to additive heritability. Our model includes the environmental variable as a fixed effect and accounts for noise heterogeneity. Error bars mark  $\pm 2$  standard errors. The asterisk and double asterisk correspond to the nominal  $p < 0.05$  and  $p < 0.05/200$ , respectively.

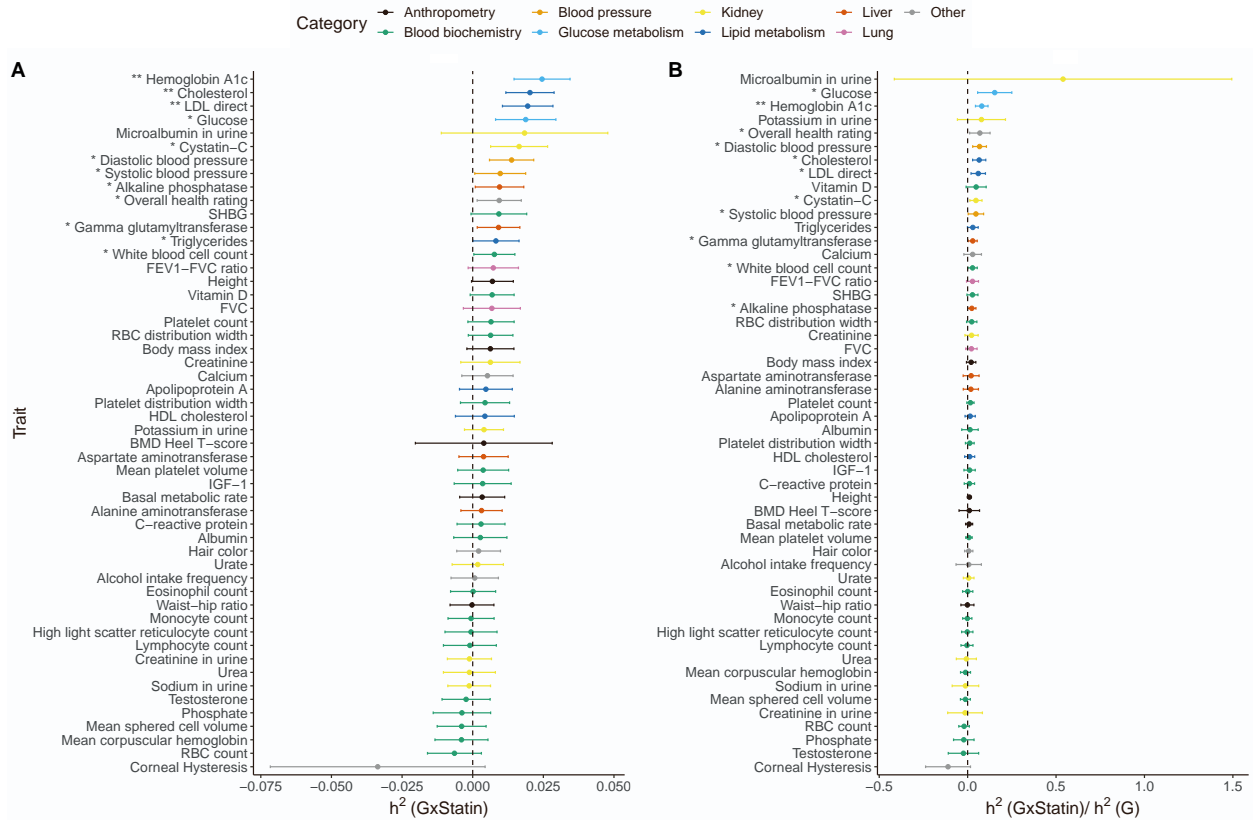


Figure S33: GxStatin across phenotypes from imputed SNPs in UK Biobank by MAF-LD partitioning. (A) GxStatin heritability and (B) the ratio of GxStatin to additive heritability. Our model includes the environmental variable as a fixed effect and accounts for noise heterogeneity. Error bars mark  $\pm 2$  standard errors. The asterisk and double asterisk correspond to the nominal  $p < 0.05$  and  $p < 0.05/200$ , respectively.

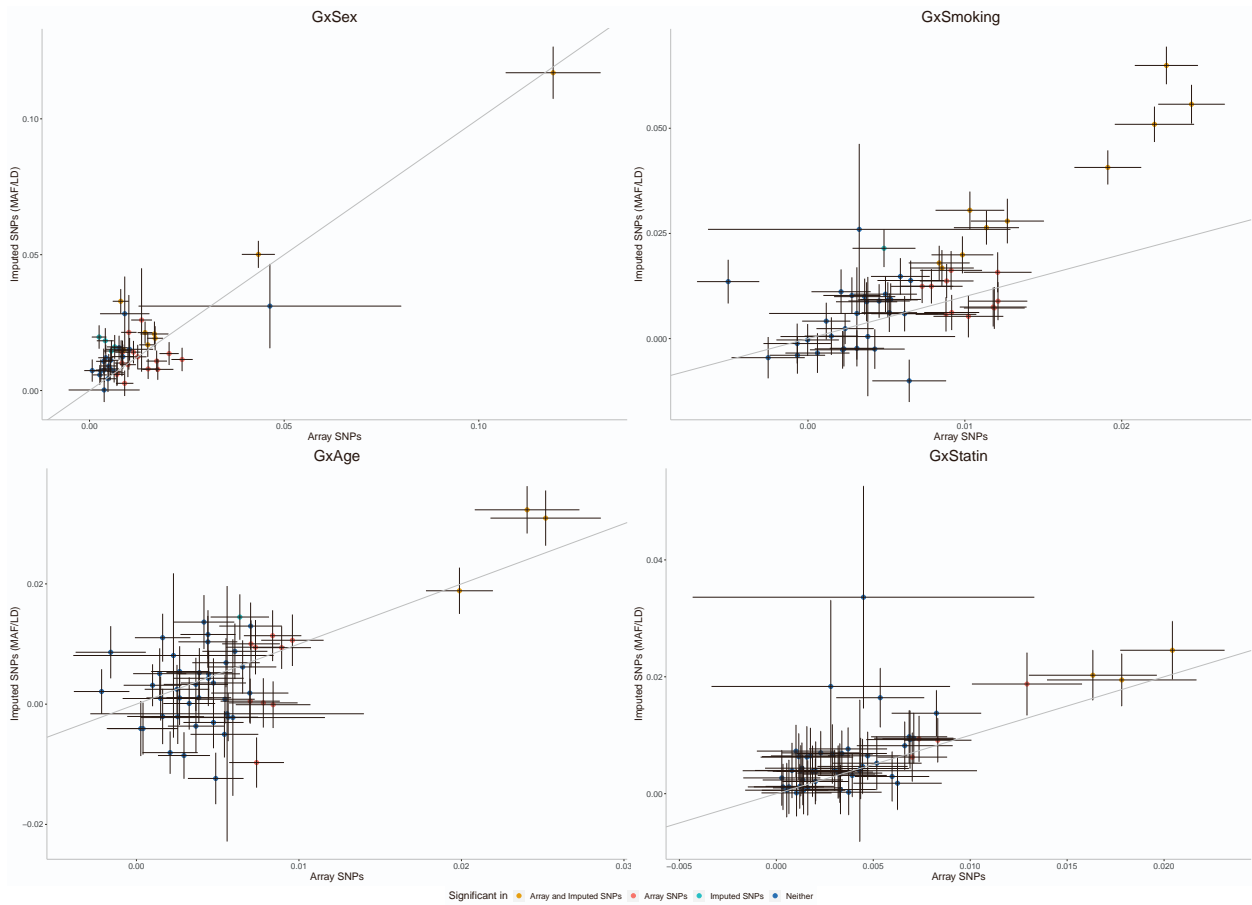


Figure S34: Comparing GxSex, GxSmoking, GxAge, and GxStatin estimates from imputed SNPs ( $MAF \geq 0.1\%$ ) and array SNPs ( $MAF \geq 1\%$ ). In this analysis, we applied GENIE to imputed SNPs with MAF/LD stratification and array SNPs with a single component. Black error bars mark  $\pm 2$  standard errors. The asterisk and double asterisk correspond to the nominal  $p < 0.05$  and  $p < 0.05/200$  respectively. The color of the dots indicates whether estimates of GxE heritability are significant under each model.



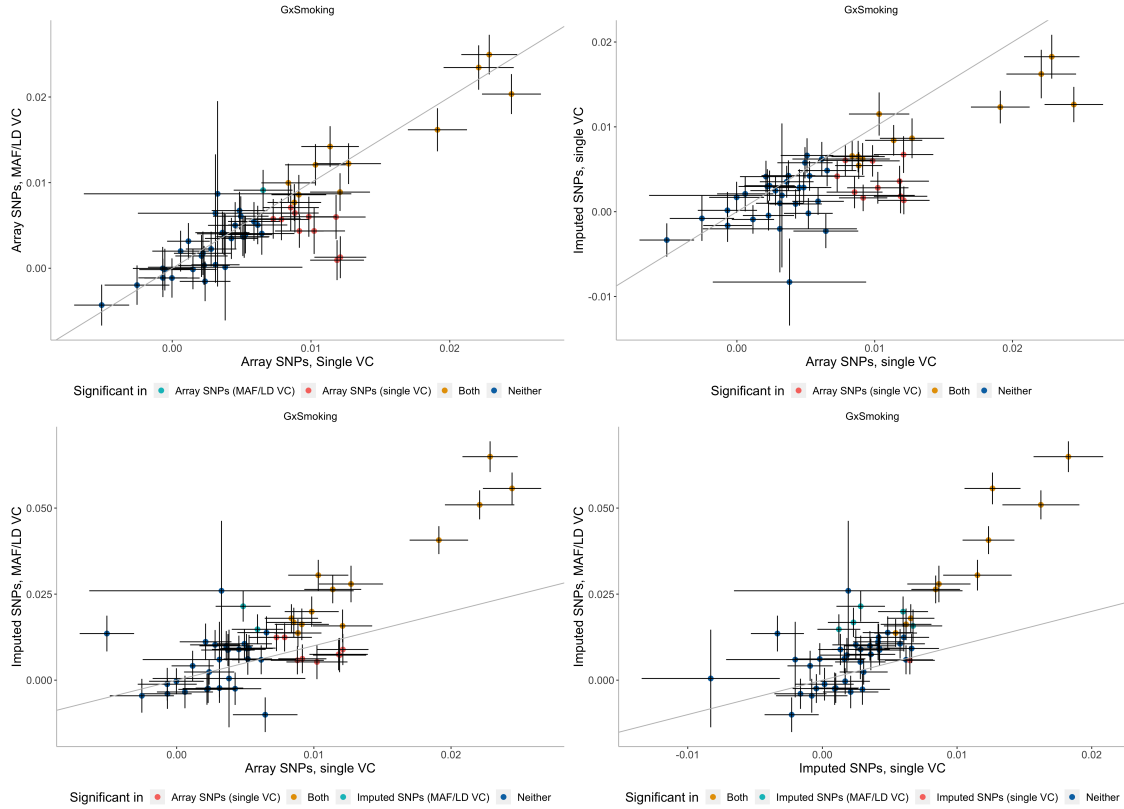


Figure S35: **Effect of MAF-LD partitioning on estimated GxE heritability.** We assessed the effect of MAF-LD partitioning on estimates of  $h_{GxSmoking}^2$  from array SNPs and imputed SNPs. We ran GENIE in two settings: (1) fitting a model with a single additive and a single GxE variance component, and (2) fitting a model with eight additive and eight GxE components defined based on four LD annotations (quartiles of LD scores) and two MAF annotations. Black error bars mark  $\pm 2$  standard errors centered on the estimates of  $h_{GxSmoking}^2$ . The color of the dots indicates whether estimates of  $h_{GxSmoking}^2$  are significant under each model.

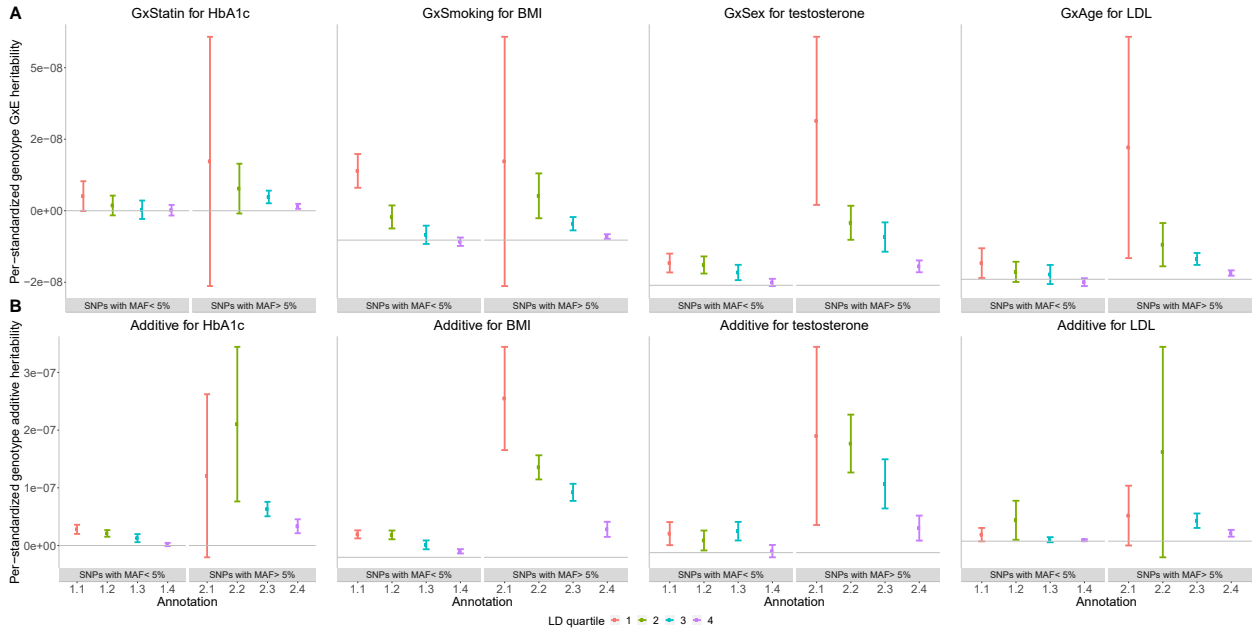


Figure S36: **Per-standardized genotype GxE and additive heritability as a function of MAF and LD.** (A) The per-standardized genotype GxE heritability for four selected traits and environments (trait-E pairs). (B) The per-allele additive heritability for the same trait-E pairs. The  $x$ -axis corresponds to MAF-LD annotations where annotation  $i.j$  includes SNPs in MAF bin  $i$  and LD quartile  $j$  where MAF bin 1 and MAF bin 2 correspond to SNPs with  $\text{MAF} \leq 5\%$  and  $\text{MAF} > 5\%$  respectively while the first quartile of LD-scores correspond to SNPs with the lowest LD-scores respectively). The  $y$ -axis shows the per-standardized genotype GxE (or additive) heritability defined as  $\frac{h_k^2}{2M_k}$  where  $h_k^2$  is the GxE (or additive) heritability attributed to bin  $k$ ,  $M_k$  is the number of SNPs in bin  $k$ . Error bars mark  $\pm 2$  standard errors centered on the estimated effect sizes.

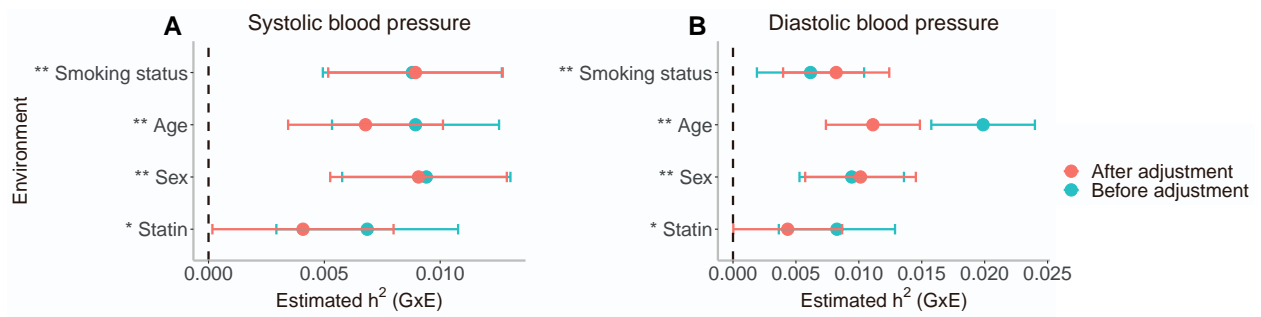


Figure S37: **Effects of adjustment for blood pressure medication on the GxE heritability estimates for systolic and diastolic blood pressure.** The estimated GxE heritability for (A) systolic and (B) diastolic blood pressure before and after the adjustment for medication. We added 15/10 mmHg to the systolic and diastolic blood pressure measurements for individuals with blood pressure medication on record in UKB, respectively<sup>7</sup>. Then we applied GENIE using the smoking status, age, sex, or statin as the environment exposure on  $N = 291,273$  individuals genotyped at 454,207 SNPs. The point estimates and  $\pm 2$  standard errors were shown, with single and double asterisks denoting  $p$ -value  $< 0.05$  and  $0.05/200$  for the results after the blood pressure medication adjustment.

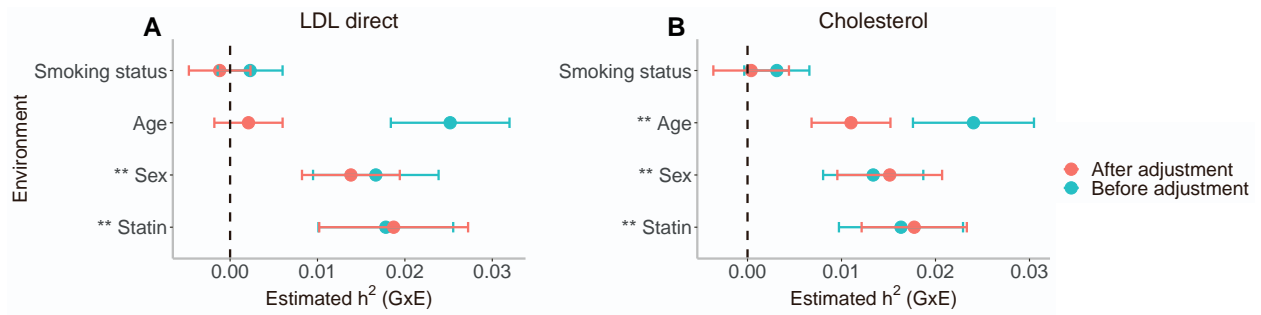


Figure S38: **Effects of adjustment for statin on the GxE heritability estimates for LDL and cholesterol.** The estimated GxE heritability for (A) LDL direct and (B) cholesterol before and after the adjustment for statin. We divided by 0.684 or 0.749 for LDL direct and cholesterol for those individuals who had taken statin medications, respectively<sup>8</sup>. Then we applied GENIE using the smoking status, age, sex, or statin as the environment exposure on  $N = 291,273$  individuals genotyped at 454,207 SNPs. The point estimates and  $\pm 2$  standard errors were shown, with single and double asterisks denoting  $p$ -value  $< 0.05$  and  $0.05/200$  for the results after the statin medication adjustment.

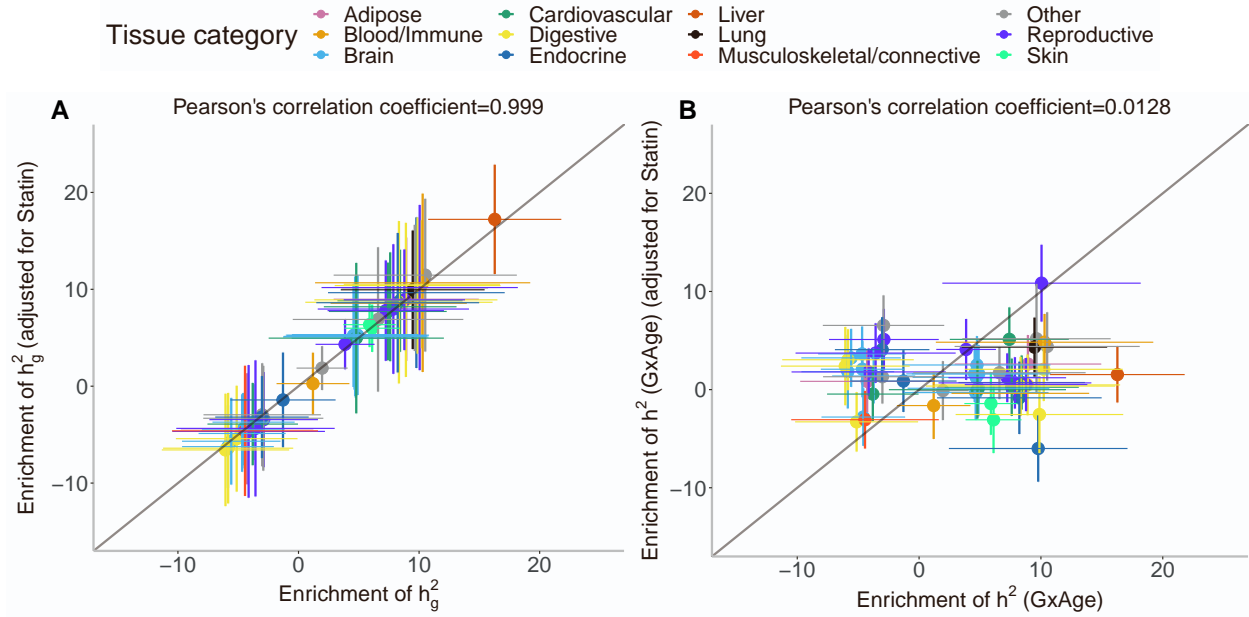


Figure S39: **Comparison of tissue-specific enrichment of G and GxAge heritability for cholesterol before and after adjustment.** The comparison of enrichment of (A) additive and (B) GxAge heritability in 53 tissue-specific genes for cholesterol before and after adjustment for statin. We divided the measured cholesterol values by 0.749 for individuals who had taken statin medications<sup>8</sup>. The enrichment in each tissue-specific annotation is conditional on 28 functional annotations that are part of the baseline LDSC annotations. The dot and error bars represent the point estimates and SE of the heritability enrichment in a tissue-specific annotation, respectively.

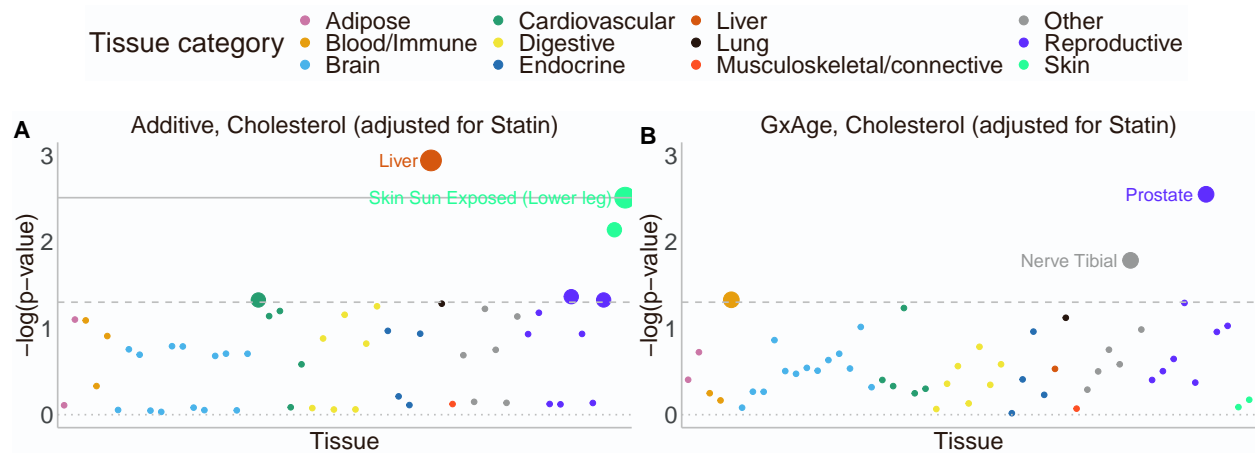


Figure S40: **Partitioning G and GxAge heritability for cholesterol (adjusted for statin) across 53 tissue-specific genes.** We plot  $-\log_{10}(p\text{-value})$  of the tissue-specific (A) G and (B) GxAge enrichment. For every tissue-specific annotation, we use GENIE to test whether this annotation is significantly enriched for per-SNP heritability, conditional on 28 functional annotations that are part of the baseline LDSC annotations. The dashed and solid lines correspond to the nominal  $p < 0.05$  and  $FDR < 0.1$  threshold, respectively. No tissue had a GxAge enrichment  $p$ -value below the  $FDR < 0.1$  threshold. We have labeled two tissues with the most significant  $p$ -values for each figure.

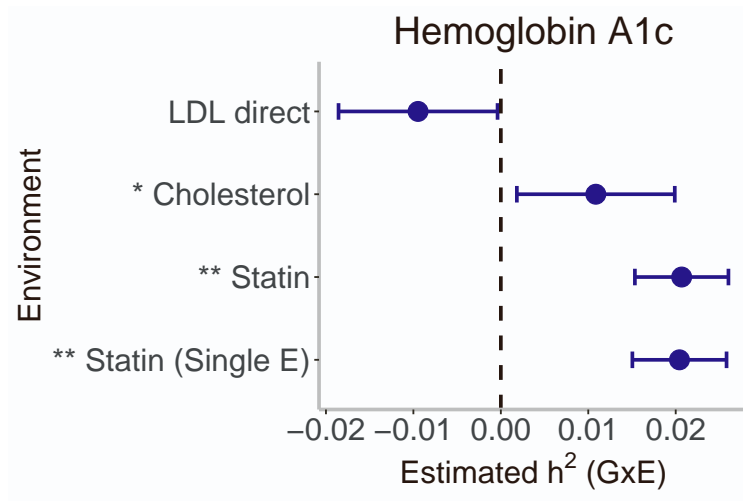


Figure S41: **Impact of LDL and cholesterol as environment exposures on the GxStatin estimates.** The GxStatin heritability for Hemoglobin A1c on  $N = 291,273$  individuals genotyped at 454,207 SNPs while incorporating LDL and cholesterol as environment exposures. The GxE heritability of three environment variables was jointly estimated in one pass of GENIE. The point estimates and  $\pm 2$  standard errors were shown, with single and double asterisks denoting  $p$ -value  $< 0.05$  and  $0.05/200$  for the specific GxE heritability estimate. Here “single E” refers to the case where statin was the single environment exposure used in the experiment. The sum of the GxE heritability of LDL, cholesterol, and statin was 2.21%. The GxStatin heritability point estimate was 2.07%, compared to 2.05% where statin is the single environmental exposure.

## Supplemental Tables

Method	Variance component	Mean	SE	Bias	Test of bias $p$ -value
GENIE	G	0.2005	0.0382	5e-04	0.9006
GENIE	GxE1	-0.0021	0.027	-0.0021	0.4302
GENIE	GxE2	0.0035	0.0257	0.0035	0.1778
GENIE	GxE3	-1e-04	0.0275	-1e-04	0.9692
GENIE	GxE4	0.0016	0.0245	0.0016	0.5094
GENIE	GxE5	0.0017	0.0267	0.0017	0.5159
GENIE	GxE6	0.0974	0.0278	-0.0026	0.3449
GENIE	GxE7	0.0981	0.0266	-0.0019	0.4673
GENIE	GxE8	0.0975	0.0257	-0.0025	0.3329
GENIE	GxE9	0.0098	0.0263	-2e-04	0.9537
GENIE	GxE10	0.0094	0.0257	-6e-04	0.8082

Table S1: **Accuracy of GENIE in the setting of multiple environmental variables:** We reported the bias, and SE of GENIE under different settings with  $L = 10$  environmental variables. Bias, mean and SE are computed from 100 replicates. We report the  $p$ -value of a test of the null hypothesis of no bias in the estimates of variance components.



Trait	Category
Alanine aminotransferase	Liver
Albumin	Blood biochemistry
Alcohol intake frequency	Other
Alkaline phosphatase	Liver
Apolipoprotein A	Lipid metabolism
Aspartate aminotransferase	Liver
BMD Heel T-score	Anthropometry
Basal metabolic rate	Anthropometry
Body mass index	Anthropometry
C-reactive protein	Blood biochemistry
Calcium	Other
Cholesterol	Lipid metabolism
Creatinine in urine	Kidney
Creatinine	Kidney
Cystatin-C	Kidney
Diastolic blood pressure	Blood pressure
Eosinophil count	Blood biochemistry
FEV1-FVC ratio	Lung
FVC	Lung
Gamma glutamyltransferase	Liver
Glucose	Glucose metabolism
HDL cholesterol	Lipid metabolism
Height	Anthropometry
Hemoglobin A1c	Glucose metabolism
High light scatter reticulocyte count	Blood biochemistry
IGF-1	Blood biochemistry
LDL direct	Lipid metabolism
Lymphocyte count	Blood biochemistry
Mean corpuscular hemoglobin	Blood biochemistry
Mean platelet volume	Blood biochemistry
Mean sphered cell volume	Blood biochemistry
Microalbumin in urine	Kidney
Monocyte count	Blood biochemistry
Overall health rating	Other
Phosphate	Blood biochemistry
Platelet count	Blood biochemistry
Platelet distribution width	Blood biochemistry
Potassium in urine	Kidney
RBC count	Blood biochemistry
RBC distribution width	Blood biochemistry
SHBG	Blood biochemistry
Sodium in urine	Kidney
Systolic blood pressure	Blood pressure
Testosterone	Blood biochemistry
Triglycerides	Lipid metabolism
Urate	Kidney
Urea	Kidney
Vitamin D	Blood biochemistry
Waist-hip ratio	Anthropometry
White blood cell count	Blood biochemistry

Table S2: Mapping between the 50 UK Biobank traits and their categories.

Tissue	Category
Adipose Subcutaneous	Adipose
Adipose Visceral (Omentum)	Adipose
Adrenal Gland	Endocrine
Artery Aorta	Cardiovascular
Artery Coronary	Cardiovascular
Artery Tibial	Cardiovascular
Bladder	Other
Brain Amygdala	Brain
Brain Anterior cingulate cortex (BA24)	Brain
Brain Caudate (basal ganglia)	Brain
Brain Cerebellar Hemisphere	Brain
Brain Cerebellum	Brain
Brain Cortex	Brain
Brain Frontal Cortex (BA9)	Brain
Brain Hippocampus	Brain
Brain Hypothalamus	Brain
Brain Nucleus accumbens (basal ganglia)	Brain
Brain Putamen (basal ganglia)	Brain
Brain Spinal cord (cervical c-1)	Brain
Brain Substantia nigra	Brain
Breast Mammary Tissue	Reproductive
Cells EBV-transformed lymphocytes	Blood/Immune
Cells Transformed fibroblasts	Other
Cervix Ectocervix	Reproductive
Cervix Endocervix	Reproductive
Colon Sigmoid	Digestive
Colon Transverse	Digestive
Esophagus Gastroesophageal Junction	Digestive
Esophagus Mucosa	Digestive
Esophagus Muscularis	Digestive
Fallopian Tube	Reproductive
Heart Atrial Appendage	Cardiovascular
Heart Left Ventricle	Cardiovascular
Kidney Cortex	Other
Liver	Liver
Lung	Lung
Minor Salivary Gland	Other
Muscle Skeletal	Musculoskeletal/connective
Nerve Tibial	Other
Ovary	Reproductive
Pancreas	Other
Pituitary	Endocrine
Prostate	Reproductive
Skin Not Sun Exposed (Suprapubic)	Skin
Skin Sun Exposed (Lower leg)	Skin
Small Intestine Terminal Ileum	Digestive
Spleen	Blood/Immune
Stomach	Digestive
Testis	Endocrine
Thyroid	Endocrine
Uterus	Reproductive
Vagina	Reproductive
Whole Blood	Blood/Immune

Table S3: Mapping between the 53 GTEx tissues and their categories.

## References

- [1] Evans, L. M., Tahmasbi, R., Vrieze, S. I., Abecasis, G. R., Das, S., Gazal, S., Bjelland, D. W., Candia, T. R., Goddard, M. E., Neale, B. M. *et al.* (2018). Comparison of methods that use whole genome data to estimate the heritability and genetic architecture of complex traits. *Nature genetics* *50*, 737.
- [2] Hou, K., Burch, K. S., Majumdar, A., Shi, H., Mancuso, N., Wu, Y., Sankararaman, S., and Pasaniuc, B. (2019). Accurate estimation of SNP-heritability from biobank-scale data irrespective of genetic architecture. *Nature genetics* *51*, 1244–1251.
- [3] Yang, J., Lee, S. H., Goddard, M. E., and Visscher, P. M. (2011). GCTA: a tool for genome-wide complex trait analysis. *The American Journal of Human Genetics* *88*, 76–82.
- [4] Bulik-Sullivan, B. K., Loh, P.-R., Finucane, H. K., Ripke, S., Yang, J., Patterson, N., Daly, M. J., Price, A. L., Neale, B. M., of the Psychiatric Genomics Consortium, S. W. G. *et al.* (2015). LD Score regression distinguishes confounding from polygenicity in genome-wide association studies. *Nature genetics* *47*, 291.
- [5] Speed, D., Hemani, G., Johnson, M. R., and Balding, D. J. (2012). Improved heritability estimation from genome-wide snps. *The American Journal of Human Genetics* *91*, 1011–1021.
- [6] Di Scipio, M., Khan, M., Mao, S., Chong, M., Judge, C., Pathan, N., Perrot, N., Nelson, W., Lali, R., Di, S. *et al.* (2023). A versatile, fast and unbiased method for estimation of gene-by-environment interaction effects on biobank-scale datasets. *Nature Communications* *14*, 5196.
- [7] Warren, H. R., Evangelou, E., Cabrera, C. P., Gao, H., Ren, M., Mifsud, B., Ntalla, I., Surendran, P., Liu, C., Cook, J. P. *et al.* (2017). Genome-wide association analysis identifies novel blood pressure loci and offers biological insights into cardiovascular risk. *Nature genetics* *49*, 403–415.
- [8] Sinnott-Armstrong, N., Tanigawa, Y., Amar, D., Mars, N., Benner, C., Aguirre, M., Venkataraman, G. R., Wainberg, M., Ollila, H. M., Kiiskinen, T. *et al.* (2021). Genetics of 35 blood and urine biomarkers in the UK Biobank. *Nature genetics* *53*, 185–194.